Abstract

LOO, LINA. Development of *Red clover necrotic mosaic virus* as a Multifunctional Nanoparticle. (Under the direction of Stefan Franzen.)

Red clover necrotic mosaic virus (RCNMV) is a member of the genus *Dianthovirus* and the family *Tombusviridae*. RCNMV is a plant virus with 180 identical capsid proteins (CP) arranged to form a T = 3 icosahedral symmetry. The capsid, with an outer diameter of 36 nm and an inner diameter of 17 nm, is enclosed to package two ssRNA: RNA-1 (3.9 kb) and RNA-2 (1.5 kb).

In nature, a 20 nucleotide hairpin structure within the RNA-2 sequence trans-activator region forms a kissing loop complex with 8 nucleotides of the RNA-1 to serve as the origin of assembly (OAS). This pseudo-knot structure selectively recruits CP to initiate the virus assembly. In one of the research directions, an oligonucleotide mimic of the OAS sequence was attached to Au, $CoFe_2O_4$, and CdSe nanoparticles ranging from 3-15 nm, to trigger virus-like assembly by RCNMV CP. The formation of virus-like particles encapsidated nanoparticles was comparable in size to the native RCNMV. Attempts to encapsidate nanoparticles with diameters > 17 nm did not result in well-formed particles.

The versatility of RCNMV capsid to package smaller cargo was explored. RCNMV experiences reversible swelling transition in a pH- and divalent ion-dependent manner. This transition leads to the reversible opening of pores (~13 Å) that permit infusion of molecules into the interior cavity. Comparison of three dyes, Rhodamine (positive charge), Luminarosine (neutral) and Fluorescein (negative charge) shows that infusion is controlled by electrostatic interactions. This method was applied to package an anticancer drug, Doxorubicin, within the capsid.

The capability of the RCNMV capsid to deliver cargo into cancer cells was explored. Peptides from various serotypes of adenovirus were conjugated to the capsid to determine the internalization efficiency. The modified RCNMV was prepared with packaged molecules in the interior cavity and targeting peptide on the exterior surface. Intracellular uptake was studied both in terms of RCNMV internalization and cargo

release. The utilization of RCNMV capsid as a multifunctional tool for therapeutic purposes demonstrates a new general therapeutic and diagnostic platform.

Development of *Red clover necrotic mosaic virus* as a Multifunctional Nanoparticle

by

Li Na Loo

A dissertation submitted to the Graduate Faculty of
North Carolina State University
in partial fulfillment of the
requirements for the Degree of
Doctor of Philosophy

Chemistry

Raleigh, North Carolina

2007

APPROVED BY:

_____
Dr. Stefan Franzen, Chair of Advisory Committee

_____ _____
Dr. Tatyana Smirnova Dr. Alexander Deiters

_____
Dr. Steven A. Lommel

BIOGRAPHY

I was born and raised in Kuala Lumpur, Malaysia. My parents have always taught me the importance of education. Growing up with five other siblings, they were my childhood playmates for most of the time. Laughs and jokes are part of our daily life. I am very fortunate to have a wonderful family who has encouraged and supported me throughout my life.

TABLE OF CONTENTS

LIST OF TABLES

CHAPTER 3

CHAPTER 4

LIST OF FIGURES

CHAPTER 1

CHAPTER 2

CHAPTER 3

CHAPTER 5

CHAPTER 1

Applications of Viruses: An overview

1.0 Introduction

Biomaterials such as DNA or peptides are often used as building blocks in nanotechnology applications[1-4]. Recently, virus particles have been studied extensively as a nanotechnology tool due to the desirable packaging and self-assembly properties[5-7]. In this thesis I will present several new applications of a plant virus, *Red clover necrotic mosaic virus* (RCNMV). The first application consists of the templated self-assembly of the RCNMV capsid protein around three types of nanoparticles. A second application consists of an alternative approach to package smaller cargo/molecules within the RCNMV capsid. Electrostatic interactions and possibly specific nucleic acid binding are used to load cargo into the interior RCNMV. This method highlights the versatility of RCNMV capsid to package foreign cargos. The exterior surface of RCNMV capsid also demonstrated as a platform to display targeting signals. The utilization of RCNMV capsid to package, target and deliver cargo into cell is described. Overall, the work described here uses a plant virus as a multifunctional nanoparticle that can package foreign cargos and serve as a cell-targeting agent.

1.1. General structure of viruses

Viruses are obligate intracellular parasites, which only replicate within a host cell. Once in a cell, viruses use the host cell machinery to replicate and assemble to form progeny. Viruses typically consist of 2 basic components: capsid and genome. The genetic material, ribonucleic acid (RNA) or deoxyribonucleic acid (DNA), are packaged by multiple copies of protein subunits, referred as capsid. Some viruses contain an additional lipid membrane on the outer surface of capsid, such viruses are termed enveloped virus. The lipid membrane is taken from the membrane of the host cells when the virus buds out from the cytoplasm. The morphology of viruses exists in different shapes such as helical, icosahedral or tetrahedral. Here, we will focus on an icosahedral capsid structure of a non-enveloped virus.

An icosahedral virus consists of 20 equilateral triangular faces, 12 vertices, and 30 edges with 2, 3, and 5-fold axes of symmetry (Figure 1). The smallest number of protein subunits needed to form an icosahedron is 60, where all the capsid proteins have identical shape and bonding to the nearby subunits (equivalent environments). For instance, the capsid of *Tobacco necrosis satellite virus* is built from 60 subunits with three protein subunits in identical position on each triangular face[8]. Viruses with multiple copies of 60 subunits contain pentameric and hexameric assemblies. The capsid proteins are interchangeable to form pentamers and hexamers, hence the angles on bonding between the proteins are not exactly equivalent. A triangulation number, T, indicates the number of subunits in the icosahedral asymmetrical unit (Figure 2). This concept of quasi-equivalance was first introduced by Caspar and Klug (1962). For instance, RCNMV is a T = 3 icosahedral virus which consists of 180 identical capsid proteins. These capsid proteins consist of three different conformational proteins, referred as A, B and C. These A, B and C subunits are arranged to form 12 pentamers and 20 hexamers.

1.2 Applications of viruses in nanotechnology

Recently, researchers have recognized the potential of virus capsids as a new class of bio-nanoparticle that can be attractive for nanotechnology applications[5-7]. The virus capsids consist of protein subunits that self-assemble to form a symmetrical structure with defined exterior and interior surfaces. The inner and outer surfaces of virus capsids are often accessible for chemical modification. Most of the viruses that have been exploited for nanotechnology applications, such as *Cowpea mosaic virus* (CPMV), can be produced in a large quantity (over 1 g/kg of infected leaves)[9]. These properties possessed by viruses made them an ideal candidate in nanotechnology applications. Here, we described the usage of viruses as tools in material science, biomedical and electronics applications.

1.2.1 Material Science Applications

In nature, viruses package their genome within a capsid. The virus capsid, devoid of the genome, can be used as a container. An initial attempt to use the virus capsid for foreign cargo encapsulation was demonstrated with the *Cowpea chlorotic mottle virus* (CCMV). CCMV is composed of 180 protein subunits assembled to form a T = 3 icosahedral virus with a diameter of 28 nm[10]. At pH > 6.5, the capsid of CCMV swells to form 60 pores (~2 nm diameter) on the capsid. At pH < 6.5, the swollen capsid can be reversed to the non-swollen conformation. By pH adjustments, precursor ions such as tungstate ($H_2W_{12}O_{42}^{10-}$) and vanadates ($V_{10}O_{28}^{6-}$) were loaded and entrapped in the CCMV capsids[11]. These ions were further mineralized to form nanoparticles within the capsid. That report demonstrated the ability of CCMV to package foreign cargo and function as vessel for mineralization reaction. Using a similar approach, the interior cavity of CCMV capsids were further explored to synthesize metal oxides such as Fe_2O_3 and Co_2O_3[12]. The possibility to synthesize nanoparticles within a virus capsid is advantageous as the growth of nanoparticles can be controlled by the size and shape of the virus capsids.

The external surface of a virus capsid consists of highly symmetrical and repetitive functional groups such as glutamate, aspartate, arginine and lysine. These functional groups can be exploited to serve as a template for nanoparticles synthesis. *Tobacco mosaic virus* (TMV), a rod shaped virus with 300 nm in length and 18 nm in diameter, exhibits remarkable stability at pH 2-10 and temperature as high as 60 ^{o}C. These properties exhibited by TMV, together with the ordered functional groups on the outer surface, have been exploited as a platform for the nucleation and growth of metal oxide. The precursor ions $[AuCl_4]^-$ and $[PtCl_6]^{2-}$ were deposited and bound to the functional groups on the exterior of TMV[13]. By chemical reduction, these ions grew to form nanoparticles with an average diameter of 10 nm on the exterior of TMV. In addition, the 4 nm central channel of TMV was also investigated as a template for nanoparticles synthesis. By loading Co^{2+} and Pt^{2+} ions into the inner channel, the ions grew within the capsid to form one dimension CoPt and $FePt_3$ nanowires with a defined diameter that is controlled by the inner cavity of TMV[14,15]. These reports demonstrated the versatility of inner and outer surface of TMV to serve as a template for nanomaterial

synthesis. The highly symmetrical structure and narrow size distributions of viruses made them an ideal template for nanoparticle synthesis.

Besides nucleation or templating for nanoparticle synthesis, virus capsids have been described for nanoparticle encapsulation. An initial study was performed to package Au nanoparticles-coated citrate by *Brome mosaic virus* (BMV) protein subunits[16]. In that report, the Au nanoparticles managed to initiate a self-assembly of BMV protein subunits, via electrostatic interactions, to form virus-like particles (VLP) with the Au nanoparticles encapsulated. The encapsulation efficiency can be increased by polyethylene glycol (PEG) modification to the Au nanoparticles, where the PEG formed a layer that mimics the viral genome[17]. This approach was further extended to package semiconductor nanoparticles[18]. So far, the methods proposed to package nanoparticles were based on a RNA-independent self-assembly process. In my research, a different approach was proposed where a complex of RNA sequences conjugated on nanoparticles acts as a recognition signal for the self-assembly of protein subunits (described in Chapter 3). The encapsulation of nanoparticles by a virus capsid, not only offers an alternative method to stabilize the nanoparticles, but also provides an external platform for ligands conjugation.

1.2.2 Biomedical Applications

Virus particles are excellent candidates to function as tools for biomedical nanotechnology. The homogeneity in size and shape as well as the ease of production of virus particles are advantageous as opposed to most reported drug delivery system such as lipids and polymers that were prepared through random aggregation[19]. In addition, the plant viruses studied are not human pathogens, which have no natural tendency to interact with human cell surface receptors.

In nature, the virus protein cages are assembled in a manner to provide full protection to its virus genome over a wide range of pH and temperature. The rigidity and robustness of the capsid can be exploited as a container for encapsulation of drug molecules. For instance, the capsid of *Hibiscus chlorotic ringspot virus* (HCRSV) was studied to package an anticancer drug, Doxorubicin[20]. In this study, a negatively charged

polyacid was mixed with Doxorubicin to create a net negative charge complex. This complex then acted as a nucleus to initiate an *in vitro* assembly of HCRSV protein subunits to form a virus-like particle, along with the Doxorubicin encapsulated inside the capsid. A different approach was applied using MS2 bacteriophage capsid for cargo encapsulation[21]. The tyrosine residues located in the interior cavity of MS2 bacteriophage was modified to attach olefin substrates. These olefin substrates acted as the functional group for Diels-Alder reaction, with the product of the reaction encapsulated within the MS2 capsid. This report highlighted the ability to manipulate the inner cavity of virus capsid to enhance specificity in encapsulation.

The ability to modify the exterior surface for multivalent presentation enables virus particles to function as an imaging agent. Based on cross-linking chemistry, the outer surface of *Cowpea mosaic virus* (CPMV) was conjugated with fluorophore AlexaFluor555[5]. The injection of CPMV-fluorophore into living chick and mouse embryos allowed the vasculature of the animals to be visualized. By using the fluorescently labeled CPMV, further experiments were performed to study the *in vivo* interaction of CPMV and mammalian cells[22]. The 54-kDa and 47-kDa mammalian binding proteins were found to bind CPMV with high affinity. The ability to visualize as well as understand the interaction of CPMV with mammalian vasculature provides important information to further enhance the biological applications of CPMV.

Virus capsids are ideal drug carriers due to the fact that they have diameters on the nanometer scale, which is critical for tumor permeability and retention[23]. *Canine parvovirus* (CPV), a member of the family *parvoviridae*, has recently been developed for tumor targeting. CPV consists of 3 different protein subunits termed VP1, VP2 and VP3[24] assembled to form a T = 1 icosahedral particle with an average diameter of 26 nm. The natural receptor for CPV is the transferrin receptor TfR on canine cells, which is also found to be over-expressed in human tumor cells[25]. Hence, the natural binding ability between CPV and tumor cells was exploited for tumor targeting. In the reported work, the VP2 of CPV was expressed using baculovirus expression system to form virus-like particles (VLP) that is morphologically similar to a native CPV. The CPV-VLP, packaged with dyes molecules, was then studied for binding and internalization into human tumor cells via TfR. This report demonstrated an alternative approach for tumor

targeting by using the natural binding interactions between virus and tumor receptor. In contrast to liposomes or inorganic nanoparticles that required artificial targeting for tumor specificity, viruses have evolved with high degree of selective targeting for cell entry.

The interface of protein subunits also presents an attractive property that can be exploited for biomedical purposes. The crystal structure of *Cowpea chlorotic mosaic virus* (CCMV) indicated the presence of 180 Ca^{2+} binding sites per virus[26]. These binding sites were located at the interface between protein subunits. The possibility to replace Gd^{3+} into the divalent ion binding sites created a virus nanoparticle with magnetic properties[27]. An experiment to explore the potential of MS2 for similar purposes has been described. The lysine residues on the outer surface of MS2 were replaced with Gd-diethylenetriamine (Gd-DPTA) with an average of 514 Gd-DPTA per virus[28]. The ability to modify the functional groups on the virus capsids either at the interface or the outer surface of the subunit demonstrated the potential of virus capsids as a new platform to function as MRI contrast agent.

Another way to create a paramagnetic viral nanoparticle is to encapsulate a magnetic nanoparticle by virus protein subunits[29]. As reported, the iron oxide nanoparticles, with an average diameter of 10 nm and 8 nm, were coated with lipid micelles (HOOC-PEG-PL) to exhibit an anionic surface charge (COOH groups) as well as hydrophobic properties (PEG). The functionalized nanoparticles managed to initiate a self-assembly of BMV protein subunits to form virus-like particles (VLP) with the magnetic nanoparticles encapsulated. The magnetic behavior of the encapsulated iron oxide nanoparticle remained similar to un-encapsulated iron oxide nanparticle. This method increases the biocompatibility of nanoparticles and also provides an external functionalization sites.

1.2.3 Electronic Applications

Viruses have also been studied to function in the electronic field. As mentioned earlier, the outer surface of a virus capsid can be exploited as a nucleation site and growth of

nanoparticles. In a reported work, Pt^{2+} ions deposited and bound to the functional groups on a TMV capsid were found to form nanoparticles with an average diameter of 10 nm[30,31]. When the TMV-Pt was placed between 2 Al electrodes, a unique memory effect was observed. As described in the report, the RNA and the TMV capsid acted as charge donor and energy barrier, respectively. When current was applied, the charge transferred from the RNA (the aromatic rings such as guanine can behave as a charge donor) was trapped in the Pt nanoparticles, and stabilized by the capsid. The reversible charge transfer and charge trapped process between the TMV capsid and Pt nanoparticles (formed on the outer surface of TMV capsid) have created a memory device. Using similar approach, another memory device was designed using *Cowpea mosaic virus* (CPMV) with the exterior capsid conjugated with quantum dots[32]. The insulating capping layer (such as ZnS) of quantum dots acted as a charge storage while the aromatic residues (tryptophan) on CPMV capsid behaved as a charge transport. By combining quantum dots and CPMV, a new material system with the electronic memory device functional was demonstrated.

The rod-shaped of TMV, with 300 nm in length, has also been studied to form fibers and wires with length up to multiple centimeters[33]. In the report, the viruses were aligned through a dewetting technique where the thickness, length as well as the orientation can be controlled. The outer surface of the assembled virus was then coated with Au and Ag nanoparticles to form anisotropic conductive arrays of wires. The technique reported here offers a rapid method to assemble viruses to form wires with electronically function, which can further be explored for applications such as bioelectronic devices.

1.2.4 Summary

The natural properties of viruses, including homogeneity structure, amenable to chemically or genetically manipulation, as well as ease of production, have enable them to function for a variety applications in nanotechnology. The transition occurred from the understanding of viruses as pathogens to applications for nanotechnology created a new

area of interdisciplinary study between virology, material science, biomedical and electronic.

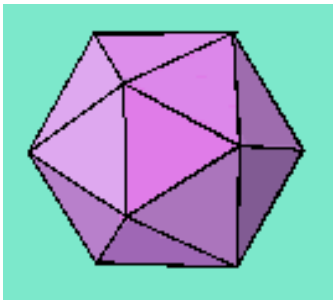

Figure 1. A regular icosahedral structure. A typical icosahedral structure has 12 vertices, 20 equilateral triangular faces and 30 edges. The vertices are on a 5-fold rotational symmetry; the center of each triangular face is on a 3-fold symmetry axis, and each edge is on a 2-fold symmetry axis.

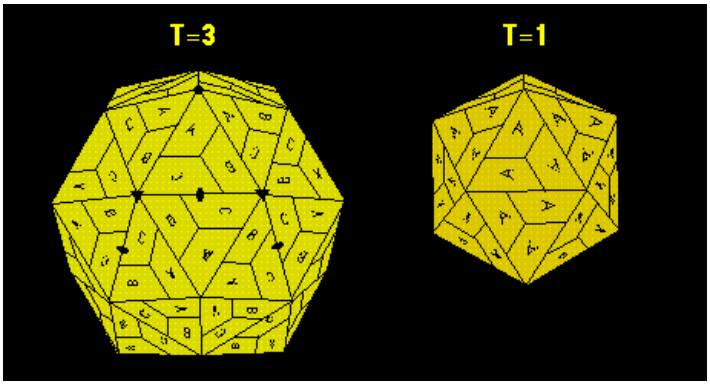

Figure 2. Comparison of T = 3 and T = 1 icosahedral virus. A T = 3 icosahedral virus consists of three chemically identical but structurally independent subunits (referred as A, B and C) in each asymmetrical unit. For a T = 1 icosahedral virus, the subunits are chemically and structurally identical in each triangular face[34]

References

(1) LaBean, T. H.; Li, H. Y. *Nano Today* **2007**, *2*, 26-35.

(2) Sherman, M. B.; Guenther, R. H.; Tama, F.; Sit, T. L.; Brooks, C. L.; Mikhailov, A. M.; Orlova, E. V.; Baker, T. S.; Lommel, S. A. *Journal of Virology* **2006**, *80*, 10395-10406.

(3) Gazit, E. *Chemical Society Reviews* **2007**, *36*, 1263-1269.

(4) Banta, S.; Megeed, Z.; Casali, M.; Rege, K.; Yarmush, M. L. *Journal of Nanoscience and Nanotechnology* **2007**, *7*, 387-401.

(5) Lewis, J. D.; Destito, G.; Zijlstra, A.; Gonzalez, M. J.; Quigley, J. P.; Manchester, M.; Stuhlmann, H. *Nature Medicine* **2006**, *12*, 354-360.

(6) Rawat, M.; Singh, D.; Saraf, S.; Saraf, S. *Biological & Pharmaceutical Bulletin* **2006**, *29*, 1790-1798.

(7) Uchida, M.; Klem, M. T.; Allen, M.; Suci, P.; Flenniken, M.; Gillitzer, E.; Varpness, Z.; Liepold, L. O.; Young, M.; Douglas, T. *Advanced Materials* **2007**, *19*, 1025-1042.

(8) Ban, N.; McPherson, A. *Nature Structural Biology* **1995**, *2*, 882-890.

(9) Falkner, J. C.; Turner, M. E.; Bosworth, J. K.; Trentler, T. J.; Johnson, J. E.; Lin, T. W.; Colvin, V. L. *Journal of the American Chemical Society* **2005**, *127*, 5274-5275.

(10) Johnson, J.; Lin, T.; Lomonossoff, G. *Annual Review of Phytopathology* **1997**, *35*, 67-86.

(11) Douglas, T.; Young, M. *Nature* **1998**, *393*, 152-155.

(12) Allen, C.; Dos Santos, N.; Gallagher, R.; Chiu, G. N. C.; Shu, Y.; Li, W. M.; Johnstone, S. A.; Janoff, A. S.; Mayer, L. D.; Webb, M. S.; Bally, M. B. *Bioscience Reports* **2002**, *22*, 225-250.

(13) Dujardin, E.; Peet, C.; Stubbs, G.; Culver, J. N.; Mann, S. *Nano Letters* **2003**, *3*, 413-417.

(14) Tsukamoto, R.; Muraoka, M.; Seki, M.; Tabata, H.; Yamashita, I. *Chemistry of Materials* **2007**, *19*, 2389-2391.

(15) Knez, M.; Bittner, A. M.; Boes, F.; Wege, C.; Jeske, H.; Maiss, E.; Kern, K. *Nano Letters* **2003**, *3*, 1079-1082.

(16) Chen, C.; Kwak, E. S.; Stein, B.; Kao, C. C.; Dragnea, B. *Journal of Nanoscience and Nanotechnology* **2005**, *5*, 2029-2033.

(17) Chen, C.; Daniel, M. C.; Quinkert, Z. T.; De, M.; Stein, B.; Bowman, V. D.; Chipman, P. R.; Rotello, V. M.; Kao, C. C.; Dragnea, B. *Nano Letters* **2006**, *6*, 611-615.

(18) Dixit, S. K.; Goicochea, N. L.; Daniel, M. C.; Murali, A.; Bronstein, L.; De, M.; Stein, B.; Rotello, V. M.; Kao, C. C.; Dragnea, B. *Nano Letters* **2006**, *6*, 1993-1999.

(19) Huang, Y. Z.; Gao, J. Q.; Lang, W. Q.; Nakagawa, S. *Biological & Pharmaceutical Bulletin* **2005**, *28*, 387-390.

(20) Ren, Y.; Wong, S. M.; Lim, L. Y. *Bioconjugate Chemistry* **2007**, *18*, 836-843.

(21) Hooker, J. M.; Kovacs, E. W.; Francis, M. B. *Journal of the American Chemical Society* **2004**, *126*, 3718-3719.

(22) Koudelka, K. J.; Rae, C. S.; Gonzalez, M. J.; Manchester, M. *Journal of Virology* **2007**, *81*, 1632-1640.

(23) Nagayasu, A.; Uchiyama, K.; Kiwada, H. *Advanced Drug Delivery Reviews* **1999**, *40*, 75-87.

(24) Tsao, J.; Chapman, M. S.; Agbandje, M.; Keller, W.; Smith, K.; Wu, H.; Luo, M.; Smith, T. J.; Rossmann, M. G.; Compans, R. W.; Parrish, C. R. *Science* **1991**, *251*, 1456-1464.

(25) Parker, J. S. L.; Murphy, W. J.; Wang, D.; O'Brien, S. J.; Parrish, C. R. *Journal of Virology* **2001**, *75*, 3896-3902.

(26) Speir, J. A.; Munshi, S.; Wang, G. J.; Baker, T. S.; Johnson, J. E. *Structure* **1995**, *3*, 63-78.

(27) Allen, M.; Bulte, J. W. M.; Liepold, L.; Basu, G.; Zywicke, H. A.; Frank, J. A.; Young, M.; Douglas, T. *Magnetic Resonance in Medicine* **2005**, *54*, 807-812.

(28) Anderson, E. A.; Isaacman, S.; Peabody, D. S.; Wang, E. Y.; Canary, J. W.; Kirshenbaum, K. *Nano Letters* **2006**, *6*, 1160-1164.

(29) Huang, X. L.; Bronstein, L. M.; Retrum, J.; Dufort, C.; Tsvetkova, I.; Aniagyei, S.; Stein, B.; Stucky, G.; McKenna, B.; Remmes, N.; Baxter, D.; Kao, C. C.; Dragnea, B. *Nano Letters* **2007**, *7*, 2407-2416.

(30) Tseng, R. J.; Tsai, C. L.; Ma, L. P.; Ouyang, J. Y. *Nature Nanotechnology* **2006**, *1*, 72-77.

(31) Trohalaki, S. *Mrs Bulletin* **2007**, *32*, 5-6.

(32) Portney, N. G.; Tseng, R. J.; Destito, G.; Strable, E.; Yang, Y.; Manchester, M.; Finn, M. G.; Ozkan, M. *Applied Physics Letters* **2007**, *90*.

(33) Kuncicky, D. M.; Naik, R. R.; Velev, O. D. *Small* **2006**, *2*, 1462-1466.

(34) http://virology.wisc.edu/cgi-bin/virusworld/htdocs.pl?docname=triangulation.html

CHAPTER 2

RED CLOVER NECROTIC MOSAIC VIRUS

2.1 Introduction to *Red clover necrotic mosaic virus*

Red clover necrotic mosaic virus (RCNMV) is a plant virus in the *Dianthovirus* genus, family *Tombusviridae*. RCNMV has moderately wide host range, which includes alfalfa, red, sweet and white clover[1]. RCNMV is a soil-borne virus that infects plants through the roots without a biological vector or through physical contact. The virus released from the root cells remains infective and stable for months in soil. When infected or inoculated, this virus causes mosaics and necrosis on the infected leaves as typical infection symptoms.

RCNMV is a monodisperse icosahedral virus with an outer diameter of 36 nm[2]. The virus capsid is made up of 180 chemically identical capsid subunits (37 kDa) arranged to form a T = 3 icosahedral symmetry. These capsid subunits consist of three different conformational proteins, referred as A, B and C. Each capsid subunit composed of three domains: RNA-interacting (R), shell (S), and protruding (P). The R domain contains basic residues that extend into the interior cavity to neutralize the RNA genome. The S domain, consists of two sets of four-stranded anti-parallel B sheet structures in a jellyroll conformation, forms the ~ 3 nm protein shell. The P domain of two subunits forms a protrusion that is ~ 3.7 nm above the protein shell. An inner cage with a diameter of 17 nm (T = 1) is present in the RCNMV capsid[3]. This structure is likely to consist of portions of virus RNA or interactions of RNA with the N-terminal of protein subunits.

The RCNMV genome consists of two single stranded RNAs: a 3.9 kb RNA-1, which encodes viral polymerase and capsid protein (CP), and a 1.5 kb RNA-2, which encodes the virus movement protein. A 34-nucleotide sequence on RNA-2, termed trans-activator (TA), forms a stem loop to base-pair with the 8-nucleotide of RNA-1, termed as trans-activator binding site (TABS). This RNA-1:RNA-2 complex allows the synthesis of subgenomic RNA (sgRNA) and further leads to the formation of capsid subunits[4]. Based on this result, the complex of RNA-1:RNA-2 has been proposed to function as the origin of assembly that initiates the self assembly of RCNMV capsid subunits to form virus particles. A second population of RCNMV with different packaging scheme of RNA

genome has also been reported. This population of virus consists of four copies of RNA-2, with a total RNA content of 5.8 kb per capsid[5].

Divalent ions are an integral part of the RCNMV structure with 390±30 Ca^{2+} and 420±25 Mg^{2+} per virus as determined by atomic absorption spectroscopy[3]. The Ca^{2+} ions are located at the capsid, while the Mg^{2+} ions are suggested to bind with virus RNA in the interior cavity of the capsid. The selective removal of Ca^{2+} alone results in minor reorientation of the CP shell (S) and protruding (P) domains. However, depletion of both divalent ions (Ca^{2+} and Mg^{2+}) induces significant conformational changes to the S and P domain that leads to formation of pores (11-13Å) within the capsid. The electrostatic-potential analysis indicated the presence of a cluster of positively charge residues at the outside of the pores, while negatively charged residues are predominately located at the inside of the pores. The formation of pores, together with the distribution of positively charged residues at the outside of pores, suggested a mechanism for the RNA genome to release from the interior cavity of RCNMV.

2.2 Research Overview

2.2.1 Encapsidation of nanoparticles by RCNMV capsid

As a T = 3 icosahedral virus, the RCNMV capsid has an outer diameter of 36 nm and an inner diameter of 17 nm. By pH and divalent ions adjustment, the capsid can be transformed from assembled to disassembled states. The natural ability of RCNMV protein subunits to assemble and disassemble can be exploited to package foreign cargo. With that goal in mind, experiments were designed to study the ability of RCNMV capsid to package nanoparticles.

Understanding the self-assembled mechanism of RCNMV in nature is driven by RNA-protein interaction, a complex of oligonucleotides, which mimics the origin of assembly (OAS) was conjugated to nanoparticles. Three different types of nanoparticles (diameter range 5-20nm) were studied which included Au, $CoFe_2O_4$, and quantum dots. The nanoparticle-OAS conjugate templates a self-assembly of RCNMV protein subunits to form virus-like particles (VLPs) with the nanoparticles encapsidated. Under these

conditions, the formation of VLPs produced particles that were similar in size to native and were stable to withstand magnetic or centrifugation purification. The attempts to encapsidate > 15 nm nanoparticles did not result in well-formed capsids. These results were consistent with the presence of a 17 nm cavity in native RCNMV.

As described in Chapter 1, the encapsulation of Au nanoparticles or quantum dots by BMV protein subunits was performed based on an RNA-independent manner. Here, a different approach was proposed to package nanoparticles by RCNMV protein subunits via a RNA-dependent manner. The requirement for specific RNA sequences offers a unique kind of control over the assembly process. This approach to VLP preparation is a straightforward method that can be applied to a wide range of starting materials, with an array of useful properties, to produce a uniform product.

2.2.2 Infusion of molecules into RCNMV capsid

The above experiments provide positive results, which demonstrate the ability of RCNMV capsid to function as a vessel for foreign cargo encapsidation. The next step is to further expand the versatility of RCNMV capsid to package smaller cargo/molecules. As described, depletion of divalent ions from the capsid results in formation of pores, which allows the inner cavity to be accessible. By the adjustment of the divalent ion concentrations, the opening and closing of surface pores can be exploited to load and unload molecules into the RCNMV capsid.

As an initial attempt, three different charged of dye molecules were studied for capsid infusion: Rhodamine (positive), Luminarosine (neutral) and Fluorescein (negative). Results indicated that the infusion mechanism is charge-dependent where positive and neutral charged molecules were feasible but the negatively charged molecule was not favorable to be infused into the capsid. Our understanding of this mechanism was then applied to package anticancer drug, Doxorubicin. Results indicated a loading density as high as ~1000 Doxorubicin per capsid can be achieved. Moreover, the Doxorubicin packaged within the capsid showed no leakage or diffusion through the opened pores. An i*n vitro* assembly of RCNMV capsid protein (CP) is an additional method that may be

used to encapsidate molecules. Here, an artificial OAS, just as described 2.2.1, was used to template the assembly of CP to form an enclosed protein cage and simultaneously package the dye molecules.

Most reported work, such as MS13 (described in Chapter 1), required genetically engineered to the capsid in order to package molecules. In contrary, this approach offers a direct and straightforward manner to package molecules without major alteration to the capsid.

2.2.3 Delivery of RCNMV-infused molecules into cancer cells

2.2.3.1 Adenovirus as a gene delivery vector

Due to the nature ability of a virus to target and transfer its genome into a cell nucleus, researchers are interested to exploit viruses as a potential tool in gene transfer applications. Several types of virus vectors which included adenovirus[6,7], adeno-associated virus[8], herpes virus[9] or lentivirus [10,11] have been studied extensively. Here, we will focus on adenovirus as a gene transfer vector. Specifically, we will focus on the cell-targeting ability of the adenovirus, which has been used as a model for targeting peptides attached to RCNMV.

Adenovirus, a non-enveloped icosahedral *ds*DNA virus with an outer diameter of 90 nm, causes infections to the respiratory tract, gastrointestinal tract and genitourinary tract. The capsid of an adenovirus composed of 252 capsomeres, 240 hexons and 12 pentons at the vertices (Figure 3). Each penton displays a fiber protein. There are approximately 52 human adenovirus serotypes that have been categorized into 6 subgroups (A-F) according to various properties such as the repeating motifs of the fiber protein[12]. In nature, an adenovirus binds its fiber protein to the cellular receptor called Coxsackie adenovirus receptor (CAR) for subgroup C adenoviruses[13] or CD46 for subgroup B adenoviruses[14]. A secondary interaction to promote internalization involves the penton base, which consists of Arg-Gly-Asp (RGD) sequences, with the integrins ($\alpha_v\beta_3$ or $\alpha_v\beta_5$) on the cell surface[15]. The cellular internalization occurs through receptor mediated endocytosis (RME) and forms a clathrin-coated pit, which further localizes in

the endosomes. Under acidic conditions (pH ~6), the adenovirus capsid has the ability to lyse the endosomal membrane. The attachment of integrin $\alpha_v\beta_5$ with the penton base protein, together with the low endosomal pH, facilitates the escape of adenovirus from the endosome[16]. In cytoplasm, the adenovirus binds with microtubules or molecular motors to facilitate the translocation to the nucleus membrane[17]. The nuclear membrane consists of pores that control the transport of macromolecules into and from the nucleus. Small ions and molecules (< 30 kDa) diffuse passively through the pores. Larger molecules require a nuclear localization signal (NLS) that is recognizes by nucleus transport protein, known as importin, to transport into nucleus. The NLS signal is recognizes by importin α, follows by importin β before reaching the nucleus membrane. The residues of 2-10 located at the amino terminus of an adenovirus fiber protein contain the nuclear localization signal (NLS)[18]. With the help from importins, the virus capsid docks at the nuclear membrane and releases the virus DNA into the nucleus[19].

An infection is initiated by the binding of the adenovirus fiber to the host cell receptor. Here, we focus on the attachment of subgroup B Ad11 to host cell CD46 receptor. The CD46 receptor, a membrane cofactor protein with molecular mass of 57-67 kDa, is a member of regulators of complement activation. One major function of the CD46 receptor is to serve as a cofactor for the plasma serine protease factor I, and mediates the cleavage of C3b and C4b[20]. The purpose of this function of the CD46 receptor is to protect the host cell from complement attack. The CD46 receptor is known to express in many tissues and relatively high in kidney[21], and in the airway and conjunctival epithelium[22]. The CD46 receptor contains four short consensus repeats, referred as SCR1-SCR4. The N-terminals of SCR1 and SCR2 have been reported to be the binding sites for subgroup B Ad 11 (Figure 4). The study by Persson et al. indicated that the conformation of CD46 is altered when the binding occurred where the SCR1 and SCR2 residues that were initially bended/ hidden are now exposed to bind with Ad11[23]. The interactions which involved van der Waals, hydrogen bonds as well salt bridge, together with the extensive contacts facilitate a tight binding between CD46 and the knob for a high efficiency of infection.

Adenovirus is an attractive tool to apply in gene transfer applications for the following reasons. It has the ability to infect a wide variety of dividing and non-dividing

cells. It is easy to mass produce. Adenovirus has the ability to accommodate up to 37 kb of foreign genetic material[24]. It is an advantage that the virus genome rarely integrates into the host chromosome[25]. One way to manipulate the usage of adenovirus is by modifying the virus genome in order to reduce virus gene expression level. To achieve this, the E1 and E3 regions of adenovirus, which is responsible for gene expression and virus replication respectively, were deleted. This class of adenovirus is being referred as first generation adenovirus vector. However, reports indicated that the first generation adenovirus vector induced significant toxicity *in vivo*, which leads to rapid clearance from the immune system[26,27].

An alternative approach to exploit the targeting by adenovirus for cell-targeting application was proposed by using synthetic peptides, which consist of RGD sequences or peptides that bind to CAR to mimic the internalization of an adenovirus. For instance, the conjugation of CAR peptide to an anti-CD40 antibody demonstrated an increased of internalization and gene expression in dendritic cells[28]. Moreover, a synthetic peptide with the RGD sequence conjugated with pDNA managed to induce cell entry via endocytosis as well as nucleus localization[29]. This approach can further be explored to facilitate the internalization of inorganic nanoparticles such as Au nanoparticles[30]. In the report, the Au nanoparticles coated with bovine serum albumin (BSA) was conjugated with peptides, which consist of nuclear localization signal (NLS) from adenovirus. After certain incubation period, the accumulations of Au nanoparticles were found in cytoplasm as well as in the nucleus of HeLa cells, suggested the ability of Au nanoparticles-conjugated NLS to escape the endosomes and pass through the nucleus pore complex.

Inspired by observations of targeting using gold nanoparticles, a similar approach is applied in my research project to induce intracellular uptake of a plant virus. Three synthetic peptides: CAR, CD46 and IBD, were conjugated on the exterior of RCNMV. The CAR and CD46 targeting peptides used here were derived from adenovirus to target Coxsackie adenoviral receptor and CD46 receptor, respectively. The IBD peptide consists of integrin binding domain and a group of lysine residues, which facilitate bindings to the integrin on cell surface. Our hypothesis is that these peptides will mimic the internalization of an adenovirus into cells and induce intracellular uptake of RCNMV.

2.2.3.2 RCNMV as a multifunctional tool to package, target and deliver molecules into cancer cells

The next goal was to study the potential of RCNMV to package, target and deliver molecules into cancer cells. The number of residues available on the outer surface of RCNMV creates a platform that can be functionalized with multiple targeting signals. The ability to modify the external surface with targeting signal, along with the packaging capacity, enables RCNMV capsid to perform as a multifunctional tool.

Initially, the capsid of RCNMV was conjugated with fluorescein-labeled targeting peptides (CAR-F, CD46-F and IBD-F). The peptides contained a terminal cysteine that was conjugated to the surface-exposed lysine residues on the RCNMV protein subunits by using succinimidyl-4-(*N*-maleimidomethyl)cyclohexane-1-carboxylate (SMCC) linker. The intracellular uptake of RCNMV-CD46 conjugates shown to have the highest extent of internalization in HeLa cells. Therefore, the CD46 peptide was chosen to deliver RCNMV-infused Rhodamine into HeLa cells. Flow cytometry results suggested a lag period between internalization and the released of Rhodamine. From here, we proceed to study the intracellular uptake of CD46 conjugated RCNMV-infused Doxorubicin in HeLa cells, as well as the effect on cell viability by using an ATP assay. An ATP assay measures the ATP production from viable cells by the addition of recombinant firefly luciferase and D-luciferin. These solutions react with ATP from the viable cells to emit lights (emission maximum at 560 nm), where the intensity can be measured and compared with the control sample.

The usage of plant viruses as a drug delivery vector has been studied extensively due to the ease of production, low toxicity and lack of replication in humans. In addition to all these properties, RCNMV has a built-in release mechanism for the drug. The sensitivity of RCNMV towards divalent ion concentrations acts as a switch to open and close surface pores. In the blood, where the calcium concentration is in the millimolar range, the capsid stays intact with the cargo packaged. Once inside a cell, the concentration of calcium is low which triggers the pores to open and release the cargo. This is a unique feature that CPMV or CCMV is lack of. The utilization of RCNMV

capsid as a multifunctional tool for therapeutic purposes demonstrated a new general drug delivery platform.

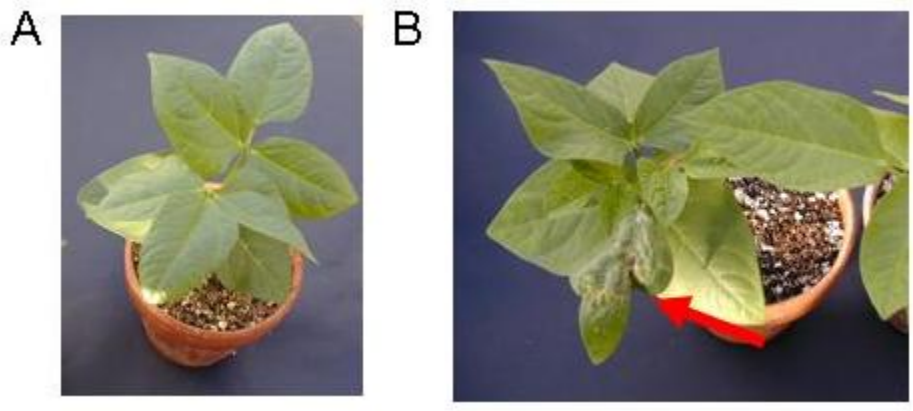

Figure 1.Comparison of a (A) healthy and (B) infected *Nicotiana benthamiana* plant. RCNMV cause necrotic lesions on infected leaves as typical infection symptom (arrow indicated).

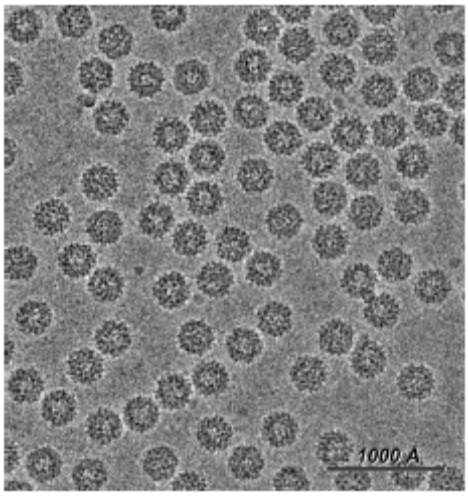

Figure 2. Cryoelectron micrograph of RCNMV. The average diameter of RCNMV is 36nm[3].

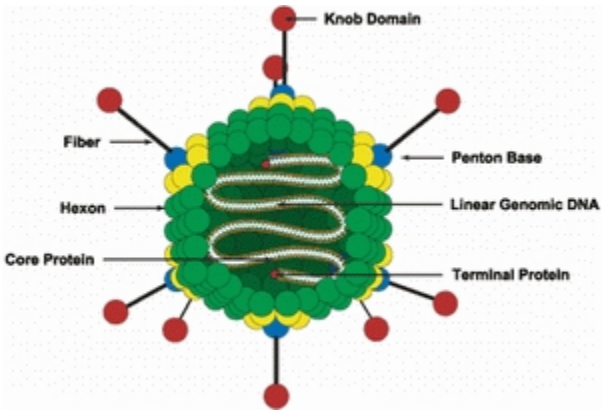

Figure 3.Adenovirus morphology. The capsid of an adenovirus, with an average diameter of 90 nm, composed of 252 capsomeres, 240 hexons and 12 pentons at the vertices. The knob on each penton base acts as a targeting signal and binds with cellular receptor.[32]

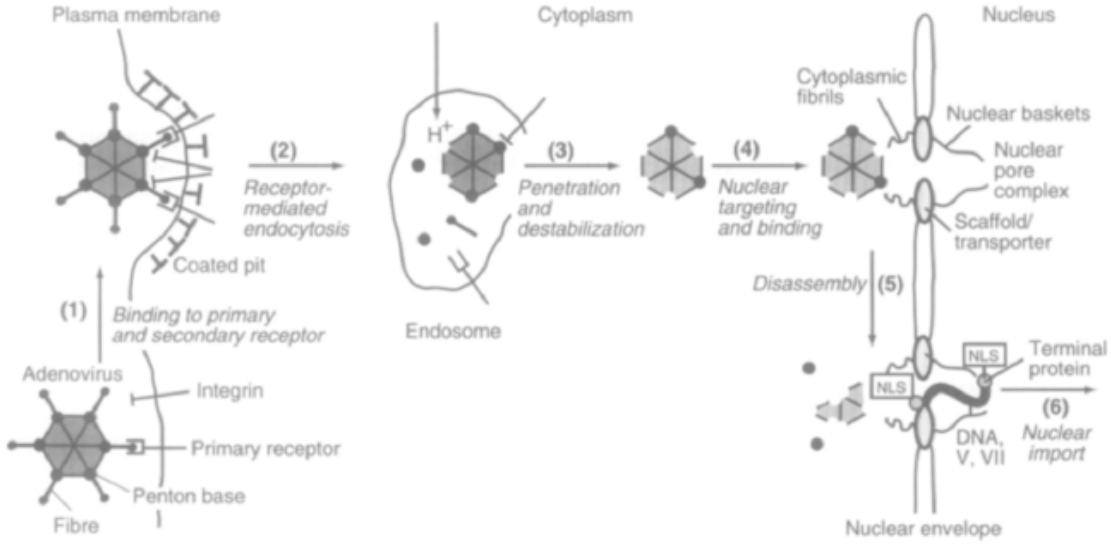

Figure 4 Schematic of cell entry of an adenovirus. (1) The fiber on the penton base binds to the cellular receptor. (2) A secondary interaction involves the penton base and the integirns on the cell; this interaction promotes endocytosis. (3) The low endosomal pH and the interaction with the integrins facilitate the escape of adenovirus from endosome. (4) The adenovirus transports to the nucleus through a nuclear localization sequence recognized by the nucleus transport protein, known as importins. (5) At the nucleus membrane, the DNA of adenovirus is delivered into the nucleus.[31]

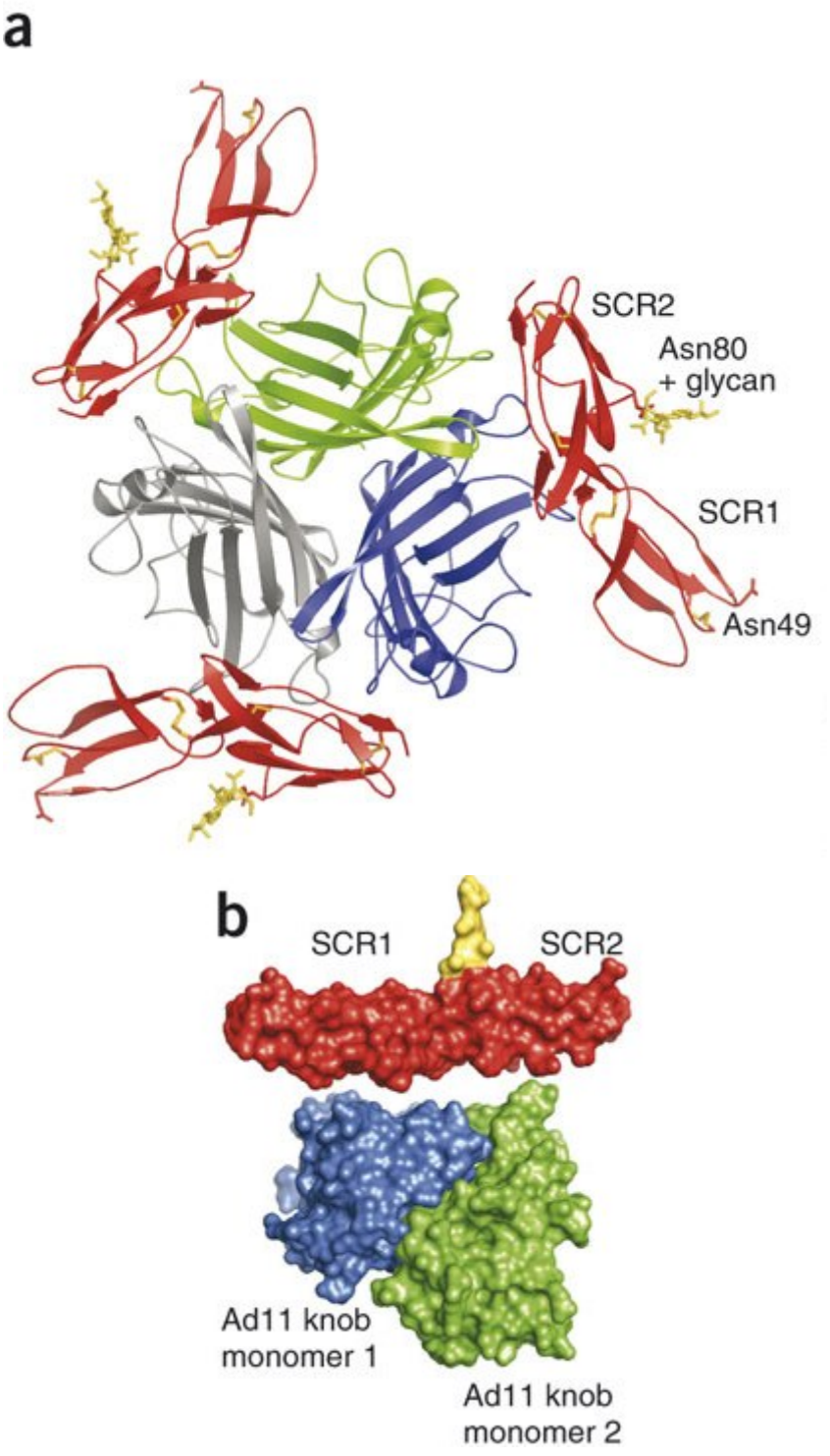

Figure 5 Binding of Ad 11 to CD46 receptor. (A) Ribbon drawing of the interaction. The trimer subunits of Ad11 are in green, blue and grey. SCR1 and SCR2 of C46 are in red. (B) Surface representation of the interaction[23].

References

(1) Hiruki, C. *Advances in Virus Research* **1987**, *33*, 257-300.

(2) Xiong, Z.; Lommel, S. A. *Virology* **1989**, *171*, 543-554.

(3) Sherman, M. B.; Guenther, R. H.; Tama, F.; Sit, T. L.; Brooks, C. L.; Mikhailov, A. M.; Orlova, E. V.; Baker, T. S.; Lommel, S. A. *Journal of Virology* **2006**, *80*, 10395-10406.

(4) Chan, W. C. W.; Nie, S. M. *Science* **1998**, *281*, 2016-2018.

(5) Basnayake, V. R.; Sit, T. L.; Lommel, S. A. *Virology* **2006**, *345*, 532-539.

(6) Ogawara, K.; Rots, M. G.; Kok, R. J.; Meijer, D. K. F.; Molema, G.; Haisma, H. J. *Molecular Therapy* **2004**, *9*, S251-S251.

(7) Stone, D.; Ni, S. H.; Li, Z. Y.; Gaggar, A.; DiPaolo, N.; Feng, Q. H.; Sandig, V.; Lieber, A. *Journal of Virology* **2005**, *79*, 5090-5104.

(8) Maheshri, N.; Koerber, J. T.; Kaspar, B. K.; Schaffer, D. V. *Nature Biotechnology* **2006**, *24*, 198-204.

(9) Burton, E. A.; Fink, D. J.; Glorioso, J. C. *Current Opinion in Molecular Therapeutics* **2005**, *7*, 326-336.

(10) Croyle, M. A.; Callahan, S. M.; Auricchio, A.; Schumer, G.; Linse, K. D.; Wilson, J. M.; Brunner, L. J.; Kobinger, G. P. *Journal of Virology* **2004**, *78*, 912-921.

(11) Bomsel, M. *Nature Medicine* **1997**, *3*, 42-47.

(12) van Raaij, M. J.; Mitraki, A.; Lavigne, G.; Cusack, S. *Nature* **1999**, *401*, 935-938.

(13) Bergelson, J. M.; Cunningham, J. A.; Droguett, G.; KurtJones, E. A.; Krithivas, A.; Hong, J. S.; Horwitz, M. S.; Crowell, R. L.; Finberg, R. W. *Science* **1997**, *275*, 1320-1323.

(14) Sirena, D.; Lilienfeld, B.; Eisenhut, M.; Kalin, S.; Boucke, K.; Beerli, R. R.; Vogt, L.; Ruedl, C.; Bachmann, M. F.; Greber, U. F.; Hemmi, S. *Journal of Virology* **2004**, *78*, 4454-4462.

(15) Wickham, T. J.; Mathias, P.; Cheresh, D. A.; Nemerow, G. R. *Cell* **1993**, *73*, 309-319.

(16) Wang, K.; Guan, T. L.; Cheresh, D. A.; Nemerow, G. R. *Journal of Virology* **2000**, *74*, 2731-2739.

(17) Leopold, P. L.; Ferris, B.; Grinberg, I.; Worgall, S.; Hackett, N. R.; Crystal, R. G. *Human Gene Therapy* **1998**, *9*, 367-378.

(18) Hong, J. S.; Engler, J. A. *Virology* **1991**, *185*, 758-767.

(19) Meier, O.; Greber, U. F. *Journal of Gene Medicine* **2004**, *6*, S152-S163.

(20) Segerman, A.; Atkinson, J. P.; Marttila, M.; Dennerquist, V.; Wadell, G.; Arnberg, N. *Journal of Virology* **2003**, *77*, 9183-9191.

(21) Nakanishi, I.; Moutabarrik, A.; Hara, T.; Hatanaka, M.; Hayashi, T.; Syouji, T.; Okada, N.; Kitamura, E.; Tsubakihara, Y.; Matsumoto, M.; Seya, T. *European Journal of Immunology* **1994**, *24*, 1529-1535.

(22) Sinn, P. L.; Williams, G.; Vongpunsawad, S.; Cattaneo, R.; McCray, P. B. *Journal of Virology* **2002**, *76*, 2403-2409.

(23) Persson, B. D.; Reiter, D. M.; Marttila, M.; Mei, Y. F.; Casasnovas, J. M.; Arnberg, N.; Stehle, T. *Nature Structural & Molecular Biology* **2007**, *14*, 164-166.

(24) Bett, A. J.; Prevec, L.; Graham, F. L. *Journal of Virology* **1993**, *67*, 5911-5921.

(25) Harui, A.; Suzuki, S.; Kochanek, S.; Mitani, K. *Journal of Virology* **1999**, *73*, 6141-6146.

(26) Gilgenkrantz, H.; Duboc, D.; Juillard, V.; Couton, D.; Pavirani, A.; Guillet, J. G.; Briand, P.; Kahn, A. *Human Gene Therapy* **1995**, *6*, 1265-1274.

(27) Yang, Y. P.; Su, Q.; Wilson, J. M. *Journal of Virology* **1996**, *70*, 7209-7212.

(28) Pereboev, A. V.; Asiedu, C. K.; Kawakami, Y.; Dong, S. S.; Blackwell, J. L.; Kashentseva, E. A.; Triozzi, P. L.; Aldrich, W. A.; Curiel, D. T.; Thomas, J. M.; Dmitriev, I. P. *Gene Therapy* **2002**, *9*, 1189-1193.

(29) Colin, M.; Maurice, M.; Trugnan, G.; Kornprobst, M.; Harbottle, R. P.; Knight, A.; Cooper, R. G.; Miller, A. D.; Capeau, J.; Coutelle, C.; Brahimi-Horn, M. C. *Gene Therapy* **2000**, *7*, 139-152.

(30) Tkachenko, A. G.; Xie, H.; Liu, Y. L.; Coleman, D.; Ryan, J.; Glomm, W. R.; Shipton, M. K.; Franzen, S.; Feldheim, D. L. *Bioconjugate Chemistry* **2004**, *15*, 482-490.

(31) Greber, U. F.; Kasamatsu, H. *Trends in Cell Biology* **1996**, *6*, 189-195.

(32) www.krackeler.com/products/fid/2862

CHAPTER 3

Encapsidation of Nanoparticles by *Red clover necrotic mosaic virus*

Abstract

Icosahedral virus capsids demonstrate a high degree of selectivity in packaging cognate nucleic acid genome components during virion assembly. The 36 nm icosahedral plant virus Red clover necrotic mosaic virus (RCNMV) packages its two genomic ssRNAs via a specific capsid protein (CP) genomic RNA interaction. A 20-nucleotide hairpin structure within the genomic RNA-2 hybridizes with RNA-1 to form a bimolecular complex, which is the origin of assembly (OAS) in RCNMV that selectively recruits and orients CP subunits initiating virion assembly. In this report, an oligonucleotide mimic of the OAS sequence was attached to Au, CoFe2O4, and CdSe nanoparticles ranging from 3-15 nm, followed by addition of RNA-1 to form a synthetic OAS to direct the virion-like assembly by RCNMV CP. Dynamic Light Scattering (DLS) and Transmission Electron Microscopy (TEM) measurements were consistent with the formation of virus-like particles (VLPs) comparable in size to native RCNMV. Attempts to encapsidate nanoparticles with diameters larger than 17 nm did not result in well-formed viral capsids. These results are consistent with the presence of a 17 nm cavity in native RCNMV. Covalent linkage of the OAS to nanoparticles directs RNA-dependent encapsidation and demonstrates that foreign cargo can be packaged into RCNMV virions. The flexibility of the RCNMV CP to encapsidate different materials, as long as it is within encapsidation constraint, is a critical factor to be considered as a drug delivery and diagnostic vehicle in biomedical applications.

3.1 Introduction

Nanoparticles with useful optical and magnetic properties have been widely investigated as tools for biomedicine. The addition of biomolecules on the surface provides a method to create a multifunctional nanoparticle that is capable of cell-specific targeting and diagnostic applications. For instance, magnetic nanoparticles functionalized with tumor-targeting molecules, chlorotoxin (Cltx), are able to target a specific site for magnetic resonance imaging.[1] Quantum dots conjugated with Immunoglobulin (IgG) and streptavidin were studied to label cancer cells.[2] Gold nanoparticles conjugated with oligonucleotides were utilized as intracellular vectors for the control of protein expression.[3] The ability of protein to behave as a stabilizer or targeting vector is dependent on the organization of the protein structure on nanoparticles, which is often difficult to control. Thus, it is desirable to find alternative strategies that increase the control over surface chemistry and provide greater control based on self-assembly properties. Generally, surfactants and polymers have been used to increase particle stability and proteins have been used to provide targeting capability. For example, the poor water solubility of quantum dots is overcome by using surfactants such as mercaptoalkanoic acids[4] or encapsulation by block copolymers.[5] Synthetic polymers such as polyvinyl alcohol (PVA)[6] were also studied as a coating agent to stabilize magnetic nanoparticles. Polyethylene glycol[7] was used to prepare stable gold nanoparticle suspensions for targeting applications. Proteins such as bovine serum albumin (BSA)[8,9] and streptavidin[10] have long been used on nanoparticles to provide multiple attachment sites for targeting peptides. However, it is difficult to determine the number of proteins associated with the nanoparticle surface.

Viruses are natural protein cages with multiple functions. Their size, load capacity, structural organization and self-assembly are desired characteristics that hold great promise for biomedical applications. Studies have demonstrated that the capsid of *Cowpea chlorotic mottle virus* (CCMV) devoid of its genome offers a constrained system that can be exploited as a container and provide protection for an encapsulated cargo.[11,12] Genetically engineered CCMV protein subunit exhibits a different charge environment

inside the capsid to encapsulate a range of drugs and nanoparticles.[13] In addition, the outer surfaces of viruses present a platform that can be chemically modified to display peptides, oligonucleotides, fluorescent labels or nanoparticles.[13-20] The attachment of artificial epitopes for antigen presentation[21] or nanoparticle magnetic resonance imaging contrast agents[22] on the virus protein surface enables it to function as a medical diagnostic tool. Furthermore, the ability of a virus to selectively target cells can be applied for diagnostic or cell-specific targeting applications. For instance, the adenoviral receptor-mediated endocytosis (RME) and nuclear localization signals (NLS) are virus-derived peptides that have been used as the most potent targeting agents.[23,24]

Red clover necrotic mosaic virus (RCNMV), a plant virus in the Dianthovirus genus, family Tombusviridae consists of 180 identical protein subunits (37 kDa) arranged to form a T = 3 icosahedral virion with an outer diameter of 36 nm and an inner cavity of ~17 nm.[25] The RCNMV genome consists of two single stranded RNAs: a 3.9 kb RNA-1, which encodes viral polymerase and capsid protein (CP), and a 1.5 kb RNA-2, which encodes the virus movement protein.[26] The RCNMV virion structure has been determined to 8Å resolution by cryo-electron microscopy.[25] The bulk of the genomic RNA forms a T = 1 inner cage, with a diameter of 17 nm, within the protein capsid.[25] Like many other T = 3 viruses,[27] assembly of RCNMV is initiated by recognition of CP by a bimolecular RNA structure, known as the origin of assembly (OAS), which further leads to assembly of the CP into a capsid. The requirement for an RNA-RNA interaction prior to assembly of the CP provides a scaffold to create a well-characterized nanoparticle structures.

Recently, we have demonstrated a new principle for nanoparticle nano-scale self-assembly.[28] Nanoparticles were tethered with an artificial RCNMV OAS, which consists of a 20-base deoxyuridine-modified DNA oligonucleotide, which is the analog of the RNA-2 stem loop (5'-AGAGGUAUCGCCCCGCCUCU-3'). The sequence called DNA-2 hybridizes with full length RNA-1 to form a functional artificial OAS. The artificial OAS templates the assembly of RCNMV CP to form an enclosed protein cage (Scheme 1). The preparation of virus-like particle (VLP) with internal metallic cores is not unique to RCNMV. Since the initial report of capturing nanoparticles by self assembly of CCMV in the presence of mineralized cores,[12] more efficient and diverse methods have been developed. Encapsulation of Au nanoparticles[29,30] and quantum dots[31] within the

Brome mosaic virus (BMV) protein shell independent of RNA have been demonstrated. Internalization of nanoparticles in VLPs can be prepared using the capsids as natural reactors for scaffold synthesis.[32-34] The inner surface of viral capsids that formed in the absence of RNA can also be exploited as a scaffold for the synthesize of inorganic materials.[11,12] Through a pH-dependent gating mechanism, the protein shell of CCMV swells and allows molecules to diffuse into the interior cage of the virion through the opening of surface pores. The available evidence suggests that the CCMV protein shell maintains its integrity throughout the process. A more controlled assembly approach to encapsidate nanoparticles by virus protein shell was reported using synthetic DNA nucleotide sequence to mimic the high affinity capsid binding site of native RNA in BMV.[35]

In the present study we elucidated this method to Au nanoparticles, magnetic nanoparticles and quantum dots. The main objective of this paper is to demonstrate that nanoparticles can be encapsidated by coat protein via a RNA-dependent manner, as opposed to previous studies that utilized an RNA-independent interaction for encapsulation of nanoparticles.

3.2 Materials and Methods

Nanoparticles and Quantum Dots

5, 10, 15 and 20 nm Au nanoparticles were purchased from Ted Pella Inc. Bis(p-sulfonatophenyl)phenylphosphine dihydrate (BSPP) was used as received from Strem Chemicals. Reagents to synthesize cobalt iron oxide, CoFe2O4 nanoparticles, which included CoCl2.6H2O, FeCl2.4H2O and methylamine, were obtained from Aldrich. Mercaptopropionic acid coated-quantum dots (MPA-Qds) was received as a gift from Applied Biosystem, Inc. ~1 mg of Qds was dissolved in 1 ml solution of 4-(dimethylamino-pyridine)(DMAP) in N,N-dimethylformamide (DMF) (20 mg of DMAP in 1 ml of DMF).

RCNMV coat protein (CP)

The source of free CP for this study was obtained from purified wild-type RCNMV virus. Virus was cultured in Nicotiana clevelandii that, at the time of inoculation, were 4-6 weeks old. Plants were initially infected by rub inoculation with infectious RCNMV full-length RNA transcripts while subsequent infections were propagated by sap transmission from the infected tissue from the primary plant. Infected plants were maintained in a temperature controlled glasshouse at 18-26 oC. Viruses were harvested from plants 7-10 days post inoculation. Purified CP of RCNMV was obtained by disruption of wild type RCNMV at pH > 9 in the presence of EDTA that removed stabilizing divalent ions. The virus RNA was separated from CP by a LiCl precipitation step. The liberated CP was purified from undisrupted virus using a 100 kDa molecular weight cutoff purification membrane.

RCNMV RNA-1

Full-length RCNMV RNA-1 used for encapsidation was obtained by transcription from a Sma1 linearized plasmid vector in which the bacteriophage T7 RNA polymerase promoter was fused to full-length RCNMV cDNA clones. The virus RNA was isolated from excess nucleotide triphosphates in the transcription reaction by ethanol precipitation.

***In vitro* assembly of RCNMV capsid protein (CP)**

20 µl of RCNMV CP (0.5 mg/ml) was brought up to a total volume of 100 µl with Glycine-NaOH, pH 10. For the analysis of the pH effect on in vitro assembly, the RCNMV CP solution is dialyzed, using Slide-A-Lyzer Dialysis Cassette (10 kDa molecular weight cutoff) against 50 mM Tris buffer at 3 different pHs (5.5, 6.0 and 6.5) for overnight at room temperature. The assembled VLPs formed at each pH is collected and analyzed by DLS.

Preparation of DNA conjugated nanoparticles

The 5'-thiol deoxyuridine modified DNA oligonucleotide, DNA-2, with the sequence (SH-5'- AGAGGUAUCGCCCCGCCUCU-3') was synthesized by MWG Biotech. In order to deprotect the thiol group, 1 ml of 100 mM solution of dithiothreitol (DTT) was

added to the DNA-2. This mixture was allowed to react for 30 minutes at room temperature. Excess DTT was removed using a Micro Bio-Spin P-30 (Biorad).

DNA: Au Conjugates Au nanoparticles coated with BSPP were synthesized as described.[36] A 1:300 mole ratio of Au nanoparticles to DNA-2 were incubated at 37 oC for 8 hours in 100 µl of 10 mM phosphate buffer, pH 7. The mixture was then brought up to 500 µl with 0.1 M NaCl/10 mM phosphate buffer, pH 7 and incubated for an additional 40 hours. Unattached DNA was removed by centrifugation at 14,000 rpm for 25 minutes. The supernatant, which consists of the unreacted DNA, was removed followed by dispersed of the precipitation in 500 ul of 10 mM phosphate buffer, pH 7 and re-centrifuged. This step was repeated twice. The DNA/Au conjugates were then resuspended in 10 mM phosphate buffer, pH 7.

DNA: $CoFe_2O_4$ synthesis and conjugation $CoFe_2O_4$ nanoparticles with mean sizes of 4, 10, and 15 nm were synthesized as described.[37] Transmission electron microscopy (TEM) and dynamic light scattering (DLS) analysis of the nanoparticles confirmed a size variation of < 30% in each batch. 10 mg of $CoFe_2O_4$ nanoparticles were added with 50 µl of DNA-2 (96 µM). The solution was allowed to stir overnight at room temperature. DNA/ $CoFe_2O_4$ conjugates were collected with a magnetic bar and washed with 50 % ethanol three times to remove unreacted DNA-2.

DNA: Quantum dot Conjugates Mercaptopropionic acid coated-quantum dots (MPA-Qds) were combined with DNA-2 in a mole ratio of 1:40. The mixture was incubated in 37 oC water bath for 12 hours. The solution was brought up to 500 µl with 0.1 M NaCl/10 mM phosphate buffer, pH 7 and incubated at 37 oC for an additional 12 hours. Unreacted DNA-2 was removed by passing the reaction mixture through a Microcon YM30 membrane.[38]

Encapsidation of nanoparticles into VLPs

DNA/nanoparticle conjugates were added with 1 µl of T7 RCNMV RNA-1 transcripts (4 mg/ml). This mixture was allowed to incubate for 10 minutes, followed by the addition of 5 µl of purified RCNMV CP (10 mg/ml) harvested from wild-type virus reared in *Nicotiana clevelandii* plants. Encapsidation reactions were carried out by dialyzed the sample against 50 mM Tris-HCl, pH 5.5 overnight at room temperature, using a Slide-A-

Lyzer Dialysis Cassette (10 kDa molecular weight cutoff). VLPs encapsidated nanoparticles were isolated by ultra centrifugation through a sucrose cushion at 218,000 g for 20 minutes in a SW-55 rotor with a model L8-70 Beckman ultracentrifuge.

Optical characterization of VLPs encapsidated nanoparticle

UV-vis absorption spectra were carried out on a Hewlett-Packard HP8453 diode array absorption spectrophotometer. TEM images were acquired using a (Philips) CM12 electron microscope operating at 100 kV accelerating voltage located at University of North Carolina, School of Dentistry, Chapel Hill, NC. Images were created with a Gatan 780 DualView camera system. All TEM samples, unless otherwise noted, were negatively stained with 2 % uranyl acetate to enhance image contrast. Samples were prepared by placing 10 μl of VLPs encapsidated nanoparticles solution onto a carbon-coated grid and stained with 2 % uranyl acetate. Excess liquid was blotted and the grid was allowed to dry. Digital Micrograph software was used to measure the diameters of the virus-like particles and inner cores from the TEM images. High resolution TEM and electron diffraction pattern images were recorded with a JEOL 2010F TEM, operating at 200 kV accelerating voltage from the Department of Materials Science and Engineering, North Carolina State University. DLS data were collected on a Malvern Zetasizer 1000HS spectrometer. The scattering data was best fit using the Contin algorithm.

3.3 Results

Characterization of the *in vitro* assembly of RCNMV capsid protein (CP)

The *in vitro* assembly properties of the CP were investigated to determine the suitability of RCNMV CP to encapsidate nanoparticles. The reassembly of CP isolated from RCNMV virus in the absence of genomic RNA was determined at pHs 5.5, 6.0, and 6.5. These capsids devoid of RNA are considered empty capsids. The apparent diameter of the empty capsids measured using DLS at three pH values is given in Table 1. Comparing the diameter of particles formed under these pHs, empty particles formed at pH 5.5 observed to have the diameter closest to the native RCNMV. Further analysis by TEM

indicated that VLP devoid of the virus genome formed at this pH observed to have different morphologies (Figure 1) and were unable to withstand centrifugation. From these data we conclude (1) that pH 5.5 is chosen for subsequent encapsidation experiments, since this pH yields particle with the closest diameter to the native RCNMV and (2) VLPs devoid of the virus genome have a diameter of ~30 nm with a different morphology. The formation of smaller than native VLP was also shown for *Southern bean mosaic virus*[39] where the CP was found to form T = 1 particles when placed in favorable conditions in the absence of virus RNA.

Characterization of the *in vitro* properties of the synthetic OAS element

The synthetic DNA-2 must hybridize with RNA-1 in order to function as a synthetic OAS. The OAS of RCNMV comprised of two regions of the virusl genome that interact to form a pseudoknot-like structural complex.[40] Two experiments were performed to determine whether DNA-2 forms a similar complex. First the thermodynamic properties of the synthetic DNA-2 were determined by UV monitored thermal denaturation. Analysis of the thermodynamic parameters reveals that the synthetic DNA-2 contains two stable conformations (Table 2). The duplex form is observed in the millimolar range of DNA-2 concentration, particularly at high NaCl concentration. However, the hairpin conformation has the largest population at low concentration. Thus, hairpin formation is dominant at the low concentration (nM) of DNA-2 used in the encapsidation experiment. The observed melt temperatures, T_m, are consistent with the existence of a hairpin as the dominant form (Table 2). The table also includes the theoretical T_m for both the duplex and hairpin.[41]. Duplex formation was observed in NMR spectra and UV melt profiles at mM and μM concentrations of DNA-2, respectively (data not shown).

The ability of the synthetic DNA-2 to bind to RNA-1, as shown in Figure 2A, was studied by a band shift assay. It has previously been shown that the native OAS comprised of a bimolecular complex RNA-2 with short oligonucleotide analogs of RNA-1 *in vitro* [42]. The interaction of DNA-2 (20-mer) with RNA-1(8-mer oligonucleotide) was observed using a band shift assay shown in Figure 2B. The apparent association constant

was similar for both the artificial OAS (DNA-2/RNA-1) and the native OAS (RNA-2/RNA-1).[40]

Encapsidation of 5, 10, and 15 nm Au nanoparticles

Given that RCNMV CP will self-assemble to produce different sizes and morphologies of VLPs under a range of conditions, experiments were performed to determine if nanoparticles would act as nucleating cores for CP self-assembly. Scheme 1 shows the following steps: A.) DNA-2 was tethered to Au nanoparticles using conditions that limit the oligomers bound per particle B.) transcript RNA-1 added to DNA-conjugated Au and the sample was incubated for 10 minutes. This incubation period allowed the RNA-1 to covalently attach to the complementary sequences on the modified oligonucleotides. C.) RCNMV CP was then added to the mixture. Particle assembly was initiated by dialyzed the sample against 50 mM Tris-HCl, pH 5.5 overnight at room temperature. After purified through a 50% sucrose cushion centrifugation, TEM images showed VLPs consist of closed protein shell, with an electron dense inner core (Figure 3). The purified VLPs were homogenous in size with an average diameter of 33.5±3.0 nm (15-25 VLPs per grid square), 30.0±3.0 nm (5-10 VLPs per grid square) and 34.0±2.0 nm (30-50 VLPs per grid square), for encapsidation of 5, 10 and 15 nm Au respectively (Figure 4). The average sizes of the electron dense VLPs inner cores were consistent with the size of Au nanoparticles used in these encapsidation experiments (Table 3). The attempt to encapsidate a 20 nm Au nanoparticle yielded no VLPs even before purification procedure was employed. The lack of assembly around a 20 nm particle is consistent with an upper packaging constraint equaling the 17 nm cavity in wild-type virions. The failure to encapsidate a 20 nm Au nanoparticle provides additional evidence that 5, 10 and 15 nm Au nanoparticles were in fact encapsidated within RCNMV CP, since non-specific coating of a nanoparticle by CP does not rely on the size of Au nanoparticle.

The 50% sucrose cushion required to concentrate the VLPs encapsidated Au, compared to the 20% sucrose utilized in native virus purification, indicated the significant structural robustness of the VLPs. To further determine the difference in density, VLPs encapsidated Au was subjected to 20-50% sucrose gradient centrifugation

(Figure 5). The VLP encapsidated Au observed to sediment at lower band (heavier density) than the native RCNMV. The absorbance profile on fractionated sucrose gradient indicated that the highest value of absorbance for both protein (A_{280}nm) and Au (A_{520}nm) of VLP encapsidated Au was at fraction 1, equivalent to 50% sucrose. In comparison, native RCNMV was detected at fraction 8, which corresponded to 20% sucrose. Based on the refractive index measurements, density of VLP encapsidated Au was 1.2299 g/ml, compared to native RCNMV, which was 1.1368 g/ml.

The VLP encapsidated Au were subjected to a 2 % agarose gel electrophoresis (Figure 6). When compared to DNA modified Au and unmodified Au, a significant reduction in mobility was observed for Au after CP packaging, providing physical evidence of VLPs formation. Absorbance measurements showed that the plasmon resonance of encapsidated Au shifted to 530 nm as compared to 520 nm of Au before encapsidation (Figure 7). The red-shift of plasmon resonance was probably due to the increase of the refractive index in response to the protein layer.[43] Preliminary studies to characterize the encapsidated Au by selected area electron diffraction revealed that the characteristic rings matched with the known reflecting planes of f.c.c. Au. Moreover, analyses by HR-TEM indicated that lattice fringes were observed on Au encapsidated by VLP. The combination of electron diffraction and HR-TEM analyses indicated the composition of Au remained even after encapsidation by VLP (Figure 8).

The OAS attachment to Au nanoparticles was also characterized. VLP encapsidated Au nanoparticles were exposed to pH > 9 to induce structural disruption. Phenol extraction was performed to precipitate RNA-1. Based on the measured absorbance the ratio of RNA-1 to Au nanoparticle was determined to be 1:1 using the UV-vis extinction coefficient. This ratio is also consistent with the observed ratio of RNA-1 to CP. The A_{260}/A_{280} ratio of native RCNMV is 1.6. Based on the absorbance measurement, the ratio of DNA/RNA (A_{260}) to protein (A_{280}) of VLP is 1.43, which is approximately 10% lower than native virus as expected since the VLP consists of native RNA-1 (3.9 kb) and DNA-2, which is a sequence of only 20 nucleotides in place of native RNA-2, which is 1.5 kb.

Control experiments were conducted to determine the requirement for the presence of the RCNMV OAS for encapsidation. In the first control, the assembly was

conducted with 10 nm Au nanoparticles coated with bissulfonato(phenyl)phenylphosphine (BSPP) in the absence of RNA-1 or the DNA oligomer. While VLPs with encapsidated Au cores were observed by TEM prior to centrifugation (Figure 9), the pelleted fraction lacked them. The disintegration of the VLPs during centrifugation was likely due to a lack of structural integrity provided by an internal RNA/protein complex. A second control experiment was performed that utilized a random 20-nucleotide DNA oligomer attached to the Au nanoparticles. No VLPs were observed in the pelleted fraction after centrifugation. Finally, when a non-RCNMV RNA template was used in assembly reactions, no VLPs were obtained in the pelleted fraction. These results indicate the absolute requirement for the cognate RNA OAS to stabilize the encapsidation of the nanoparticle.

Encapsidation of 4, 10 and 15 nm $CoFe_2O_4$ nanoparticles

To further study the versatility of RCNMV CP as an agent for encapsidation the methods described above were applied to 4, 10, and 15 nm $CoFe_2O_4$ nanoparticles. Prior to VLP purification, TEM images indicated the presence of VLPs encapsidated $CoFe_2O_4$ nanoparticles, empty VLPs, minor aggregation of $CoFe_2O_4$ nanoparticles, as well as failed products ($CoFe_2O_4$ nanoparticles that were not fully covered by CP)(Figure 10). Following the initial mixing, the sample was collected and concentrated using a magnetic bar to separate VLPs encapsidated $CoFe_2O_4$ nanoparticles from excess CP and empty VLPs. The sample was further purified through a 30 % sucrose cushion by ultra-centrifugation to remove aggregated $CoFe_2O_4$ nanoparticle and other failed products. Figure 11 are TEM images of VLPs encapsidated $CoFe_2O_4$ purified by magnetic concentration and centrifugation. A negative stain of the sample showed the presence of the intact protein shell encapsidated $CoFe_2O_4$ nanoparticles. Encapsidation of a 4, 10 and 15 nm $CoFe_2O_4$ nanoparticle yield 33.1±2.2 nm (8-20 VLPs per grid square), 34.2±1.4 nm (9-13 VLPs per grid square) and 34.0±2.0 nm (40-55 VLPs per grid square) diameter VLPs, respectively. In an unstained sample, the measured inner cores were observed to be consistent with the diameter of the $CoFe_2O_4$ nanoparticles used in the assembly procedure (Table 3). The attempts to encapsidate nanoparticles > 15 nm in diameter led

to formation of unstable particles that did not withstand purification by sucrose cushion centrifugation, which is consistent with the results obtained when the encapsidation experiment was performed on 20 nm Au nanoparticles.

Characterization of encapsidated $CoFe_2O_4$ performed by XPS indicated that the spectra for Co 2p and Fe 2p of $CoFe_2O_4$ nanoparticles before and after encapsidation by VLP showed similar group of peaks (Figure 12). The Co $2p_{3/2}$ peak from $CoFe_2O_4$ encapsidated by VLP (binding energy of 772.49 eV) observed to match the binding energy of Co $2p_{3/2}$ for $CoFe_2O_4$ nanoparticles before encapsidation. Similar observation was also reported for Fe 2p, where the peak corresponded to Fe $2p_{3/2}$ (binding energy of 704.89 eV) for $CoFe_2O_4$ nanoparticles before encapsidation coincided with Fe $2p_{3/2}$ for $CoFe_2O_4$ encapsidated by VLP.

DLS analysis of VLPs encapsidated 10 nm $CoFe_2O_4$ nanoparticles indicated that VLP exhibited pH-dependent swelling comparable to native RCNMV (Figure 13). When exposed to pH 8, the diameter of VLPs increased from 33.5 ± 3.0 to 54.2 ± 3.0 nm. At pH > 9, VLPs disassembled to release the encapsidated $CoFe_2O_4$ nanoparticles as indicated in Figure 12B. The lower peak (11.3 nm) corresponds to $CoFe_2O_4$ nanoparticles while the higher peak (81.0 nm) indicated the disrupted VLPs. These data also support the hypothesis that the $CoFe_2O_4$ nanoparticles were encapsidated within CP and not attached on the outer surface of the protein. If nanoparticles were attached on the outer protein shell, high pH VLP disruption would result in a single peak with the nanoparticles remained attached on disrupted CP.

Encapsidation of Quantum dots (Qds)

Encapsidation of quantum dots was carried out using procedures similar to those described above. Analysis of TEM images before purification indicated a large amount of empty particles and distorted VLP (Figure 14). After purification by centrifugation through a 50 % sucrose cushion these empty particles and distorted VLPs were not observed. When an identical sample was negatively stained, the protein cage remained intact and surrounded the interior core (Figure 14C). The VLPs (5-15 VLPs per grid square) were found to be homogenous in size with an average diameter of 31.6± 3.3 nm

and an electron-dense core with an average diameter of 4 nm, commensurate in size with the quantum dots. The remaining VLPs after isolation process indicated the high stability of the encapsidation of quantum dots by RCNMV CP. Preliminary studies on encapsidated Qds were performed based on fluorescence measurements. The emission wavelength of Qds encapsidated by VLP appeared to be shifted 1-2 nm as compared to the Qds before encapsidation (Figure 15). This result is consistent with the observation reported for Qds packaged by BMV where a shift of emission wavelength was also detected.[31]

3.4 Discussion

The present study demonstrates a novel method that utilizes the RCNMV OAS to direct self-assembly of virus CP that leads to encapsidation of nanoparticles within the protein shell. A functional 20-nucleotide deoxyuridine-modified DNA analog of the RNA-2 of OAS is attached to a nanoparticle and then base-paired through an 8-nucleotide complementary sequence in genomic RNA-1 (3.9 kb total length) to form the functional OAS. Nanoparticles presenting the OAS can nucleate the self-assembly of the capsid protein. The requirement of these elements for VLP formation is similar to the elements for native RNA dependent encapsidation of RCNMV. This method yields uniform sized of VLP, independent to the composites and sizes of cores used in this report. The average diameter of the VLP formed from the seven different cores tested, 32.8 nm, was only slightly less than that of the native virus at 36.6 nm. Attempts to encapsidate nanoparticles with diameters larger than 17 nm failed to yield well-formed VLPs. In other words, the critical limit for encapsidation of nanoparticles is < 17 nm. This observation is expected as structural studies indicate the inner cavity of the virus to be approximately 17 nm in diameter.[25]

A common aspect in the *in vitro* self assembly of icosahedral plant viruses is the use of pH to facilitate capsomere assembly.[44,45] A pH reduction likely ionizes the many charged residues characteristic of CP, resulting in protein-protein and RNA-protein

interactions that promote capsid assembly to form native-like particles.[46] For BMV, the balance of electrostatic charges can be achieved for the VLP encapsidation by coating the surface of of nanoparticles by DNA or PEG.[30,35] For RCNMV, the requirement for encapsidation of a nanoparticle to form VLP is dependent on the presence of two critical components: the OAS and a nucleating core of appropriate size. The absence of either one of these components either prevented formation of VLPs or generated VLPs that were significantly smaller than the native virion. The requirement for RNA to form stable VLP for tombusviridae suggested a different self-assembly mechanism may be involved as compared to bromoviridae.

The self-assembly design process and VLP formed in the present study may have advantages over other approaches. The requirement for a synthetic DNA element and an RNA scaffold affords a unique kind of control over the assembly process. This approach to VLP preparation is a straightforward method that can be applied to a wide range of starting materials, with an array of useful properties, to produce a uniform product. The sizes of VLP produced are significantly smaller than those reported for most other non-viral nanoparticle approaches.[47] While it is unclear if there is an optimal size for diagnostic and therapeutic nanoparticles, a VLP in the 30 nm range would be small enough to be delivered directly to the nucleus of mammalian cells by passing through the nuclear membrane pores. An additional advantage of this method is the ability of the particles to withstand magnetic or centrifugation purification demonstrates a structural integrity that is necessary to obtain usable quantities of material for any biomedical application. This protein surface of this VLP can also serves as a platform for peptide-conjugation, which further enhances the functionality of the particle. The VLPs obtained by the method reported here have advantages that can address problems associated with the use of nanoparticles in biomedical applications.

Acknowledgement SF acknowledges support through NIH grant NCI CA098194. We would like to thank Applied Biosystems, Inc. for providing the quantum dots used in this study. We thank Dr.Wallace Ambrose in the School of Dentistry at UNC for help with

TEM and Dr.Tim Sit for help with the RCNMV molecular biology. We thank Dr.Gerd Josef-Manfred Dusher for help with HR-TEM and electron diffraction of Au.

Table 1.DLS measurement of the mean hydrodynamic diameter (DH) of empty VLPs formed at various pH values.

pH	mean hydrodynamic diameter (D_H), nm
5.5	29.8±3.0
6.0	45.6±2.0
6.5	48.5±2.3 , 73.1±2.0

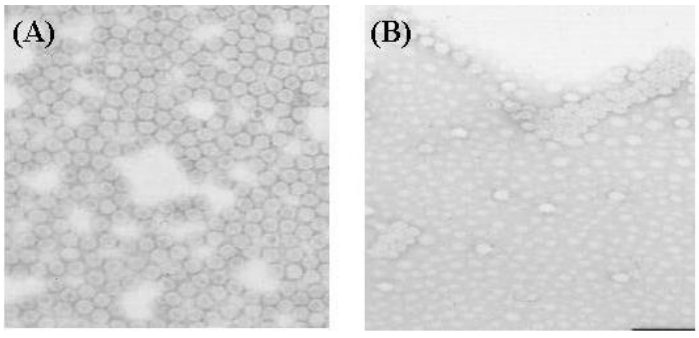

Figure 1.TEM image of (A) native RCNMV and (B) empty virus reassembled at pH 5.5. Average diameter of empty virus was 29.8±3 nm.

Table 2.Experimental and theoretical melting temperature, T_m (℃), of DNA-2 (20-mer) at three different concentrations.

Concentrations of DNA (μM)	Melting Temperature, T_m (℃)		
	Experimental	Theoretical	
		Duplex[41]	Hairpin[48]
0.2	43.5± 0.5	-6.5	43.5
2	45.2± 0.7	1.5	43.5
16	43.9±0.6	9.1	43.5

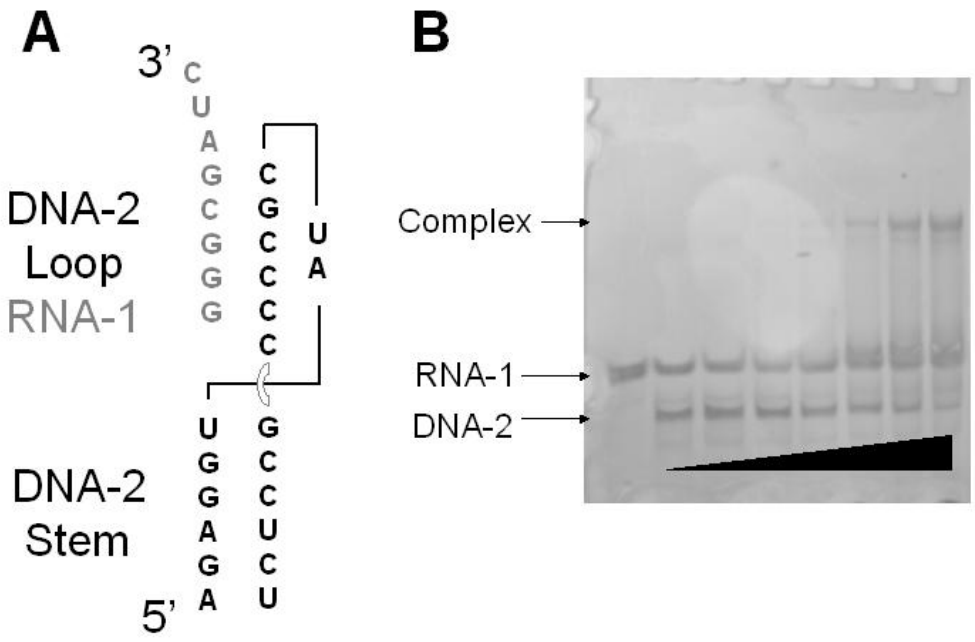

Figure 2.Characterizations of synthetic OAS. A) The sequences of DNA-2 and RNA-1 are depicted in the kissing loop complex that comprises a model for the OAS. B) Gel shift assay to measure the binding constant for interaction of the DNA-2 (20-mer) with the RNA-1 (8-mer oligonucleotide).

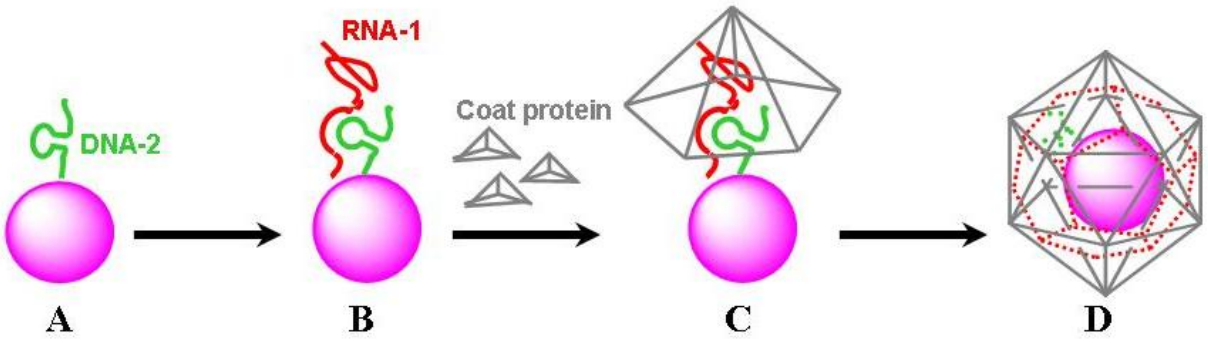

Scheme 1.Schematic of nanoparticles encapsidation by RCNMV coat protein. (A) Conjugation of nanoparticle with DNA-2 (B) Addition of RNA-1 interacts with DNA-2 to form the functional OAS (C) The artificial OAS templates the assembly of coat protein (D) Formation of virus-like particle with nanoparticle encapsidated.

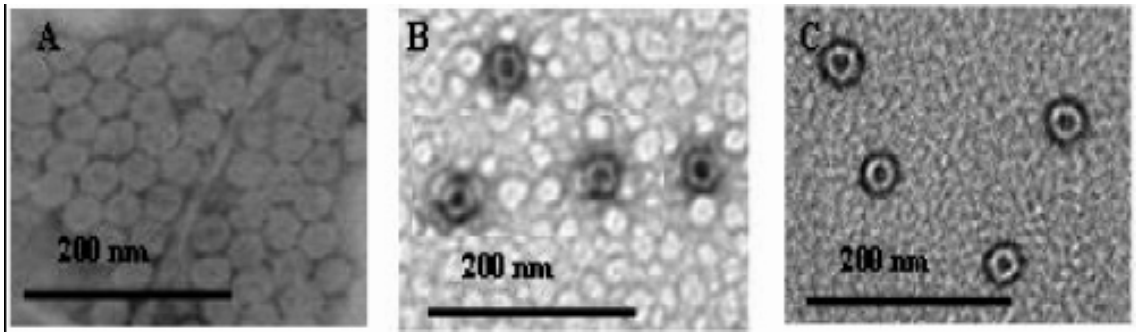

Figure 3.Encapsidation of 10nm Au nanoparticles by RCNMV CP. TEM images of (A) native RCNMV and encapsidation of 10 nm Au nanparticles within RCNMV CP (B) prior to and (C) after purification by sucrose centrifugation.

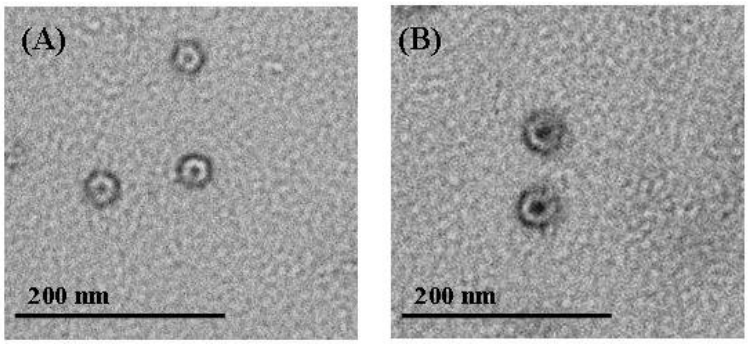

Figure 4.Encapsidation of 5 and 15 nm Au nanoparticles by RCNMV CP. TEM images of virus-like particles encapsidated (A) 5 nm and (B) 15 nm Au nanoparticles.

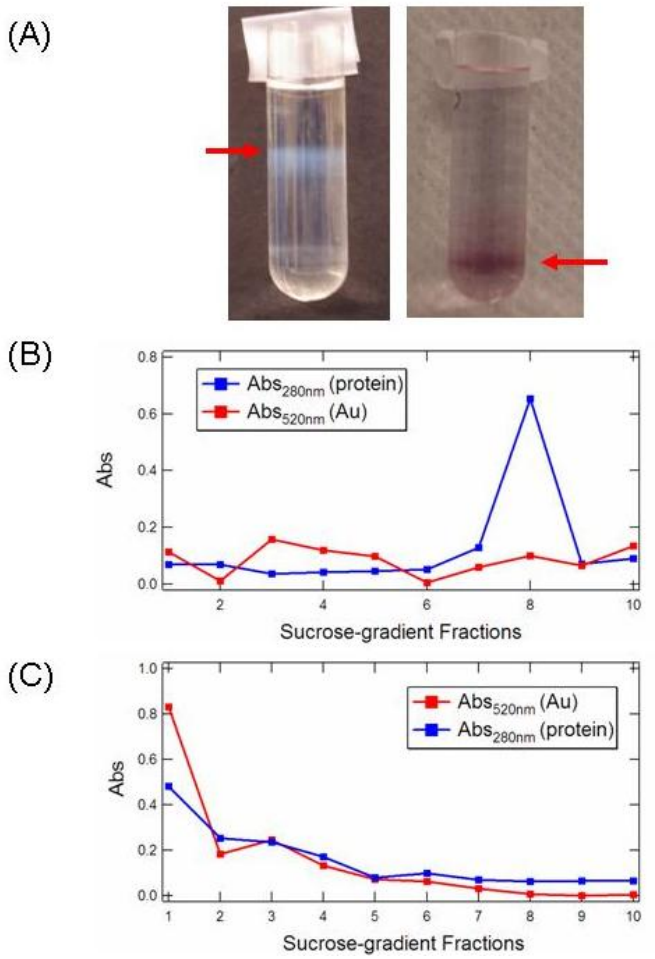

Figure 5.VLP encapsidated Au and native RCNMV subjected to 20-50 % sucrose gradient centrifugation. (A) Distribution profile of RCNMV (left) and VLP encapsidated Au (right) after centrifugation. Arrows indicate the samples sedimentation after centrifugation. Fractions collected from the bottom were measured with absorbance at 280nm and 520nm for protein and Au, respectively. Absorbance profile of each sucrose gradient fractions obtained from (B) RCNMV and (C) VLP encapsidated Au. Data are presented with the densest fractions on the left.

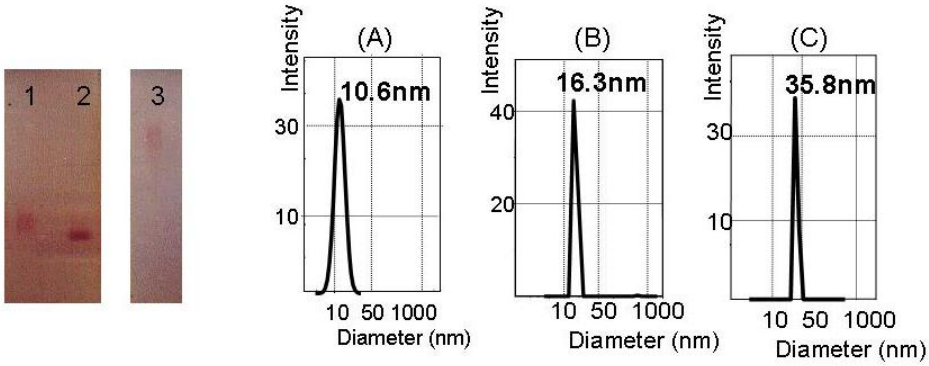

Figure 6.Characterization of VLP encapsidated 10 nm Au by a 2 % agarose gel electrophoresis and Dynamic Light Scattering. (Left) When compared to the mobility of Au conjugated with DNA-2 (Lane 1) and Au coated with Bis(p-sulfonatophenyl)phenylphosphine dihydrate (BSPP) (Lane 2), gel electrophoresis illustrated a significant reduction in mobility of the 10 nm Au nanoparticles after CP packaging (Lane 3) providing physical evidence of VLPs formation. (Right) Hydrodynamic radius, as determined by DLS, of (A) 10 nm Au coated with BSPP (B) Au conjugated with DNA-2 and (C) VLP encapsidated Au nanoparticles.

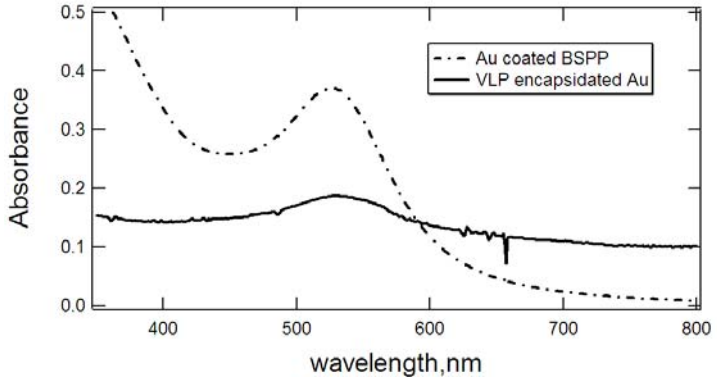

Figure 7.Comparison of the absorbance spectrums of Au coated with Bis(p-sulfonatophenyl)phenylphosphine dehydrate (BSPP) and Au encapsidated by VLP. The plasmon resonance of Au has shifted from 520 nm to 530 nm after encapsidated by VLP.

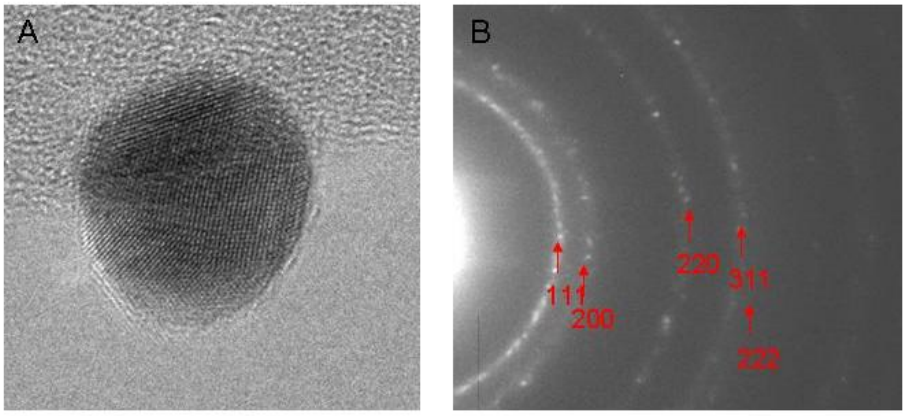

Figure 8.Characterization of VLP encapsidated 10 nm Au by electron diffraction and HR-TEM. (A) A representative high resolution TEM image showing lattice fringes of Au encapsidated by VLP. (B) Electron diffraction pattern of Au encapsidated by VLP. The diffraction pattern showed rings characteristic matched with the known reflecting planes of f.c.c Au.

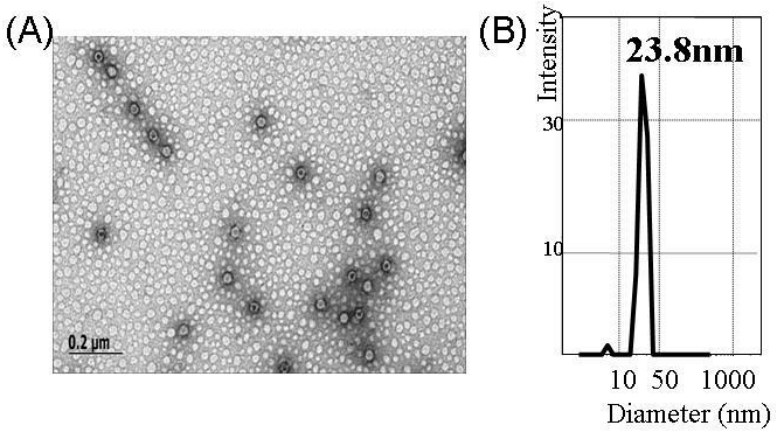

Figure 9.Encapsidation of a 10nm Au coated Bis(p-sulfonatophenyl)phenylphosphine dehydrate (BSPP) by RCNMV CP in the absence of OAS. (A) TEM image and (B) DLS of virus-like particles (VLP) encapsidated 10 nm Au coated BSPP prior to sucrose purification. The particles formed in the absence of OAS were not stable to withstand the purification.

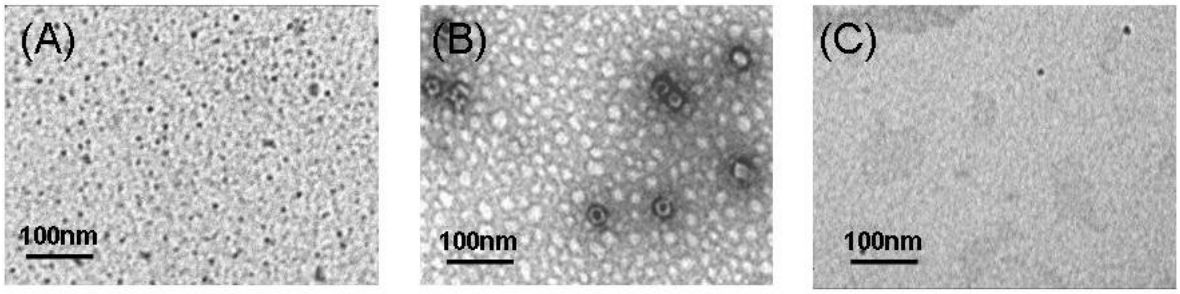

Figure 10.Encapsidation of 4 nm $CoFe_2O_4$ nanoparticles by RCNMV CP. TEM images of (A) 4 nm $CoFe_2O_4$ nanoparticles (B) negatively stained sample of VLP encapsidated 4 nm$CoFe_2O_4$ nanoparticles prior to purification and (C) unstained sample of VLP encapsidated 4 nm $CoFe_2O_4$ nanoparticles after purification.

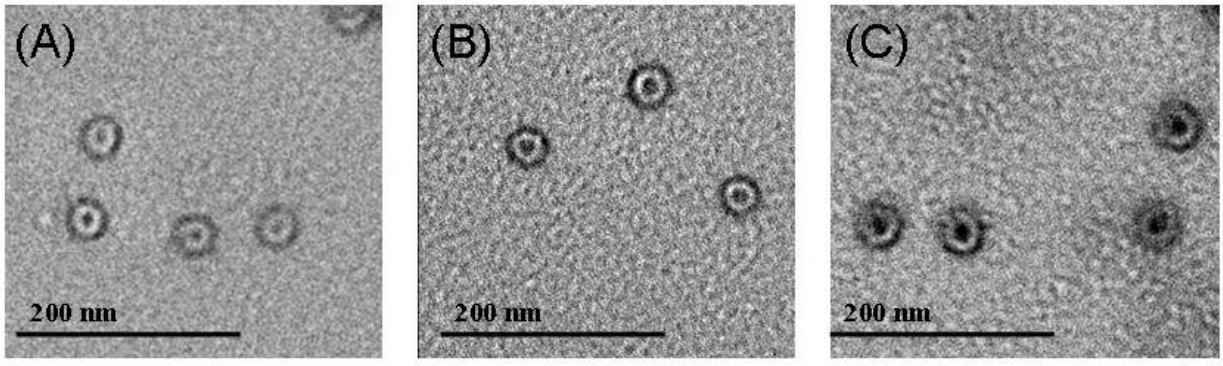

Figure 11.Encapsidation of 4, 10 and 15 nm $CoFe_2O_4$ nanoparticles by RCNMV CP. Negatively stained TEM images of VLP encapsidated (D) 4 nm $CoFe_2O_4$ (E) 10 nm $CoFe_2O_4$ and (F) 15 nm $CoFe_2O_4$ nanoparticles after purification.

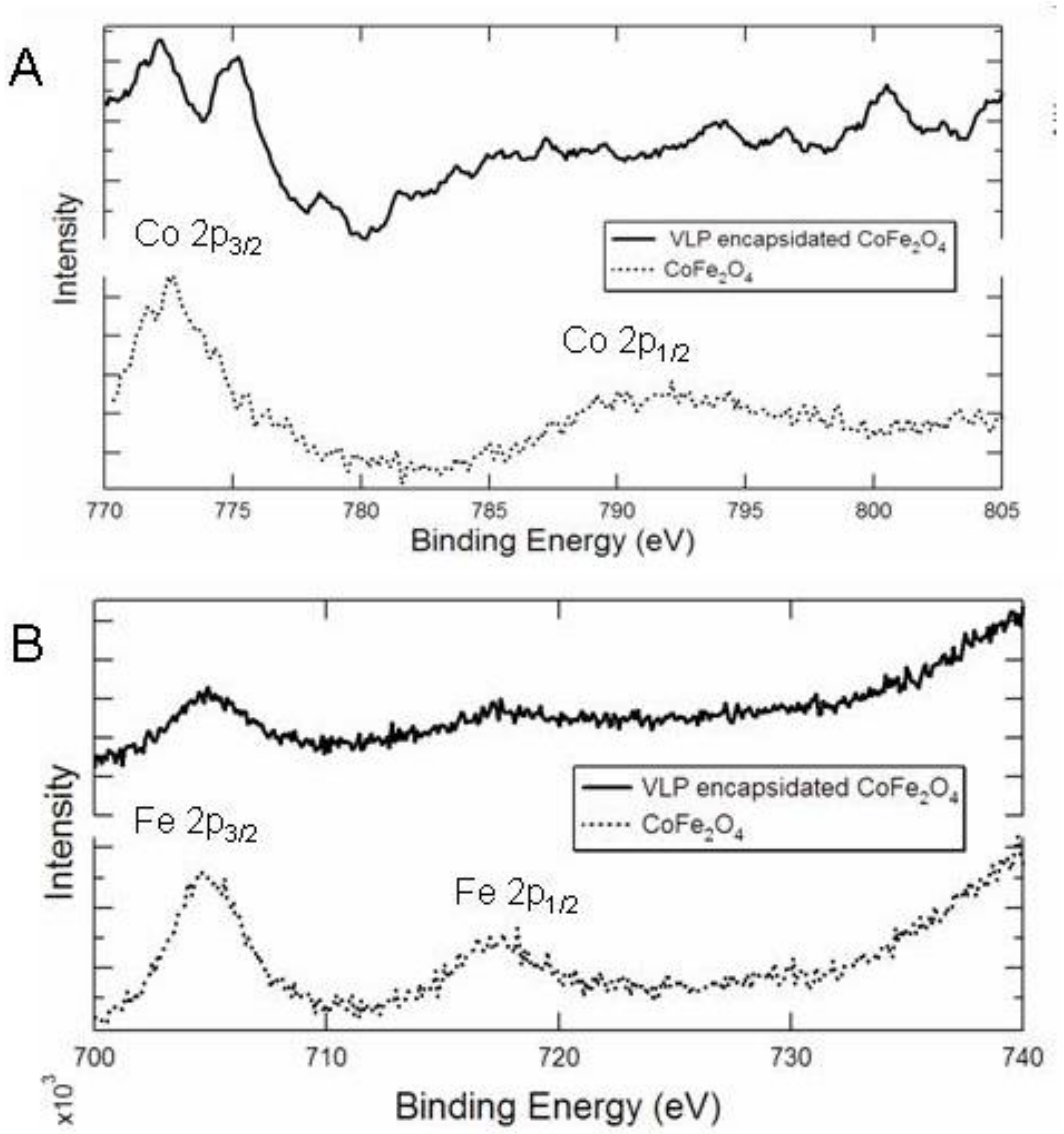

Figure 12.Characterization of VLP encapsidated 10 nm $CoFe_2O_4$ nanoparticles by XPS. XPS spectra of (A) Co and (B) Fe of $CoFe_2O_4$ nanoparticles before and after encapsidated by VLP.

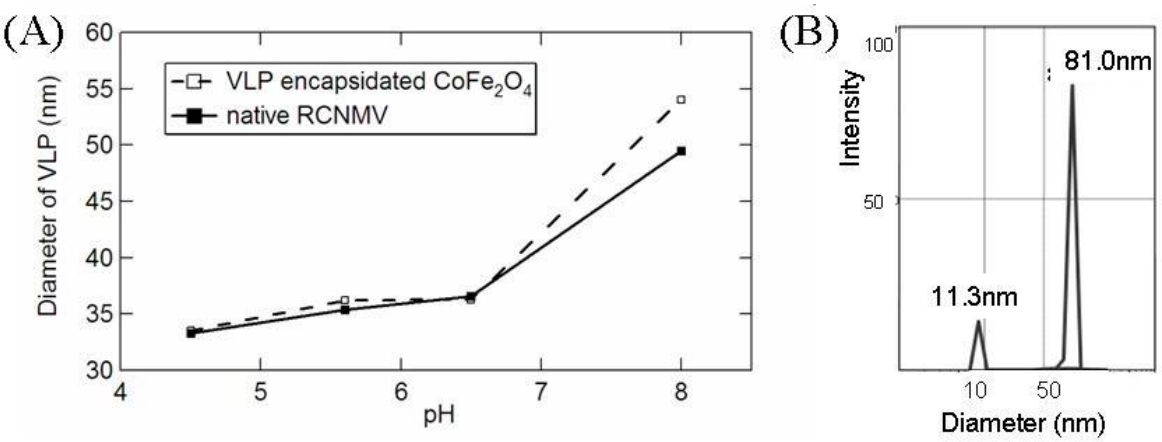

Figure 13.Characterization of VLP encapsidated 10 nm $CoFe_2O_4$ nanoparticles under various pH. (A) Hydrodynamic radius of native RCNMV and VLP encapsidated 10 nm $CoFe_2O_4$ in the range of pH 4.5 to 8 as determined by DLS. (B) DLS of VLP encapsidated 10 nm $CoFe_2O_4$ at pH> 9. Structural disruption of VLP indicated the released of encapsidated $CoFe_2O_4$ nanoparticles.

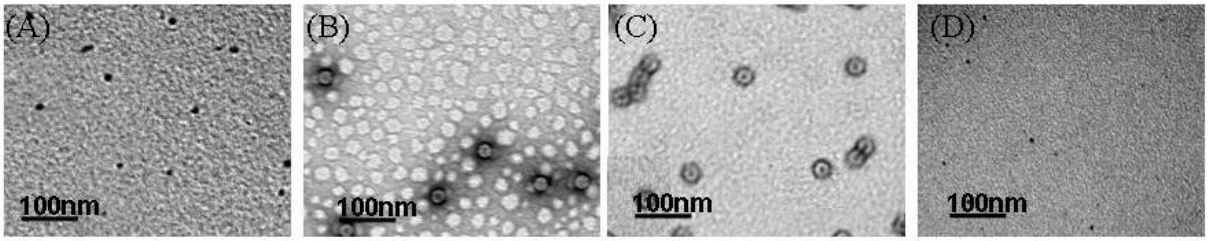

Figure 14.Characterization of VLP encapsidated 4 nm quantum dots. TEM images of (A) 4 nm quantum dots (B) negatively stained sample of VLP encapsidated quantum dots prior to purification (C) negatively stained sample of VLP encapsidated quantum dots after purification and (D) unstained sample of VLP encapsidated quantum dots after purification.

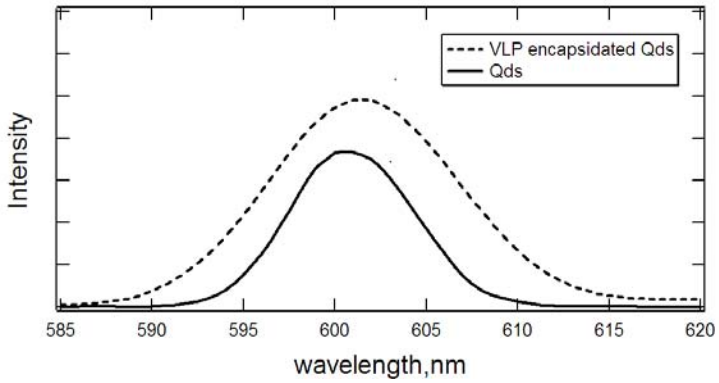

Figure 15.Comparison of emission spectrums of Qds before and after encapsidated by VLP. The emission wavelength of Qds shifted 1-2 nm after encapsidated by VLP.

Table 3.Effect of encapsidated nanoparticle diameter on the inner and outer diameters of VLP as measured by TEM.

Nanoparticle diameter (nm)	VLP outer diameter (nm)	VLP inner diameter (nm)
Au (5.0±0.5 nm)	30.0 ± 3.0	6.0 ± 0.5
Au (10.0± 1.0 nm)	33.5 ± 3.0	10.0 ± 2.0
Au (15.0±1.5 nm)	34.0 ± 2.0	15.0 ± 2.0
$CoFe_2O_4$(4.0±1.2 nm)	33.1 ± 2.2	4.0 ± 0.5
$CoFe_2O_4$(10.0±3.0 nm)	34.2 ± 1.4	9.8 ± 1.1
$CoFe_2O_4$(15.0±4.5 nm)	34.0±2.0	15.0±2.0
Quantum Dots (4.0±1.0 nm)	31.6 ± 3.3	4.0 ± 1.5

References

(1) Veiseh, O.; Sun, C.; Gunn, J.; Kohler, N.; Gabikian, P.; Lee, D.; Bhattarai, N.; Ellenbogen, R.; Sze, R.; Hallahan, A.; Olson, J.; Zhang, M. Q. *Nano Letters* **2005**, *5*, 1003-1008.

(2) Wu, X. Y.; Liu, H. J.; Liu, J. Q.; Haley, K. N.; Treadway, J. A.; Larson, J. P.; Ge, N. F.; Peale, F.; Bruchez, M. P. *Nature Biotechnology* **2003**, *21*, 452-452.

(3) Rosi, N. L.; Giljohann, D. A.; Thaxton, C. S.; Lytton-Jean, A. K. R.; Han, M. S.; Mirkin, C. A. *Science* **2006**, *312*, 1027-1030.

(4) Chan, W. C. W.; Nie, S. M. *Science* **1998**, *281*, 2016-2018.

(5) Dubertret, B.; Skourides, P.; Norris, D. J.; Noireaux, V.; Brivanlou, A. H.; Libchaber, A. *Science* **2002**, *298*, 1759-1762.

(6) D'Souza, A. J. M.; Schowen, R. L.; Topp, E. M. *Journal of Controlled Release* **2004**, *97*, 385-385.

(7) Latham, A. H.; Williams, M. E. *Langmuir* **2006**, *22*, 4319-4326.

(8) Tkachenko, A. G.; Xie, H.; Coleman, D.; Glomm, W.; Ryan, J.; Anderson, M. F.; Franzen, S.; Feldheim, D. L. *Journal of the American Chemical Society* **2003**, *125*, 4700-4701.

(9) Feldherr, C.; Akin, D.; Littlewood, T.; Stewart, M. *Journal of Cell Science* **2002**, *115*, 2997-3005.

(10) Lagerholm, B. C.; Wang, M. M.; Ernst, L. A.; Ly, D. H.; Liu, H. J.; Bruchez, M. P.; Waggoner, A. S. *Nano Letters* **2004**, *4*, 2019-2022.

(11) Douglas, T.; Young, M. *Nature* **1998**, *393*, 152-155.

(12) Douglas, T.; Young, M. *Advanced Materials* **1999**, *11*, 679-+.

(13) Allen, M.; Bulte, J. W. M.; Liepold, L.; Basu, G.; Zywicke, H. A.; Frank, J. A.; Young, M.; Douglas, T. *Magnetic Resonance in Medicine* **2005**, *54*, 807-812.

(14) Medintz, I. L.; Sapsford, K. E.; Konnert, J. H.; Chatterji, A.; Lin, T. W.; Johnson, J. E.; Mattoussi, H. *Langmuir* **2005**, *21*, 5501-5510.

(15) Strable, E.; Johnson, J. E.; Finn, M. G. *Nano Letters* **2004**, *4*, 1385-1389.

(16) Wang, Q.; Kaltgrad, E.; Lin, T. W.; Johnson, J. E.; Finn, M. G. *Chemistry & Biology* **2002**, *9*, 805-811.

(17) Gillitzer, E.; Suci, P.; Young, M.; Douglas, T. *Small* **2006**, *2*, 962-966.

(18) Peabody, D. S. *Journal of Nanobiotechnology* **2003**, *1*, 5-13.

(19) Khor, I. W.; Lin, T. W.; Langedijk, J. P. M.; Johnson, J. E.; Manchester, M. *Journal of Virology* **2002**, *76*, 4412-4419.

(20) Lewis, J. *Nature medicine* **2006**, *12*, 354-360.

(21) Joelson, T.; Akerblom, L.; Oxelfelt, P.; Strandberg, B.; Tomenius, K.; Morris, T. J. *Journal of General Virology* **1997**, *78*, 1213-1217.

(22) Anderson, E. A.; Isaacman, S.; Peabody, D. S.; Wang, E. Y.; Canary, J. W.; Kirshenbaum, K. *Nano Letters* **2006**, *6*, 1160-1164.

(23) Tkachenko, A. G.; Xie, H.; Liu, Y. L.; Coleman, D.; Ryan, J.; Glomm, W. R.; Shipton, M. K.; Franzen, S.; Feldheim, D. L. *Bioconjugate Chemistry* **2004**, *15*, 482-490.

(24) Feldherr, C. M.; Akin, D.; Cohen, R. J. *Journal of Cell Science* **2001**, *114*, 4621-4627.

(25) Sherman M, R. H. G., Florence Tama, Tim L. Sit, Charles L. Brooks,; Albert M. Mikhailov, E. V. O., Timothy S. Baker,Steven A. Lommel *Journal of Virology* **2006**, *80*, 10395-10406.

(26) Basnayake, V. R. *Ph.D Dissertation* **2006**.

(27) Tang, L. *Nature structural biology* **2001**, *8*, 77-83.

(28) Loo, L.; Guenther, R. H.; Basnayake, V. R.; Lommel, S. A.; Franzen, S. *Journal of the American Chemical Society* **2006**, *128*, 4502-4503.

(29) Dragnea, B.; Chen, C.; Kwak, E. S.; Stein, B.; Kao, C. C. *Journal of the American Chemical Society* **2003**, *125*, 6374-6375.

(30) Sun, J.; DuFort, C.; Daniel, M. C.; Murali, A.; Chen, C.; Gopinath, K.; Stein, B.; De, M.; Rotello, V. M.; Holzenburg, A.; Kao, C. C.; Dragnea, B. *Proceedings of the National Academy of Sciences of the United States of America* **2007**, *104*, 1354-1359.

(31) Dixit, S. K.; Goicochea, N. L.; Daniel, M. C.; Murali, A.; Bronstein, L.; De, M.; Stein, B.; Rotello, V. M.; Kao, C. C.; Dragnea, B. *Nano Letters* **2006**, *6*, 1993-1999.

(32) Knez, M. **2003**, - *3*, - 1082.

(33) Reiss, B. D.; Mao, C. B.; Solis, D. J.; Ryan, K. S.; Thomson, T.; Belcher, A. M. *Nano Letters* **2004**, *4*, 1127-1132.

(34) Balci, S.; Bittner, A. M.; Hahn, K.; Scheu, C.; Knez, M.; Kadri, A.; Wege, C.; Jeske, H.; Kern, K. *Electrochimica Acta* **2006**, *51*, 6251-6257.

(35) Chen, C.; Kwak, E. S.; Stein, B.; Kao, C. C.; Dragnea, B. *Journal of Nanoscience and Nanotechnology* **2005**, *5*, 2029-2033.

(36) Loweth, C. J.; Caldwell, W. B.; Peng, X. G.; Alivisatos, A. P.; Schultz, P. G. *Angewandte Chemie-International Edition* **1999**, *38*, 1808-1812.

(37) Rondinone, A. J.; Samia, A. C. S.; Zhang, Z. J. *Journal of Physical Chemistry B* **2000**, *104*, 7919-7922.

(38) Mitchell, G. P.; Mirkin, C. A.; Letsinger, R. L. *Journal of the American Chemical Society* **1999**, *121*, 8122-8123.

(39) Erickson, J. W.; Silva, A. M.; Murthy, M. R. N.; Fita, I.; Rossmann, M. G. *Science* **1985**, *229*, 625-629.

(40) Guenther, R. H.; Sit, T. L.; Gracz, H. S.; Dolan, M. A.; Townsend, H. L.; Liu, G. H.; Newman, W. H.; Agris, P. F.; Lommel, S. A. *Nucleic Acids Research* **2004**, *32*, 2819-2828.

(41) Markham, N. O.; Parry, E. M.; Stefanovic, M.; Gallagher, P. G.; Low, P. S.; Bodine, D. M. *Blood* **2005**, *106*, 473A-474A.

(42) Sit, T. L.; Vaewhongs, A. A.; Lommel, S. A. *Science* **1998**, *281*, 829-832.

(43) Henglein, A.; Mulvaney, P.; Linnert, T. *Faraday Discussions* **1991**, 31-44.

(44) Ren, Y. *The Journal of general virology* **2006**, *87*, 2749-2754.

(45) Phelps, J. P.; Dao, P.; Jin, H. F.; Rasochova, L. *Journal of Biotechnology* **2007**, *128*, 290-296.

(46) Fox, J. *Virology* **1998**, *244*, 212-218.

(47) Oberdorster, G.; Oberdorster, E.; Oberdorster, J. *Environmental Health Perspectives* **2005**, *113*, 823-839.

(48) Dimitrov, R. A.; Zuker, M. *Biophysical Journal* **2004**, *87*, 215-226.

CHAPTER 4

Infusion of dye molecules into *Red clover necrotic mosaic virus*

Abstract

The interior cavity of a native virus protein cage can serve as a container for the encapsulation of molecules. In this paper, the capsid of *Red clover necrotic mosaic virus* (RCNMV) was studied to package dye molecules. RCNMV has been reported to undergo reversible swelling transition in a pH- and divalent ion-dependent manner. This transition leads to the reversible opening of pores (11-13 Å) that permit infusion of molecules into the interior of the virus capsid. At pH 8 and in the presence of 200 mM ethylenediaminetetraacetic acid (EDTA), dye molecules were infused into the interior cavity of RCNMV through the open surface pores. Infusion within the cavity was effected by dialysis of the virion at pH 7 in the presence of calcium. Release of infused dye molecules was achieved by exposure the virus to EDTA at pH 10. Comparison of three dyes, Rhodamine (positive charge), Luminarosine (neutral) and Fluorescein (negative charge) shows that infusion is controlled by electrostatic interactions. This infusion method was further explored to package Doxorubicin, a positively charged chemotherapeutic agent, within the RCNMV capsid. Results indicated that the RCNMV capsid is able to package ~1000 molecules of Doxorubin per virus. Encapsidation of dye molecules by *in vitro* assembly of RCNMV capsid protein (CP) was also studied using the origin of assembly, DNA-2 and RNA-1, to template the formation of a virus-like particle in a dye solution. The capability of RCNMV capsid to infuse and selectively release of cargo represents a potential tool for drug delivery.

4.1 Introduction

Virus capsids consist of multiple copies of subunits that self-assemble to form a protein-cage like architecture. These protein cages offer monodisperse and rigidity structure with an interior cavity that is ideal to function as a container for cargo encapsidation. Several approaches employing virus capsids as a container to package molecules[1-3] and nanoparticles[4-6] have been reported. We recently demonstrated that self-assembly of *Red clover necrotic mosaic virus* (RCNMV) capsid protein (CP) around nanoparticles conjugated with oligonucleotides to mimic the origin of assembly, not only created encapsulation specificity but also enhanced the stability of virus-like particles (described in Chapter 3). To further explore the versatility of the RCNMV capsid for nano-cargo packaging and delivery we describe a small molecule/ cargo infusion process.

RCNMV is a soil-transmitted 36 nm icosahedral plant infecting virus with a capsid composed of 180 copies of a 37 kDa CP packaging either 1 copy each of a 4 kb single-stranded RNA-1 and a 1.5 kb RNA-2 or 4 copies of RNA-2.[7] Divalent ions are an integral part of the RCNMV structure with 390±30 Ca^{2+} and 420±25 Mg^{2+} per virus.[8] The selective removal of Ca^{2+} results in minor reorientation of the CP shell (S) and protruding (P) domains. However, depletion of both divalent ions (Ca^{2+} and Mg^{2+}) induces significant conformational changes to the S and P domain that leads to formation of pores (11-13 Å) within the capsid. The pores observed at the pseudo-3-fold axes expose the capsid interior to the outer environment. Here, we are taking advantage of the reversible opening and closure of pores within the capsid to incorporate molecules into the interior cavity of RCNMV. Based on the presence of anionic genome in the capsid, our hypothesis is that dye molecules with appropriate compensating charge will enter the inner cavity through the opened pores. Our understanding of the mechanism is then applied to package drug molecules by RCNMV capsid.

The pH- and divalent-ion-dependent swelling mechanism of RCNMV is studied to infuse and encapsidate dye molecules within the protein shell. As illustrated in Scheme 1A, the divalent ions on RCNMV were removed by adding EDTA, 200 mM at pH 8. Formation of pores on the protein surface of RCNMV allows small dye molecules from the exterior solution to infuse into the virus. The encapsidation of dye molecules within

RCNMV is completed when the surface pores are closed by dialysis in 200 mM Ca^{2+} at pH 6. An i*n vitro* assembly of RCNMV capsid protein (CP) is an additional method that may be used to encapsidate dye molecules. The RCNMV genome consists of 2 single stranded RNAs: a 3.9 kb RNA-1, and a 1.5 kb RNA-2.[9] Like many other T=3 viruses,[10,11] assembly of RCNMV is initiated by recognition of CP to a specific RNA structure, the origin of assembly (OAS), which leads to encapsidation of the virus genome. In the *in vitro* assembly experiments reported here a 20-base deoxyuridine-modified DNA oligonucleotide analog of the RNA-2 stem loop (5'- AGAGGUAUCGCCCCGCCUCU-3') was used to hybridize with a full length RNA-1 to form the functional OAS. The artificial OAS templates the assembly of CP to form an enclosed protein cage and simultaneously package the dye molecules (Scheme 1B).

4.2 Materials and Methods

RCNMV propagation and purification

Growth and purification of RCNMV were as described.[8] In brief, RCNMV RNA transcripts were inoculated on *Nicotiana clevelandi* plants and maintained under standard greenhouse conditions for 7 to 10 days. Virus were collected from infected leaves and purified. The concentration of virus is determined by absorbance measurement with an extinction coefficient of 6.46.

Infusion of dye molecules into RCNMV

1.25 mg/ml of RCNMV was dialyzed in a Slide-A-Lyzer 10K MWCO dialysis cassette (Pierce Biotechnology, Rockford, IL) against 200 mM EDTA at pH 8 for 5-6 hours. Dialyzed RCNMV was collected and incubated with 2000:1 ratio of dye-to-virus at 4 ^{o}C for 12-16 hours. After the incubation period, the sample was dialyzed against 200 mM Ca^{2+} at pH 6 for 24 hours. The sample, which contained RCNMV-infused dye ($RCNMV_{dye}$), was then collected. Excess dyes were removed by Microcon filter unit with 30 kDa cutoff (Millipore, Billerica, MA) by centrifugation at 16,000 g for 30 minutes. This filtration was repeated until the fluorescence signal of the $RCNMV_{dye}$ was reduced

to the background level, an indication of complete removal of excess dyes from the sample. The identical protocol as described above was also performed to infuse Doxorubicin into RCNMV ($RCNMV_{Dox}$). After dialyzed against EDTA, 5000:1 ratio of Doxorubicin-to-virus was incubated for 12-16 hours, followed by dialyzed against Ca^{2+}. The excess Doxorubicin was then removed using sucrose gradient centrifugation as described below.

***In vitro* assembly of RCNMV capsid protein to encapsidate dye molecules**

50 µl of deoxyuridine modified ssDNA (5'- AGAGGUAUCGCCCCGCCUCU-3'), 2.106 mM, was added into a solution of dye molecules with a mole ratio of 1:25, followed by 2 µl of 4 µM T7 RCNMV RNA-1 transcripts. The sample was allowed to incubate for 1 hour before adding 10 ul of purified RCNMV capsid protein (10 mg/ml) into the mixture. *In vitro* assembly of RCNMV capsid protein was carried out by dialyzed against 50 mM Tris buffer at pH 6.5 for 24 hours. The sample which contained assembled coat protein of RCNMV (encapsulated dye molecules) was then collected.

Quantification of dyes or Doxorubicin infused per RCNMV

The infused dyes or Doxorubicin was released from the capsid by EDTA treatment at pH 10. 200 mM EDTA at pH 10 was added into a Microcon filter unit with 10 kDa cutoff (Millipore, Billerica, MA), which contained 0.5 mg/ml of $RCNMV_{dye}$ or $RCNMV_{Dox}$ with a volume ratio of 1:1. After ~30 minutes of incubation at room temperature, the sample was centrifuged for 30 minutes at 16,000 g. The dyes or Doxorubicin released from the disassembled capsid were separated and quantified by fluorescence measurement. To determine the capability of infused dyes to diffuse through pores, the $RCNMV_{dye}$ or $RCNMV_{Dox}$ was treated by 200 mM EDTA at pH 8 with a volume ratio of 1:1. After ~30 minutes of incubation, the dyes or Doxorubicin that diffused through the pores was separated from the capsid by centrifugation for 30 minutes at 16,000 g in a Microcon filter unit (10 kDa cutoffs). Standard curves of native RCNMV, dyes and Doxorubicin were generated for quantitative measurement to determine the ratio of dyes or Doxorubicin infused per RCNMV. Identical protocol was applied to quantify the number of dyes encapsidated by virus-like particles.

Sucrose density gradient centrifugation

To expedite the process of removing the excess Doxorubicin, RCNMV-infused Doxorubicin ($RCNMV_{Dox}$) was loaded onto a 20-50 % sucrose gradient centrifugation (180000 g, 5 ^{o}C, and 55 minutes) in a SW-55 rotor with a model L8-70 Beckman ultracentrifuge. The preformed gradients were prepared by layering, in succession, 1 ml of 20, 30, 40 and 50% (w/w) sucrose into ultra-clear centrifuge tubes (Beckman). The gradients were kept for overnight at 4 ^{o}C to allow diffusion to form linear sucrose density gradients. The native RCNMV (0.5 mg/ml), as a control sample, was also studied under the same experimental conditions. Fifteen 0.25 ml fractions of the sucrose gradient were collected from bottom to top for absorbance measurement at 260 nm. The fraction with the highest absorbance value (purified $RCNMV_{Dox}$) was collected for further analysis.

Iodixanol gradient centrifugation

The RCNMV-infused Doxorubicin ($RCNMV_{Dox}$) was layered on a 20-60 % iodixanol gradient (Optiprep, Axis Shield) into polyallomer bell-top quick seal tubes (Beckman) and centrifuged in a SW-55 rotor with a model L8-70 Beckman ultracentrifuge (27900 *g*, 16 hours, 5 °C). After centrifugation, the gradients were fractionated into 0.25 ml fractions. 50 ul of each collected fraction was mixed with equal volume of Bradford reagent (Pierce Biotechnology, Rockford, IL) and the absorbance was measured at 595 nm using a microplate reader (Bio-Tek Synergy HT). The fraction with the highest absorbance value (purified $RCNMV_{Dox}$) was collected. The refractive indexes of samples were measured using a refractometer to determine the densities, based on the formula $\rho=3.4394\eta- 3.5970$, where ρ is the density (g/ml) and η is the refractive index.

Fluorescence Spectrometer

Fluorescence measurements were performed by Perkin Elmer LS-50B Spectrofluorometer. Rhodamine 590 Chloride was measured with an excitation wavelength at 500 nm and emission wavelength at 560nm. Luminarosine was excited at 425 nm and fluorescence emission was observed at 530 nm. Fluorescein was measured with an excitation wavelength at 470 nm and the emission wavelength at 530 nm. In three cases, excitation and emission slit widths were set to 2.5 nm and 5.0 nm, respectively.

Transmission Electron Microscopy (TEM)

TEM images were acquired using a (Philips) CM12 microscope operating at 100 kV accelerating voltage located at the University of North Carolina, School of Dentistry, Chapel Hill, NC. Images were created with a Gatan 780 DualView camera system. All TEM samples, unless otherwise noted, were negatively stained with 2 % uranyl acetate to enhance image contrast.

4.3 Results and Discussion

Three different charged dye molecules were tested for capsid infusion: Rhodamine (positive), Luminarosine (neutral) and Fluorescein (negative). The loading capacity of the RCNMV capsid for each dye molecule was ascertained by complete disassembly of the infused capsid with EDTA treatment at pH 10 to release the infused molecules (Table 1). Rhodamine, a positively charged molecule exhibited the highest infusion rate of 83±10 molecules/virus, which is probably due to the electrostatic interaction with the anionic virus genome. The neutral charged dye, Luminarosine, loaded to 76±5 molecules/virus. Luminarosine is a fluorescent nucleobase with the ability to interact with nucleotides, which likely explains its relatively high loading. In contrast, Fluorescein with only 2±1 molecules/virus had the lowest infusion rate, presumably due to electrostatic repulsion between its negative charge and the anionic RNA virus genome. Moreover, the amino acid residues on the surface of the capsid surrounding the site of pore formation possess a net negative charge,[8] which may prevent the Fluorescein from entering the capsid. These measurements support the hypothesis that dye infusion is facilitated by an electrostatic interaction with the viral genome. In order to determine the capability of the infused dyes to diffuse through the opened pores, pre-infused capsids termed $RCNMV_{dye}$, were exposed to 200 mM EDTA at pH 8, under identical conditions for infusion as described in Scheme 1A. A low but detectable amount of dye was observed to release under this condition. This observation suggested an alternative mechanism of dye release by diffusion through re-opened pores without complete capsid disruption.

To determine the loading capacity of RCNMV for Rhodamine, different mole ratios of Rhodamine per RCNMV were incubated (150:1, 500:1, and 4000:1) during the infusion protocol depicted in Scheme 1A. The results indicated that a maximum of ~90 Rhodamine molecules can be infused per RCNMV (Figure 1). TEM analysis revealed that infusion of Rhodamine did not result in a detectable change in the capsid diameter or morphology when compared to native RCNMV (Figure 2). Unlike Rhodamine, incubation of Luminarosine at a mole ratio of 150:1 reported almost no uptake of the dye in the virus. This observation suggested that the electrostatic interaction with the viral genome plays a major role in the infusion manner, even when low number of excess dyes was available, which explains the success infusion for Rhodamine but not for Luminarosine.

Selective depletion of Ca^{2+} (by EGTA treatment) resulted in changes to the capsid organization but did not induce the opening of pores[8]. A control experiment was performed where Rhodamine was incubated with RCNMV pre-treated with EGTA (instead of EDTA), at a mole ratio of 500:1 (Rhodamine-to-RCNMV), followed by dialyzing against Ca^{2+}. Identical protocols to remove the excess Rhodamine and release of infused Rhodamine were subsequently performed. Based on fluorescence measurements, 6.2±3.4 Rhodamine molecules infused per virus (Figure 3). In a second control experiment, Rhodamine was incubated with untreated RCNMV (not treated with EGTA or EDTA). The emission spectrum indicated the released Rhodamine signal was as low as the background signal, suggesting no Rhodamine infusion. Collectively these results indicated that Rhodamine infusion is strictly dependent upon total divalent ion extraction and pore formation, since the failure to open the pores leads to almost no infusion of Rhodamine.

This information was then applied to package Doxorubicin, a positively charged chemotherapeutic agent, within RCNMV capsid. The incubation of Doxorubicin at a mole ratio of 5000:1(Doxorubicin-to-RCNMV) following the Scheme 1A infusion protocols used for Rhodamine was performed. The RCNMV-infused Doxorubicin ($RCNMV_{Dox}$) was banded by ultracentrifugation in a 20-50 % sucrose gradient to separate the $RCNMV_{Dox}$ from the non-infused RCNMV and the excess Doxorubicin. The infusion of Doxorubicin into the RCNMV capsid uniformly increased the density of the

entire virus population, hence, results a shift of density and banded at 40 % sucrose, as compared to native RCNMV which yielded a band at 30% sucrose (Figure 4). The TEM image (Figure 2C) indicated that the integrity of $RCNMV_{Dox}$ remained intact and the diameter (34.5±3.7 nm) is similar to the native RCNMV.

$RCNMV_{Dox}$ was further subjected to a 20-60 % iodixanol (Optiprep) gradient centrifugation. The centrifugation of native RCNMV resulted in 2 visible bands, where the lower and upper band corresponded to native and expanded (swollen) form of the virus, respectively. On the contrary, $RCNMV_{Dox}$ formed a distinct band that reached equilibrium at a higher density (lower in the gradient) than native RCNMV (Figure 5A). Absorbance on the fractionated iodixanol gradients indicated a major peak of $RCNMV_{Dox}$ at fraction 2, corresponded to 60 % iodixanol, while native RCNMV was found at fraction 8, equivalent to 50 % iodixanol. To eliminate the possibility that the increased density of $RCNMV_{Dox}$ as observed was due to attachment of Doxorubicin on the virus outer surface, a control experiment was performed where Doxorubicin was incubated with untreated RCNMV and centrifuged under the same conditions. The distribution profile of this control sample was the same as native RCNMV (Figure 6). The control experiment, together with the notable difference in density observed for native RCNMV and $RCNMV_{Dox}$ further confirmed that the Doxorubicin was indeed infused into the capsid. Based on the refractive index measurements, density of $RCNMV_{Dox}$ was 1.324 g/ml, compared to native RCNMV which was 1.247 g/ml. Calculations based on the difference of the density indicated that ~1,000 Doxorubicin molecules are infused per RCNMV.

When $RCNMV_{Dox}$ was exposed to EDTA at pH 8, the fluorescence intensity of Doxorubicin was as low as the background signal, which implies Doxorubicin does not diffuse through the pores under those conditions. This observation is different from Rhodamine and Luminarosine, where approximately 10 % of the total encapsulated dyes were diffused through the pores after EDTA, pH 8 treatment (Table 1). Doxorubicin is an anthracycline drug that is known to intercalate in DNA. We hypothesize that the interaction between Doxorubicin and the viral genome inhibits the diffusion of Doxorubicin through the pores. Hence, Doxorubicin was not detected when $RCNMV_{Dox}$ was treated with EDTA, pH 8.

An *in vitro* assembly of RCNMV capsid protein was also proposed to package dye molecules within the virus capsid (Scheme 1B). In order to stimulate artificial encapsidation of dye molecules, we have used a DNA mimic of RNA-2 to create an OAS that can be applied to initiate the assembly process. This sequence is designated as DNA-2. Positively charged Rhodamine, neutral Luminarosine and negatively charged Fluorescein, respectively, were incubated with the DNA-2 as described in the experimental section. Subsequently, RNA-1 transcript was added to this mixture followed by the purified capsid protein of RCNMV. Upon examination by TEM (Figure 2D-E), the mean diameter of the VLP was 23.7±0.9 nm, analogous to a T = 1 particle. Further investigations are required to characterize the virus-like particles formed under this condition. So far, preliminary data from TEM and DLS indicated that encapsidation of Rhodamine within the assembled VLP did not induce a significant change in size compared to assembled VLP-unencapsidated Rhodamine (Figure 7). The number of Rhodamine, Fluorescein and Luminarosine released from VLP after EDTA, pH 10 and pH 8 treatments are reported in Table 2.

As suggested by the results, the encapsidation number for Rhodamine within the VLP was 42 % higher than that observed in native RCNMV despite its smaller size. One possible explanation is that the use of a shorter genome (20-mer DNA-2, rather than full length 1.5 kb RNA-2) within assembled VLP created available space that allowed more Rhodamine to be packaged. Moreover, incubation between polyanion DNA-2 and cationic Rhodamine as described in the protocol allowed direct electrostatic interaction to occur prior to assembly, hence, increasing the accessibility of binding sites for Rhodamine packaging within the VLP. However, this trend was not observable for Luminarosine. The binding of Luminarosine encapsidation was 65 % lower in VLP than in native RCNMV, presumably because of the smaller volume of the VLP. The encapsidation of anionic Fluorescein was reduced by the electrostatic interaction with the polyanionic RNA genome, and yielded the lowest number of encapsidated molecules.

A variety of approaches have been demonstrated to package cargo using protein containers. One approach involves covalent modification to an inner cavity of a protein cage to display a particular residue to increase the specificity of encapsulation[12-14]. Here, a plant virus, with a natural low density inner cavity (cargo hold) is used to package

molecules through the pH and divalent-ion dependent reversible pore opening and closing. This method provides an alternative approach based on direct and straightforward mechanism to package molecules without major alteration to the integrity of the capsids. Results indicated that Doxorubicin packaged by RCNMV capsid showed no diffusion through the opened pores, which eliminated the possibility of drug leakage. This property distinguishes the capsid infusion approach from formulations such as liposomes-encapsulated Doxorubicin, which do leak over time[15]. The clinically approved liposomal doxorubicin formulation (Doxil), with an average diameter of 90 nm, has been reported to package ~15,000 Doxorubicin per vesicle[16]. The loading densities of Doxorubicin (number of Doxorubicin:particle volume) are 0.0053/ nm^3 and 0.0051/ nm^3 in RCNMV and Doxil, respectively. The loading efficiency together with the tight non-leaky packaging of the RCNMV capsid offers superior candidate for development as a drug carrier.

RCNMV is stable in soil where the divalent ions concentrations are high (millimolar range) but trigger to open surface pores and release their genome inside a cell when the divalent ions concentrations are low (micromolar level). This method is advantageous as the RCNMV capsid can perform as a container to protect and sequester a cargo until it reaches the targeted cell to be released. Moreover, with the isoeletric point of 6.8, RCNMV maintains capsid integrity at high pH as compared to other plant viruses such as TBSV (isoeletric point is 4.8)[17] which also utilizes a similar opening and closing of surface pores upon changes of pH and divalent ions concentrations for genome cargo egress [18].

The development of plant viruses as biomedical tools has been previously evaluated. The incorporation of gadolinium into *Cowpea chlorotic mottle virus* (CCMV) created a paramagnetic nanoparticle that is useful as an MRI contrast agent[19]. The modification of *Cowpea mosaic virus* (CPMV) to display foreign peptides has been demonstrated for vaccine development[20]. In addition, studies to analyze the intracellular uptake of CPMV in vitro and in vivo have also been conducted. For instance, the undesirable uptake of CPMV in endothelial cells as well as immune response can be reduced by chemical attachment of a polyethylene glycol coat on the viral surface[21,22].

The in vivo interactions between mammalian cells membranes and CPMV[23]provide information, which is critical to develop virus particles as a cell-targeting tool.

4.4 Conclusion

This study demonstrates a method that exploits the natural RCNMV pH and divalent ions-dependent genome release encoded into its polymeric protein capsid to encapsidate and release dye molecules. The *in vitro* assembly approach proposed here provided an alternative method to package molecules within the virus capsid. Overall, this study revealed that infusion of positive and neutral charged dye molecules were feasible, but negatively-charged dye molecules were not readily infused into the virus. Additionally, the loading density of the neutral Luminarosine and the Doxorubicin may be increased because of interactions with the virus genome. The results demonstrated an extremely high loading density of ~1,000 dyes per virus for the chemotherapeutic Doxorubicin. The method reported here offers an approach that enables the use of virus capsid as a vector for the controlled loading and unloading cargos.

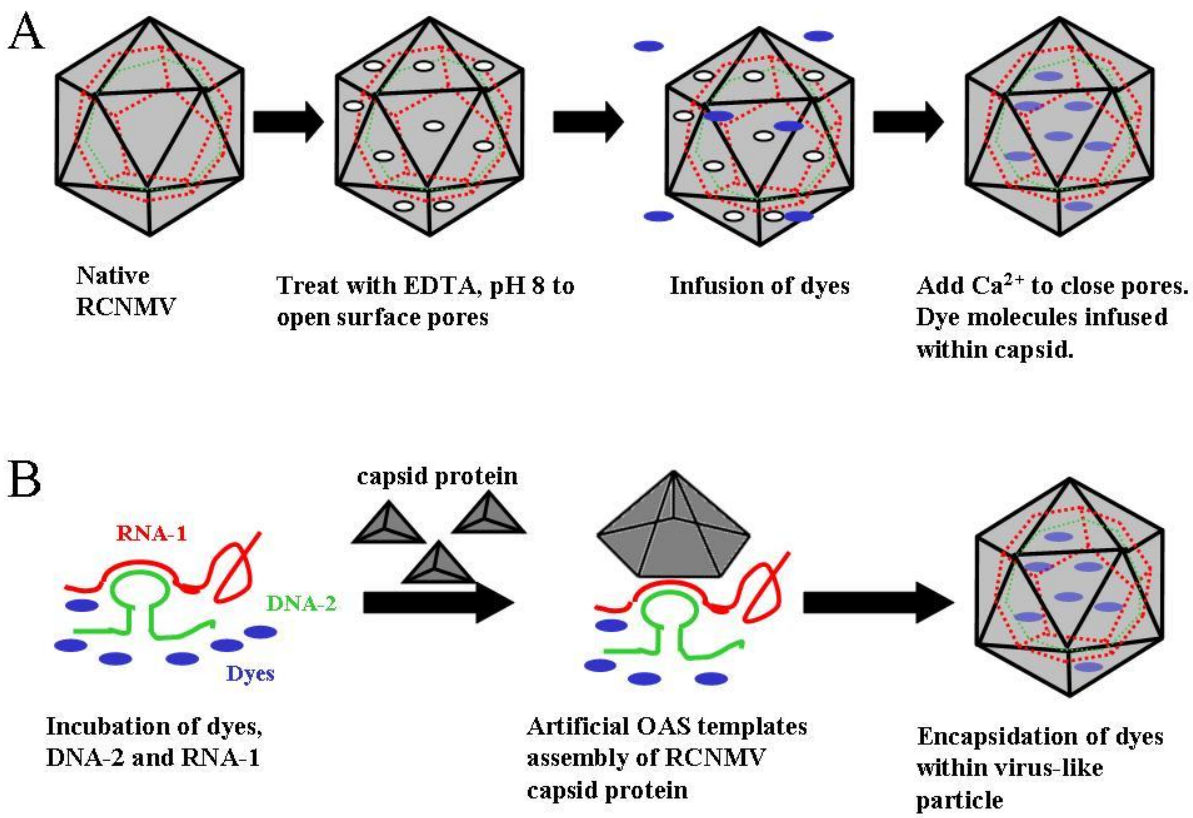

Scheme 1.A schematic of the steps involved to package dye molecules within RCNMV capsid. (A) Infusion of dye molecules into native RCNMV. (B) *In vitro* assembly of RCNMV capsid protein to encapsidate dye molecules.

Table 1.Number of dye molecules released per RCNMV capsid after EDTA treatment at pH 10 and pH 8. $RCNMV_{dye}$ was treated with EDTA, 200 mM, pH 10 or pH 8, at a volume ratio of 1:1. The dye released from RCNMV capsid was separated and collected for fluorescence measurements.

Dye (charge)	EDTA, pH 10 [a]	EDTA, pH 8 [b]
Rhodamine (positive)	83±10	6±4
Luminarosine (neutral)	76±5	7±3
Fluorescein (negative)	2±1	1±1
Doxorubicin (positive)	4300±1300	<1

[a] Virus disassembled to release infused molecules. [b] Surface pores re-opened (without virus disruption) to diffuse molecules from the capsid.

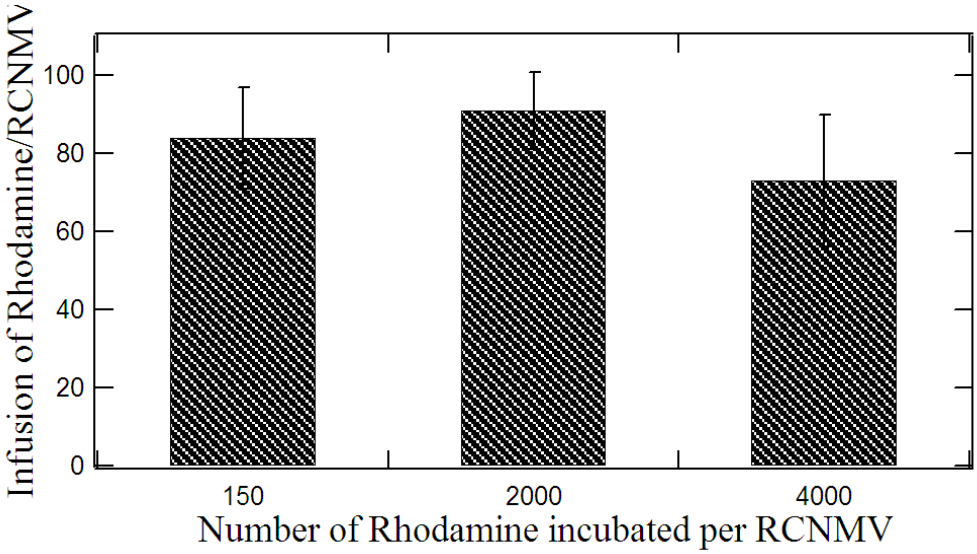

Figure 1.Number of Rhodamine infused per RCNMV under various RCNMV/Rhodamine ratios during incubation period. 3 different ratios of Rhodamine-to-RCNMV were incubated to determine the maximum loading capacity of Rhodamine per virus. Data indicated a maximum of ~90 Rhodamine can be infused per RCNMV.

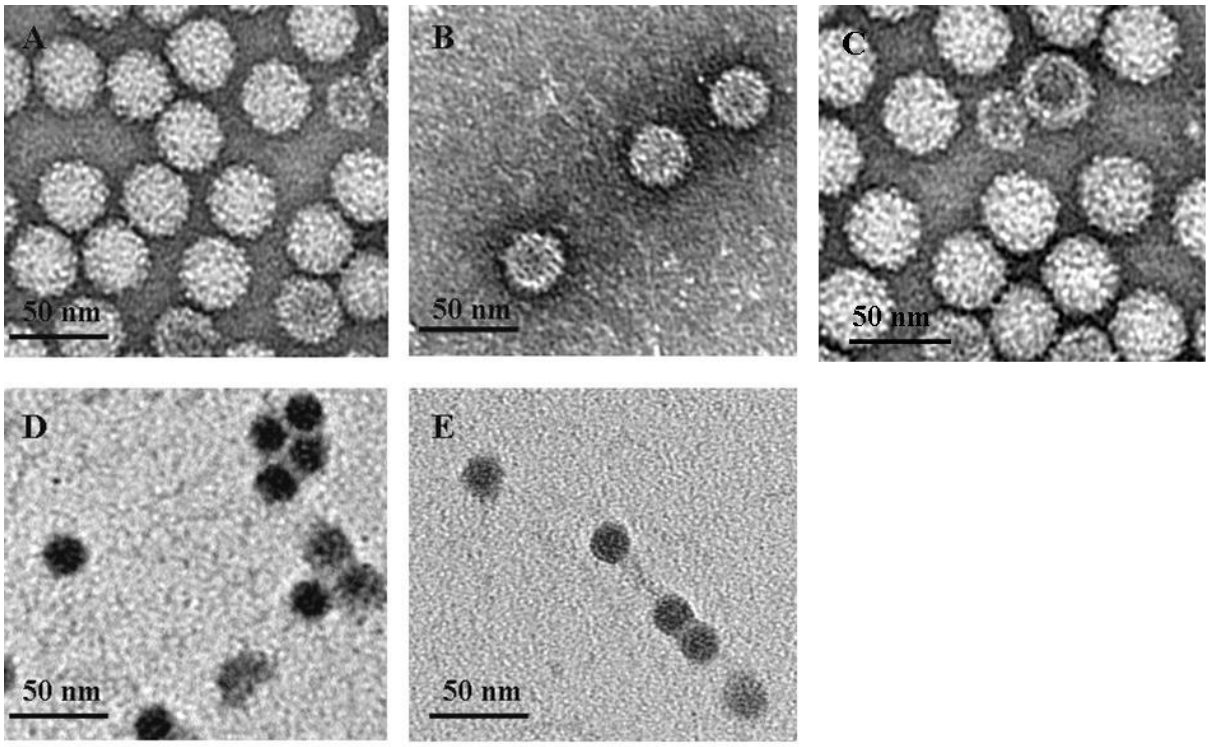

Figure 2.Characterization of RCNMV-infused dye and virus-like particles-infused dye by TEM. TEM images of (A) native RCNMV, (B) RCNMV infused Rhodamine, (C) RCNMV infused Doxorubicin (D) virus-like particles and (E) virus-like particle infused Rhodamine.

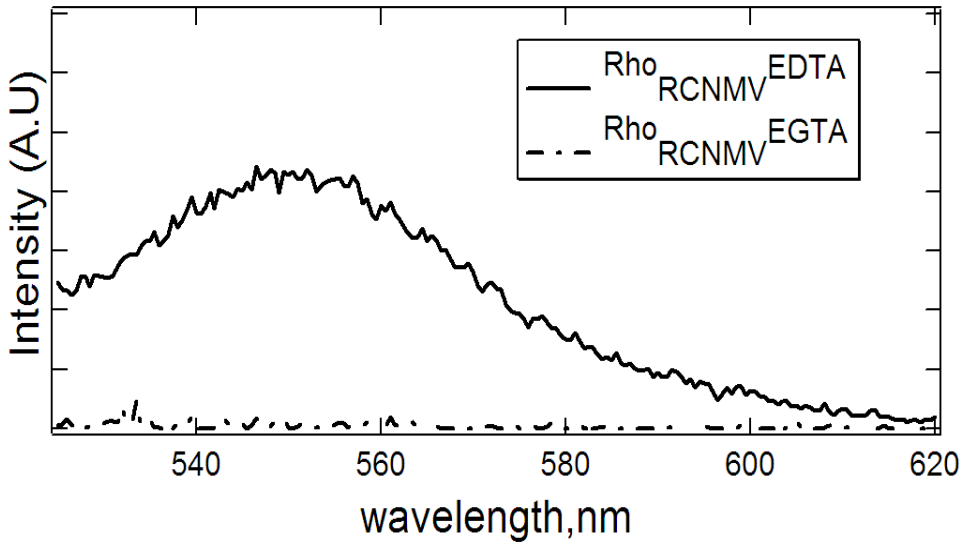

Figure 3.Emission spectrum of Rhodamine released from RCNMV pre-treated with EDTA (^{Rho}RCNMV^{EDTA}) and RCNMV pre-treated with EGTA (^{Rho}RCNMV^{EGTA}). The protocol to infuse Rhodamine into RCNMV-pretreated with EGTA, followed by the removal of excess Rhodamine and the released of infused Rhodamine was identical as described for infusion of Rhodamine into RCNMV-pretreated with EDTA. After EDTA, pH 10 treatment, Rhodamine released from the disassembled capsid was measured. The Rhodamine intensity from ^{Rho}RCNMV^{EGTA} was negligible if compared to the Rhodamine intensity from ^{Rho}RCNMV^{EDTA}. In other word, the failure to open the pores leads to low or no Rhodamine infusion.

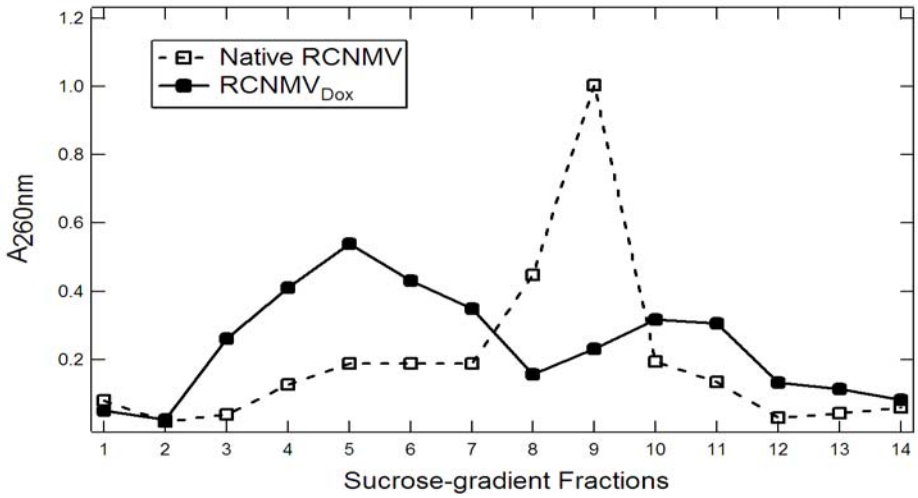

Figure 4.Absorbance of each sucrose gradient fractions obtained from native RCNMV and RCNMV$_{Dox}$. Data are presented with the densest fractions to the left. The highest absorbance for native RCNMV was observed at fraction 9, which corresponded to 30 % sucrose. The infusion of Doxorubicin into the RCNMV capsid increased the density of the particle, and banded at fraction 5, equivalent to 40 % of sucrose.

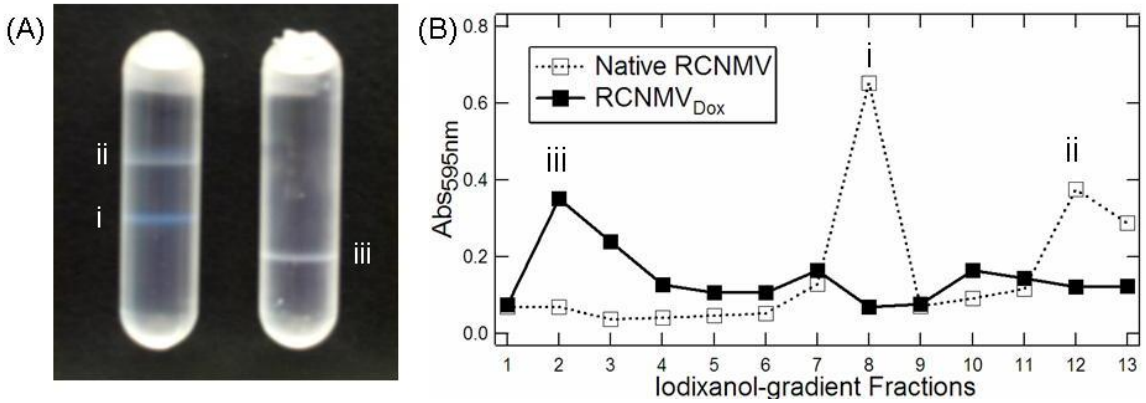

Figure 5.RCNMV$_{Dox}$ subjected to 20-60 % iodixanol gradient centrifugation. (A) Distribution profile of native RCNMV (left) and RCNMV$_{Dox}$ (right) through a 20-60 % iodixanol gradient after centrifugation. (B) Absorbance of each iodixanol gradient fractions. Data are presented with the densest fractions on the left. Peaks labelled with (i), (ii) and (iii) corresponded to bands observed on the tubes.

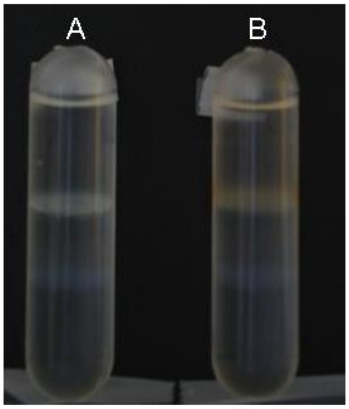

Figure 6.Iodixanol (Optiprep) gradient centrifugation. The distribution profile of (A) native RCNMV and (B) negative control sample through a 20-60 % iodixanol gradient after centrifugation. Negative control sample was prepared by incubation of Doxorubicin with untreated RCNMV (not treated with EDTA or EGTA).

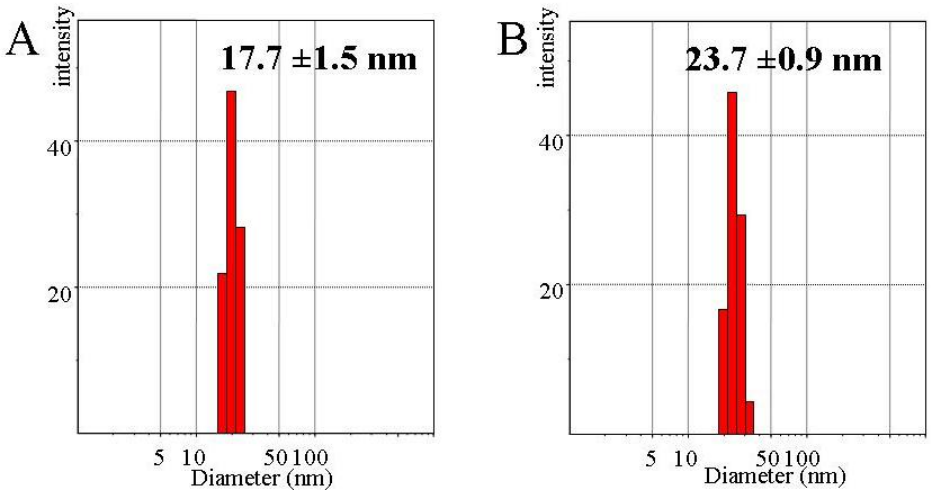

Figure 7.Hydrodynamic radius of (A) VLP and (B) VLP encapsulated Rhodamine as measured by Dynamic Light Scattering.

Table 2.Number of dye molecules released per virus-like particle (VLP) after EDTA treatment at pH 10 and pH 8. VLP_{dye} was treated with EDTA, 200 mM, pH 10 or pH 8, at a volume ratio of 1:1. The dye released from VLP was separated and collected for fluorescence measurements.

Dye (charge)	EDTA, pH 10 [a]	EDTA, pH 8 [b]
Rhodamine (positive)	147±15	16±7
Luminarosine (neutral)	26±8	19±9
Fluorescein (negative)	3±1	3±2

[a] Virus disassembled to release infused molecules. [b] Surface pores re-opened (without virus disruption) to diffuse molecules from the capsid.

References

(1) Knez, M.; Sumser, M.; Bittner, A. M.; Wege, C.; Jeske, H.; Martin, T. P.; Kern, K. *Advanced Functional Materials* **2004**, *14*, 116-124.

(2) Douglas, T.; Young, M. *Nature* **1998**, *393*, 152-155.

(3) Ren, Y.; Wong, S. M.; Lim, L. Y. *Bioconjugate Chemistry* **2007**, *18*, 836-843.

(4) Sun, J.; DuFort, C.; Daniel, M. C.; Murali, A.; Chen, C.; Gopinath, K.; Stein, B.; De, M.; Rotello, V. M.; Holzenburg, A.; Kao, C. C.; Dragnea, B. *Proceedings of the National Academy of Sciences of the United States of America* **2007**, *104*, 1354-1359.

(5) Dixit, S. K.; Goicochea, N. L.; Daniel, M. C.; Murali, A.; Bronstein, L.; De, M.; Stein, B.; Rotello, V. M.; Kao, C. C.; Dragnea, B. *Nano Letters* **2006**, *6*, 1993-1999.

(6) Loo, L.; Guenther, R. H.; Basnayake, V. R.; Lommel, S. A.; Franzen, S. *Journal of the American Chemical Society* **2006**, *128*, 4502-4503.

(7) Basnayake, V. R.; Sit, T. L.; Lommel, S. A. *Virology* **2006**, *345*, 532-539.

(8) Sherman, M. B.; Guenther, R. H.; Tama, F.; Sit, T. L.; Brooks, C. L.; Mikhailov, A. M.; Orlova, E. V.; Baker, T. S.; Lommel, S. A. *Journal of Virology* **2006**, *80*, 10395-10406.

(9) Basnayake, V. R. *Ph.D Dissertation* **2006**.

(10) Tang, L. *Nature structural biology* **2001**, *8*, 77-83.

(11) Qu, F. *Journal of virology* **1997**, *71*, 1428-1435.

(12) Flenniken, M. L.; Liepold, L. O.; Crowley, B. E.; Willits, D. A.; Young, M. J.; Douglas, T. *Chemical Communications* **2005**, 447-449.

(13) Hooker, J. M. **2004**, - *126*, - 3719.

(14) Schlick, T. L.; Ding, Z. B.; Kovacs, E. W.; Francis, M. B. *Journal of the American Chemical Society* **2005**, *127*, 3718-3723.

(15) Charrois, G. J. R.; Allen, T. M. *Biochimica Et Biophysica Acta-Biomembranes* **2004**, *1663*, 167-177.

(16) Gabizon, A.; Shmeeda, H.; Horowitz, A. T.; Zalipsky, S. *Advanced Drug Delivery Reviews* **2004**, *56*, 1177-1192.

(17) Lorber, B.; Sauter, C.; Ng, J. D.; Zhu, D. W.; Giege, R.; Vidal, O.; Robert, M. C.; Capelle, B. *Journal of Crystal Growth* **1999**, *204*, 357-368.

(18) Hogle, J.; Kirchhausen, T.; Harrison, S. C. *Journal of Molecular Biology* **1983**, *171*, 95-100.

(19) Allen, M.; Bulte, J. W. M.; Liepold, L.; Basu, G.; Zywicke, H. A.; Frank, J. A.; Young, M.; Douglas, T. *Magnetic Resonance in Medicine* **2005**, *54*, 807-812.

(20) Brennan, F. R.; Bellaby, T.; Helliwell, S. M.; Jones, T. D.; Kamstrup, S.; Dalsgaard, K.; Flock, J. I.; Hamilton, W. D. O. *Journal of Virology* **1999**, *73*, 930-938.

(21) Rae, C. S.; Khor, I. W.; Wang, Q.; Destito, G.; Gonzalez, M. J.; Singh, P.; Thomas, D. M.; Estrada, M. N.; Powell, E.; Finn, M. G.; Manchester, M. *Virology* **2005**, *343*, 224-235.

(22) Raja, K. S.; Wang, Q.; Gonzalez, M. J.; Manchester, M.; Johnson, J. E.; Finn, M. G. *Biomacromolecules* **2003**, *4*, 472-476.

(23) Koudelka, K. J.; Rae, C. S.; Gonzalez, M. J.; Manchester, M. *Journal of Virology* **2007**, *81*, 1632-1640.

CHAPTER 5

Red clover necrotic mosaic virus capsid as a Multifunctional Tool to Package, Target and Deliver Molecules into Cells

Abstract

This report describes the utilization of *Red clover necrotic mosaic virus* (RCNMV) capsid as a multifunctional tool to package, target and deliver molecules into cancer cells. The exterior surface of RCNMV presents both lysine and cysteine amino acid residues that can be conjugated with various targeting peptides. Three different targeting peptides: CAR, IBD and CD46 were conjugated to the exterior surface of RCNMV using SMCC linker to examine the efficiency for internalization. We have previously described the ability of the RCNMV capsid to package Rhodamine and Doxorubicin. From here, we further proceed to develop RCNMV capsid to target and deliver the packaged molecules into cells. The therapeutic effect of modified RCNMV, simultaneously packaged Doxorubicin in the interior cavity along with the targeting peptide on the exterior surface, was examined. The utilization of RCNMV capsid as a multifunctional tool for therapeutic purposes demonstrated a new general drug delivery platform.

5.1 Introduction

The development of nanoparticles as drug carriers has been studied extensively[1,2]. These particles, which included liposomes, dendrimers, polymeric and inorganic nanoparticles, have each demonstrated unique properties advantageous for drug delivery. The amphiphilic character of liposomes confers the ability to package both hydrophilic and hydrophobic drug molecules[3]. The polymer branches of dendrimers created a wide surface area to attach different functional components[4]. The development of biodegradable polymeric nanoparticles such as chitosan[5] not only managed to overcome the toxicity problem attributed to synthetic polymers, but also have been demonstrated as an efficient carrier for DNA vaccines[6,7]. The usage of silica nanoparticles as a carrier for plasmid DNA has been demonstrated to be desirable as the inorganic nanoparticle is stable under a range of pH and temperature which provides good protection to the encapsulated cargo[8].

Virus particles are self-assembled nanoparticles with unique features that can be exploited for medical applications. The symmetrical outer surface of a virus is a versatile platform that is amenable to display various signals such as peptides, protein or fluorescent labels[9-13], which can be developed as cell-targeting or bio-imaging agents. For example, the fluorescently-labeled of *Cowpea mosaic virus* (CPMV) has been used as an intravital vascular imaging in living mouse and chick embryos[14]. The conjugation of CD46 (cellular receptor of measles virus) to CPMV managed to function as an antiviral agent to inhibit the measles virus infection efficiently *in vitro*[15]. Moreover, the rigidity and robustness of the virus capsid can be exploited as a container for encapsulation of nanoparticles[16,17] as well as drug molecules[18,19]. Other protein cages such as the human ferritin cage have also been demonstrated to package magnetic nanoparticles along with conjugated RGD peptide externally for cell-specific targeting[20]. The ability to impart functionality to the outer surface, together with the loading capacity, has made protein cages an excellent tool for development as drug delivery vectors.

Red clover necrotic mosaic virus (RCNMV), belongs to *Dianthovirus* genus and *Tombusviridae* family, is a T = 3 icosahedral soil-transmitted virus with a diameter of 36 nm. The capsid of RCNMV consists of 180 copies of capsid protein that assembles to

package either 1 copy each of a 4 kb single-stranded RNA-1 and a 1.5 kb RNA-2 or 4 copies of RNA-2[21]. The RCNMV capsid has been demonstrated as a versatile container to package various composites of nanoparticles in the diameter range of 3-15 nm via a RNA-dependent manner[21]. An alternative approach to package smaller cargo/molecules by RCNMV capsid was also proposed[22]. The RCNMV capsid undergoes a structural transition in response to divalent-ion concentration, which leads to formation of surface pores within the capsid[23]. The opening of surface pores has been demonstrated in response to reduction of calcium and magnesium concentration to levels found in cytoplasm. The transition in virus structure in response to cytoplasmic levels of these divalent ions is associated with the release-mechanism of the bipartite RNA genome *in vivo*. The same mechanism can be used *in vitro* to infuse Rhodamine as well as a therapeutic drug, Doxorubicin, within a RCNMV capsid. The release of these molecules in the cytoplasm of cells *in vitro* is demonstrated in the present study.

In this chapter, we demonstrated the capability of the RCNMV capsid to target and deliver the packaged molecules into cancer cells. Various targeting peptides were conjugated on the exterior surface of RCNMV to determine the efficiency for internalization. The modified RCNMV, simultaneously packaged molecules in the interior cavity along with the targeting peptide on the exterior surface, was then studied for intracellular uptake. The utilization of RCNMV capsid as a multifunctional tool for therapeutic purposes demonstrates a new general drug delivery platform.

5.2 Materials and Methods

Cell lines and culture

HeLa (human cervical cancer cells) and HepG2 (human hepatocarcinoma cancer cells) cell lines were purchased from American Type Culture Collection (Rockville, MD). Minimum Essential Medium Eagle (EMEM), fetal bovine serum (FBS), Dulbecco's Phosphate Buffered Saline (DPBS), T-25 and T-75 cell culture flasks were purchased from Bio-Whittaker, Inc. (Walkersville, MD). HeLa and HepG2 cells were cultured in Minimum Essential Medium Eagle (EMEM) media containing 10 % fetal bovine serum and 1 % penicillin-streptomycin at 37 ℃ in an atmosphere containing 5 % CO_2. To plate the cells into a well plate, the culture media was removed and cells were washed with DPBS twice before harvested using 5 % trypsine (Gibco Lab) solution. Then cells were seeded ~10,000 cells/well in a 6-well plate and incubated at 37 ℃ for 24 hours before experiments were performed.

RCNMV propagation and purification

Growth and purification of RCNMV were as described[23]. In brief, RCNMV RNA transcripts were inoculated on *Nicotiana clevelandi* plants and maintained under standard greenhouse conditions for 7 to 10 days. Virus were collected from infected leaves and purified. The concentration of virus was determined by absorbance measurement at 260 nm with an extinction coefficient of 6.46.

Preparation of RCNMV-infused dyes or Doxorubicin, (^{dye}RCNMV or ^{Dox}RCNMV)

Protocols to infuse dye or Doxorubicin molecules into RCNMV capsid have previously been described (Chapter 4). In brief, native RCNMV was dialyzed against 200 mM EDTA, pH 8 for 5-6 hours, followed by incubation with molecules at a mole ratio of 2000 for Rhodamine and 5000 for Doxorubicin per RCNMV. The solution was then dialyzed against 200 mM Ca^{2+}, pH 6 for 24 hours. To expedite the removal of excess molecules, the RCNMV-infused dye or Doxorubicin was purified using sucrose gradient centrifugation at 180,000 g, 55 minutes, 5 ℃ in a SW-55 rotor with a model L8-70

Beckman ultracentrifuge. The sucrose gradients were fractionated into 0.25 ml fractions and the absorbance at 260 nm was measured. The fraction with the highest absorbance value was collected. Previous chapter indicated ~90 Rhodamine and ~1000 Doxorubicin were infused per RCNMV.

Conjugation of fluorescently-labeled peptide to RCNMV (RCNMV^{peptides})

Peptides were custom-made at UNC Microprotein Sequencing & Peptide Synthesis Facility (Chapel Hill,NC). Each peptide contains a cysteine at the N terminal and fluorescently labeled with Fluorescein or Rhodamine at the C terminal. 1 mg/ml of RCNMV was incubated with Succinimidyl-4-(*N*-maleimidomethyl) cyclohexane-1-carboxylate (SMCC) (Pierce) at a mole ratio of 1:300 (RCNMV-to-SMCC). The solution was brought up to 1 ml with DPBS and incubated for 30 minutes at room temperature. Excess SMCC was removed by centrifugation at 13,200 rpm for 10 min with a Microcon-30K (Millipore, Billerica, MA). RCNMV-SMCC conjugates were then incubated with fluorescently-labeled peptide at a mole ratio of 1:300 (RCNMV-SMCC conjugates-to-peptide), added with DPBS to a final volume of 1 ml, followed by incubation for 6 hours at room temperature. Excess peptides were removed using a Microcon-30K (Millipore, Billerica, MA) by centrifugation at 13,200 rpm for 10 min. Standard curves of fluorescently-labeled peptides were generated to determine the ratio of peptide conjugated per virus.

Delivery of RCNMV-peptide conjugates (RCNMV^{peptide}) or peptide-conjugated-RCNMV-infused Rhodamine or Doxorubicin (^{Rho}RCNMV^{peptide} or ^{Dox}RCNMV^{peptide}) to cells

Cells were cultured in a 6-well plate for 24 hours to reach ~80 % confluency. Culture media was removed from the well and cells were washed with 1 ml of DPBS. 1.5 ml of media with indicated concentrations of RCNMV^{peptide}, ^{Rho}RCNMV^{peptide} or ^{Dox}RCNMV^{peptide} were incubated with cells for certain incubation period. After indicated time point of incubation, the media in each well was removed and rinsed with 1 ml of DPBS for three times. The cells were harvested with 5 % trypsine and resuspended in 1

ml of media before collected for flow cytometry analysis. All experiments were performed in triplicate.

Fluorescence-Activated Cell Sorting (FACS) analysis

Cells were analyzed by a fluorescence-activated cell sorter (Becton Dickinson, FACScalibur) equipped with an argon laser (488 nm) and analyzed using Cell Quest software. Cells suspended in media were passed with a flow rate of ~120 µl/minute. Results were based on the acquisition of 10,000 cells. The relative fluorescence intensity was calculated by dividing the mean fluorescence intensity of treated sample with mean fluorescence intensity of untreated sample. Data are represented as the mean of triplicates with error bars represent SD.

Cell viability determined by ATP assay

HeLa cells were placed in a 96-well plate at a density of 1×10^4 viable cells/well and incubated at 37 ℃ in an atmosphere containing 5 % CO_2 for 24 hours. The media in each well was replaced with 100 ul of media containing various concentrations (10^{-12} M to 10^{-8} M) of $^{Dox}RCNMV^{CD46\text{-}F}$, $^{Dox}RCNMV$ and equivalent doses of Doxorubicin. After 24 hours of incubation, the media was removed and the wells were washed twice with DPBS. The cell viability assay was performed using an ATP determination kit (Molecular Probe). The luminescence of each well was measured at 560 nm using a microplate reader (Bio-Tek Synergy HT). Cell viability was calculated as indicated: Cell viability (%) = (Int_{sample} /$Int_{control}$) x 100 % where Int_{sample} is the intensity of the treated cells and $Int_{control}$ is the intensity of the untreated cells. Six replicates were prepared for each sample.

Confocal microscopy

HeLa cells were cultured on sterilized cover slips and placed in a 6-well plate followed by incubation with 1.5 ml of culture media containing 0.15 nM of $RCNMV^{CD46\text{-}F}$ for 6 hours. The cover slips were washed with DBPS and the cells were fixed with 4 % paraformaldehyde in DBPS for ~15 min at room temperature. The cover slips were then mounted on a glass slide and allowed to dry overnight prior to microscopy analysis. Leica DMLB microscope with Nikon DMX-1200 color CCD digital camera was used to study the localization of $RCNMV^{CD46\text{-}F}$ in HeLa cells.

Transmission Electron Microscopy (TEM)

TEM images were acquired using a (Philips) CM12 microscope operating at 100kV accelerating voltage located at the University of North Carolina, School of Dentistry, Chapel Hill, NC. Images were created with a Gatan 780 DualView camera system. All TEM samples were negatively stained with 2% uranyl acetate.

5.3 Results

Conjugation of fluorescently-labeled peptides to RCNMV

A homology model, with the *Tomato bushy stunt virus* (TBSV) structure as the template, predicts that each RCNMV capsid protein (CP) contains two lysines that are located on the virus exterior and accessible for chemical modification (Figure 1A). The targeting peptides studied, which included CD46, IBD and CARS, were fluorescently labeled with Fluorescein (F) or Rhodamine (R). The lysines on the virus were conjugated with the cysteine-terminated peptides by using Succinimidyl-4-(N-maleimidomethyl) cyclohexane-1-carboxylate (SMCC) linker. The excess peptides were removed by a 20-40 % sucrose gradient centrifugation. The sucrose gradient of RCNMV-peptide conjugates was fractionated for absorbance and fluorescence measurements (Figure 1B). In all three cases, the sedimentations of fluorescently-labeled peptides were identical to the RCNMV capsid, an indication of the conjugation of peptides on RCNMV capsid. The formation of RCNMV-peptide conjugates was further verified in a SDS-PAGE gel where fluorescently-labeled peptides were found to co-migrate with the RCNMV CP (Figure 1C). Quantification by fluorescence and absorbance measurements indicated the labeling of CD46-F, CARS-F and IBD-R per RCNMV were 115±8, 146±19 and 224±40, respectively.

Kinetic uptake of RCNMV-peptides conjugates

The kinetic uptake of RCNMV-peptide conjugates in HeLa cells was measured for various incubation times (1, 6, 12, 18 and 24 hours) with the concentration of each RCNMV-peptide conjugate held constant at 0.15 nM (Figure 2). The internalization of $RCNMV^{CD46\text{-}F}$ was observed to increase proportional to the incubation time. On the other hand, the uptake of $RCNMV^{IBD\text{-}R}$ and $RCNMV^{CARS\text{-}F}$ were negligible throughout the incubation period. A further control experiment was conducted which involved the delivery of RCNMV conjugated with FITC ($RCNMV^{FITC}$). The fluorescence intensity of $RCNMV^{FITC}$ appeared to be as low as the untreated cells throughout the incubation times, suggesting the lack of internalization. This observation indicated a specific interaction of the CD46 peptide to facilitate the intracellular uptake of RCNMV in the HeLa cell line.

To eliminate the possibility that the increase in fluorescence intensity observed for the delivery of $RCNMV^{CD46\text{-}F}$ was an effect of the auto-fluorescence of cells, control experiments, which involved a non fluorescently-labeled CD46 conjugated to RCNMV ($RCNMV^{CD46}$) and unmodified RCNMV were delivered into cells for 6 hours (Figure 3). The mean fluorescence intensity was as low as the untreated cells for both control samples. Hence, the increase in fluorescence intensity from the former experiment can be attributed to the internalization of $RCNMV^{CD46\text{-}F}$.

Confocal microscopy was used as a secondary method to study the internalization of $RCNMV^{CD46\text{-}F}$. Images obtained every 0.5 microns in the vertical dimension demonstrated the majority of $RCNMV^{CD46\text{-}F}$ accumulated in the cytoplasm and some were observed to locate in the nucleus after 6 hours of incubation (Figure 4). Based upon the uptake efficiency in HeLa cells, CD46-F peptide was chosen for subsequent delivery experiments.

To further determine if the targeting peptides was cell-type specific, the internalization of RCNMV-peptide conjugates were studied in HepG2 cells for 6 hours (Figure 5). Under these conditions, $RCNMV^{CARS\text{-}F}$ observed to have the highest internalization in HepG2 cells. The results indicated that the intracellular uptake of these targeting peptides uptake is cell-type specific. A similar observation has been reported using gold nanoparticles labeled with the same peptides [24].

Delivery of CD46-F conjugated RCNMV-infused Rhodamine ($^{Rho}RCNMV^{CD46\text{-}F}$)

Using established procedures to package ~90 Rhodamine per RCNMV capsid (Chapter 4), the above peptide-labeled RCNMV capsids were prepared and loaded with Rhodamine for cell targeting experiments. Briefly, the sample was prepared by infusion of Rhodamine into the interior cavity of RCNMV using treatment with EDTA, pH 8 to extract the divalent ions, followed by incubation with Rhodamine and dialysis against Ca^{2+}, pH 6. Subsequently, the CD46-F peptide was conjugated to the exterior surface of RCNMV capsid ($^{Rho}RCNMV^{CD46\text{-}F}$). Dynamic Light Scattering (DLS) and TEM analysis revealed that $^{Rho}RCNMV^{CD46\text{-}F}$ remained similar in size to the native RCNMV (Figure 6). In addition, the modified virus was still infectious to *Nicotiana clevelandii* with typical infection symptoms observed after 14 days of inoculation. These data revealed that infusion of Rhodamine and conjugation of CD46-F showed no significant changes to the diameter of the virus and the modified virus remained structurally intact.

The $^{Rho}RCNMV^{CD46\text{-}F}$ was delivered at 31 pM into HeLa cells for various incubation periods (3, 6 and 9 hr). Flow cytometry data indicated that the internalization of $^{Rho}RCNMV^{CD46\text{-}F}$ was rapid, with approximately 100 % of cells associated with CD46-F after 3 hr of incubation. The fluorescence intensity of Rhodamine in cells remained low after 3 hr of incubation and increased gradually after 6 and 9 hours of incubation, with 13.0± 0.6 % and 36.5±0.9 % of cells associated with Rhodamine, respectively. These data suggested that there is a delay of several hours between the internalization of RCNMV and the release of Rhodamine. A control experiment, which involved the delivery of $^{Rho}RCNMV$ (not conjugated with CD46-F), was conducted under the same conditions (Figure 7). Flow cytometry data showed that the fluorescence intensity of Rhodamine was as low as that of the untreated cells over the 6 hours incubation period. These observations indicated that $^{Rho}RCNMV$ do not enter HeLa cells.

Delivery of CD46-F conjugated RCNMV-infused Doxorubicin ($^{Dox}RCNMV^{CD46\text{-}F}$)

The delivery of $^{Rho}RCNMV^{CD46\text{-}F}$ was a proof-of-concept experiment to study the ability of RCNMV capsid to simultaneously package and deliver molecules into cells. Further experiments were performed to explore the potential of the RCNMV capsid for therapeutic targeting. A previous study has demonstrated the efficiency of the RCNMV capsid to package ~1000 Doxorubicin per virus (Chapter 4). The protocol to infuse

Doxorubicin into a RCNMV capsid followed by conjugation of CD46-F onto the capsid (^{Dox}RCNMV$^{CD46\text{-}F}$) was identical to that reported for ^{Rho}RCNMV$^{CD46\text{-}F}$.

The formulation ^{Dox}RCNMV$^{CD46\text{-}F}$ at 100 pM was delivered to HeLa cells for various incubation periods (2, 6, 12, 18 and 24 hours) (Figure 8). Doxorubicin is an anticancer drug that intercalates into DNA and inhibits the progression of topoisomerase II, hence preventing replication. A longer incubation time (24 hours) was chosen for these experiments in order to study the cytotoxicity of Doxorubicin. Flow cytometry data indicated that the internalization of ^{Dox}RCNMV$^{CD46\text{-}F}$ occurred in a time-dependent manner. The intensity of fluorescein (F) in cells was approximately 2-fold greater than the control after 6 hours of incubation and continued to rise up to 9-fold greater as the incubation extended to 24 hours. The Doxorubicin released from RCNMV capsid was detected in cells after 6 hours of incubation, an observation that is consistent with the delivery of ^{Rho}RCNMV$^{CD46\text{-}F}$. The Doxorubicin intensity detected here was relatively low throughout the incubation period, as compared to the intensity of fluorescein. One possible explanation is the fluorescence quenching of Doxorubicin when it interacts with DNA in the nucleus where > 90 % of Doxorubicin intensity reported to be quenched when intercalated to DNA[25 26].

Control experiments involved the delivery of ^{Dox}RCNMV (not conjugated with CD46-F) at 100 pM and equivalent doses of Doxorubicin for 12, 18 and 24 hours were performed (Figure 10). For ^{Dox}RCNMV, the Doxorubicin intensities remained comparable to the untreated cells, indicating the failure of Doxorubicin from the ^{Dox}RCNMV to gain access to the cells. The cells incubated with free Doxorubicin showed a slight increase of Doxorubicin intensity. However, the intensity was significantly lower than the cells incubated with ^{Dox}RCNMV$^{CD46\text{-}F}$ under the same delivery conditions. These observations suggested the efficiency of the RCNMV$^{CD46\text{-}F}$ to promote the uptake of Doxorubicin in cells.

To further substantiate the delivery of ^{Dox}RCNMV$^{CD46\text{-}F}$, the morphology of cells treated with 100 pM of ^{Dox}RCNMV$^{CD46\text{-}F}$ was observed after 24 hours of exposure period and compared with the untreated cells (Figure 10). The cells treated with ^{Dox}RCNMV$^{CD46\text{-}F}$ were spherical, and shrinkage of the cytoplasm could be observed, both are indications of apoptosis (Figure 10D). The morphology of cells after ^{Dox}RCNMV treatment

remained similar to untreated cells (Figure 10B). When treated with free Doxorubicin at equivalent doses, the number of cells showing sign of apoptosis was relatively low compared to $^{Dox}RCNMV^{CD46\text{-}F}$.

The data above indicate that the delivery of 100 pM $^{Dox}RCNMV^{CD46\text{-}F}$ for 24 hours showed that there is a significant impact on cell morphology. Further experiment was performed to study the cell viability by a dose-response curve for $^{Dox}RCNMV^{CD46\text{-}F}$ and non-infused Doxorubicin, with a 24 hour time point. The IC_{50} of Doxorubicin delivered by $^{Dox}RCNMV^{CD46\text{-}F}$ was observed to be 10^{-6} M. When free Doxorubicin (not packaged within RCNMV) was delivered under the same conditions, the IC_{50} was observed to be 10^{-5} M, which is 10-fold greater than that of $^{Dox}RCNMV^{CD46\text{-}F}$. On the other hand, the delivery of Doxorubicin in $^{Dox}RCNMV$ without a targeting peptide showed significantly lower toxicity. It is not possible to measure the IC_{50} since the preparation of RCNMV is nearly at the limit of solubility in the growth medium for HeLa cells at 10^{-4} M.

5.4 Discussion

The outer surface of RCNMV can be conjugated with various targeting peptides to introduce cell-specific targeting capability. Based on precedents using gold nanoparticle constructs[24] we hypothesized that the $RCNMV^{CD46}$ construct would be an appropriate targeting vector for the HeLa cell line. We created constructs of RCNMV that contained dye or chemotherapeutic cargo loaded in the internal cavity and targeting peptides on the exterior surface. Using the nomenclature $^{cargo}RCNMV^{peptide}$, we studied the intracellular effects of targeting peptides and both cytotoxic and non-toxic cargo. The delivery of $^{Rho}RCNMV^{CD46\text{-}F}$ was initially performed as a proof-of-concept experiment. The data suggested a lag period between internalization of $^{Rho}RCNMV^{CD46\text{-}F}$ and the release of Rhodamine in cells. In addition, the control experiments (delivery of $^{Rho}RCNMV$) demonstrated the importance of targeting peptide to enhance uptake of the particle. The understanding of these preliminary results enabled us to further develop RCNMV capsid for cell-specific therapeutic delivery. The localization of $^{Dox}RCNMV^{CD46\text{-}F}$ in cells has

not been confirmed, but the delivery of RCNMV$^{CD46\text{-}F}$ demonstrated accumulation of particles in nucleus after 6 hours of incubation. This observation is crucial as it increases the chances for Doxorubicin to bind with DNA, which is required for its therapeutic effect[27]. The results obtained from cell viability assay suggested the therapeutic efficacy was approximately 10-fold higher than free Doxorubicin due to the specific targeting and delayed release in the cells.

RCNMV is a potential tool for biomedical applications. The number of residues available on the outer surface of RCNMV creates a platform that can be functionalized with multiple targeting signals in a straightforward manner. As opposed to solid nanoparticles such as polyester poly(lactic-co-glycolic acid) PLGA, surface modification to the nanoprticles is required to present functional group for ligand conjugation[28], which potential affects the integrity of the carrier. The covalent attachment of ligands to liposomes often involves a multi-step approach[29], which has the possibility to affect the structure of the particle as well as the packaged cargo. The capability to modify internally and externally of RCNMV capsid and still maintain the capsid integrity indicated the robustness of RCNMV to protect its cargo. This is critical in order to maintain the drug's therapeutic activity during the delivery process.

Together with the delayed release mechanism reported here, the RCNMV protein shell can perform as a container to protect and sequester a cargo until it reaches the targeted cell nucleus to be released. Moreover, RCNMV has a built-in release mechanism for the drug. The sensitivity of RCNMV towards divalent ion concentrations acts as a switch to open and close surface pores[23]. In blood, where the calcium concentration is in the millimolar range, the capsid stays intact with the cargo packaged. Once inside a cell, the concentration of calcium is low which triggers the pores to open and release the cargo. In addition, the high loading capacity offers by the RCNMV cavity for drug packaging enhance the ability to achieve therapeutic concentration at targeted site. The ability of RCNMV to package, protect and release its cargo when triggered suggested the potential to function in drug delivery applications.

5.5 Conclusion

In summary, we have demonstrated that RCNMV capsid can be studied as a multifunctional tool to target and deliver molecules to cancer cells. The usage of RCNMV capsid as a carrier has demonstrated to have high stability, ability for cell-specific targeting as well as rapid delivery of cargo into cells. The utilization of RCNMV capsid as a multifunctional tool for therapeutic purposes demonstrated a new general drug delivery platform.

(A)

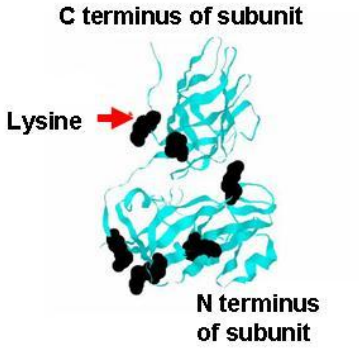

(B)

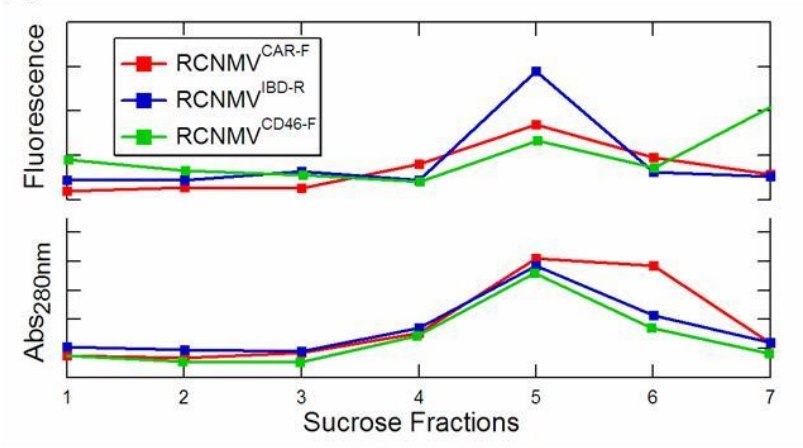

(C)

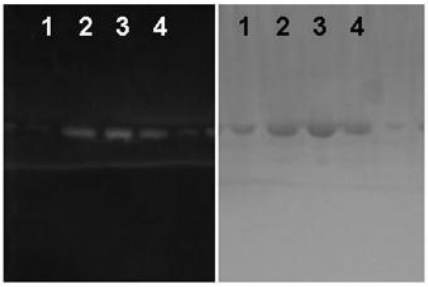

(D)

Peptide- fluorophore*	Sequence	Number of Peptide/RCNMV
Nuclear Localization Signal-F (CD46-F)	CGGFSTSLRARKA	115 ± 8
Integrin Binding Domain-R (IBD-R)	CKKKKKKGGRGD	224 ± 40
Receptor Mediated Endocytosis-F (CARS-F)	CKKKKKKSEDEY	146 ± 19

Figure 1.Conjugation of fluorescently-labeled peptides on RCNMV capsid. (A) Subunit ribbon diagram. Two lysine residues, indicated in black, appear to be exposed on the outer surface of capsid. (B) Absorbance and fluorescence profile of fractionated RCNMV-peptide conjugates. The sedimentation of fluorescently-labeled peptides was identical to RCNMV capsid (fraction 5). (C) 12% SDS-PAGE analysis of RCNMV-peptide conjugates. Identical gel visualized under ultra-violet illumination (left) and stained with Coomasie Blue (right) determined the co-localization of fluorescently labeled peptides with RCNMV capsid protein. Lane (1) native RCNMV (2) $RCNMV^{CD46-F}$ (3) $RCNMV^{IBD-R}$ and (4) $RCNMV^{CARS-F}$ conjugates. (D) Peptide sequences and number of peptide conjugated per RCNMV. *Each peptide was fluorescently labeled with Fluorescein (F) or Rhodamine (R).

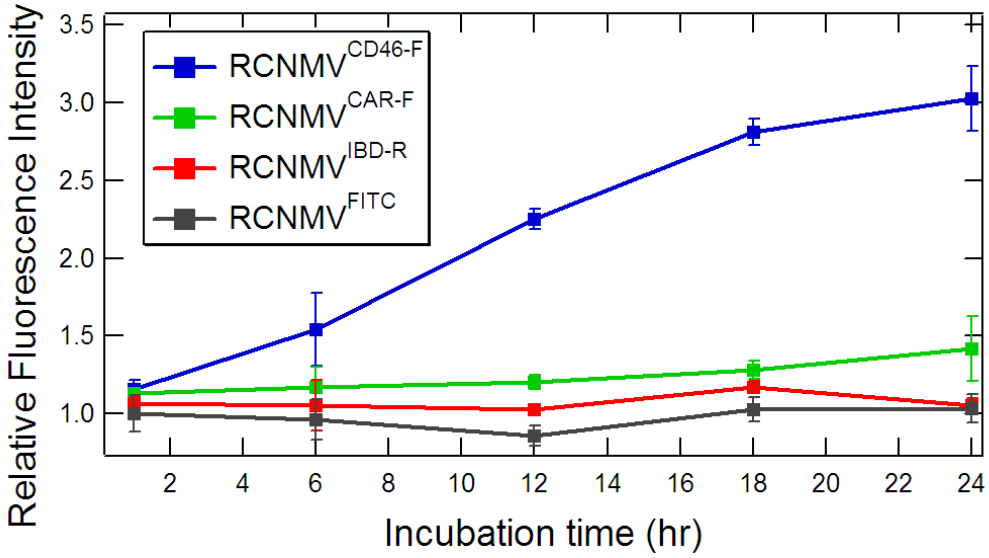

Figure 2.Kinetic uptake of RCNMV-peptide conjugates in HeLa cells. The intracellular uptake of RCNMV^{CD46-F}, RCNMV^{IBD-R}, RCNMV^{CARS-F} and RCNMV^{FITC} were studied in HeLa cells for various incubation periods. The relative fluorescence intensity was derived by dividing the mean fluorescence intensity of treated cells with the mean fluorescence intensity of untreated cells. The experiments were performed in triplicate, and the mean ± S.D are shown.

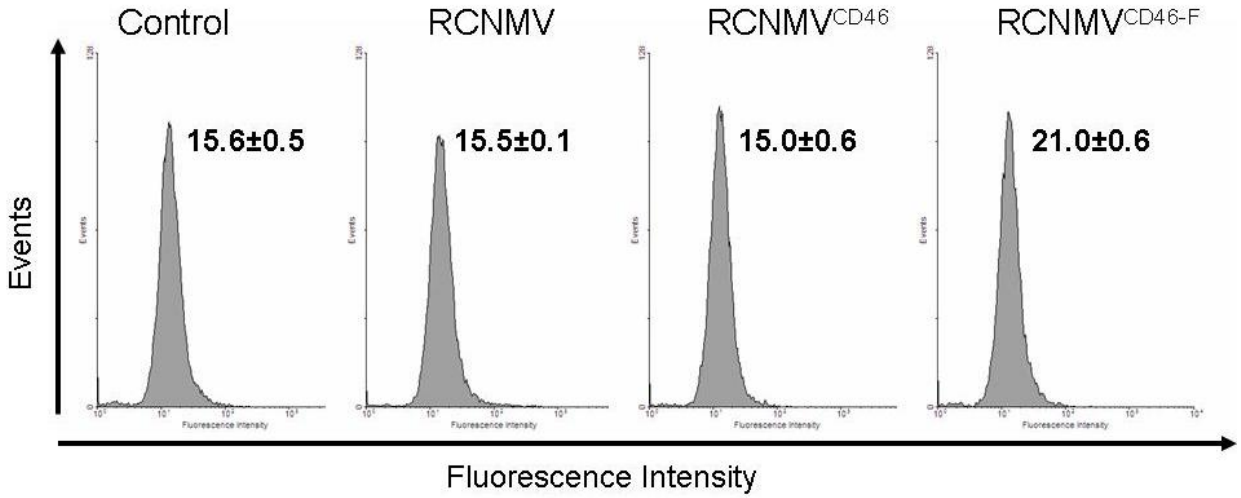

Figure 3.Delivery of native RCNMV, RCNMV^{CD46} (non-fluorescent labeled CD46) and RCNMV^{CD46-F} to HeLa cells for 6 hours. The flow cytometry data were plotted in histogram with the corresponding mean fluorescence intensity indicated.

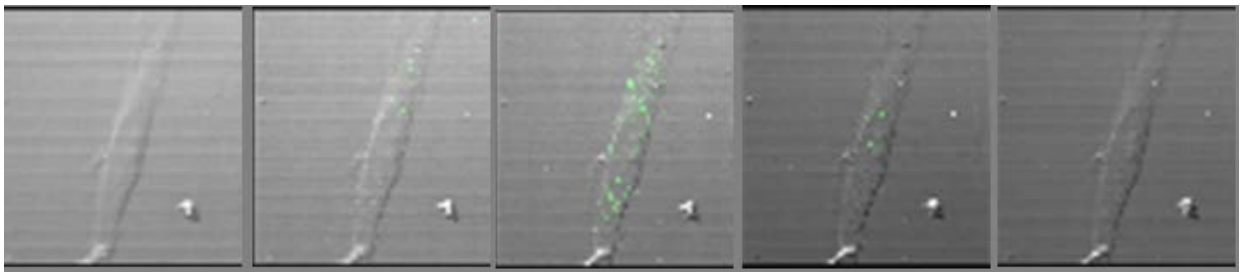

Figure 4.Confocal microscopy images of HeLa cells incubated with RCNMV$^{CD46\text{-}F}$ for 6 hours. Detectable green fluorescence from RCNMV$^{CD46\text{-}F}$ was observed in cells.

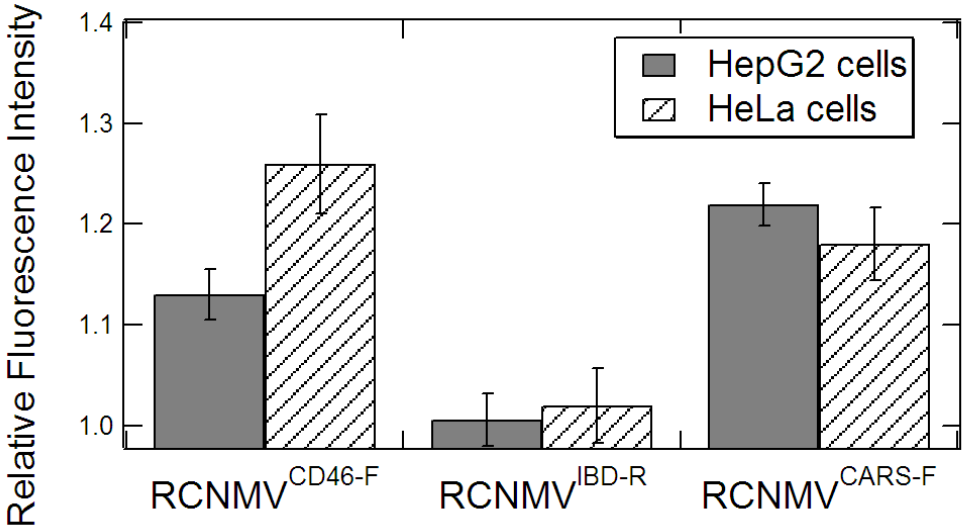

Figure 5.Comparison of RCNMV-peptide conjugates uptake in HeLa and HepG2 cells after 6 hours of incubation.

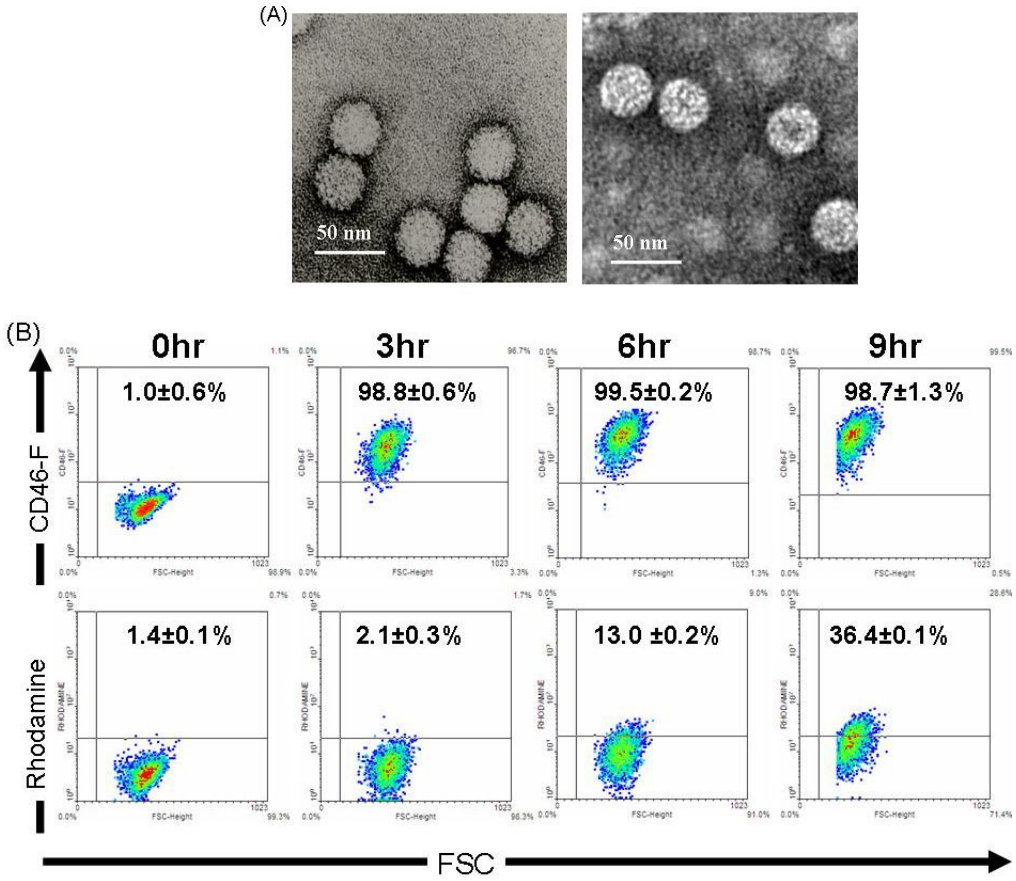

Figure 6. Characterization and intracellular uptake of ^{Rho}RCNMV$^{CD46\text{-}F}$. (A) TEM images of (left) native RCNMV and (right) ^{Rho}RCNMV$^{CD46\text{-}F}$. (B) Uptake of ^{Rho}RCNMV$^{CD46\text{-}F}$ is shown for various incubation times. FACS data were plotted in density plots with CD46-F (top row) and Rhodamine (bottom row) versus forward scattering (FSC). The percentage of cells associated with CD46-F or Rhodamine were indicated.

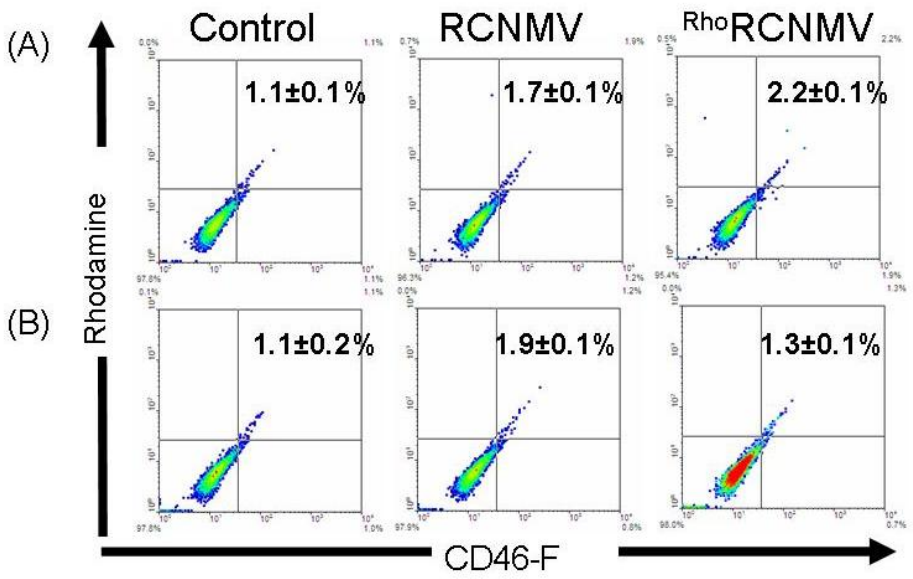

Figure 7.Delivery of native RCNMV and ^{Rho}RCNMV (not conjugated with CD46-F) into HeLa cells for (A) 1 hour and (B) 6 hours. The percentage of cells associated with both CD46-F and Rhodamine was indicated.

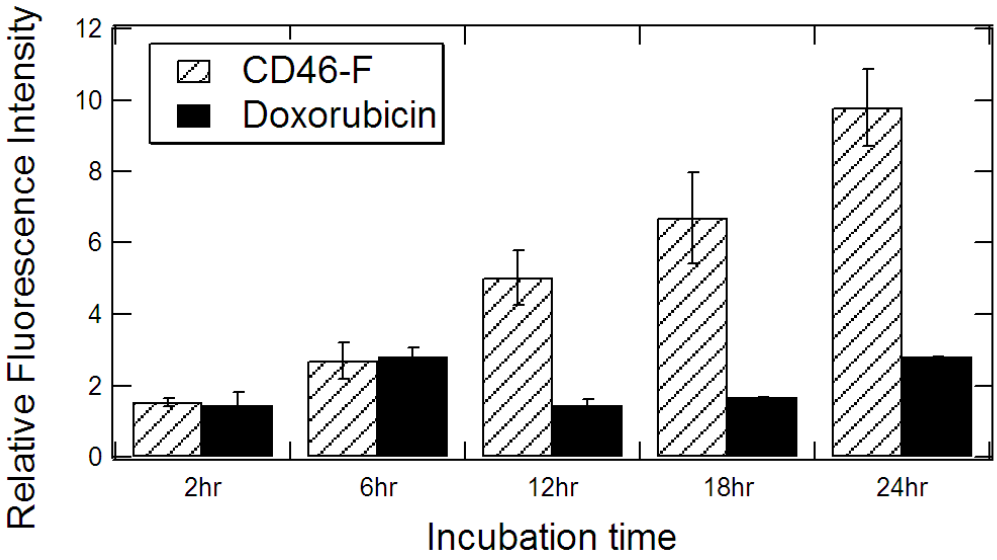

Figure 8.Kinetic uptake of ^{Dox}RCNMV$^{CD46\text{-}F}$ and the release of Doxorubicin in HeLa cells under various incubation times. The fluorescence intensities of fluorescein and Doxorubicin for treated cells were compared to the untreated cells (control).

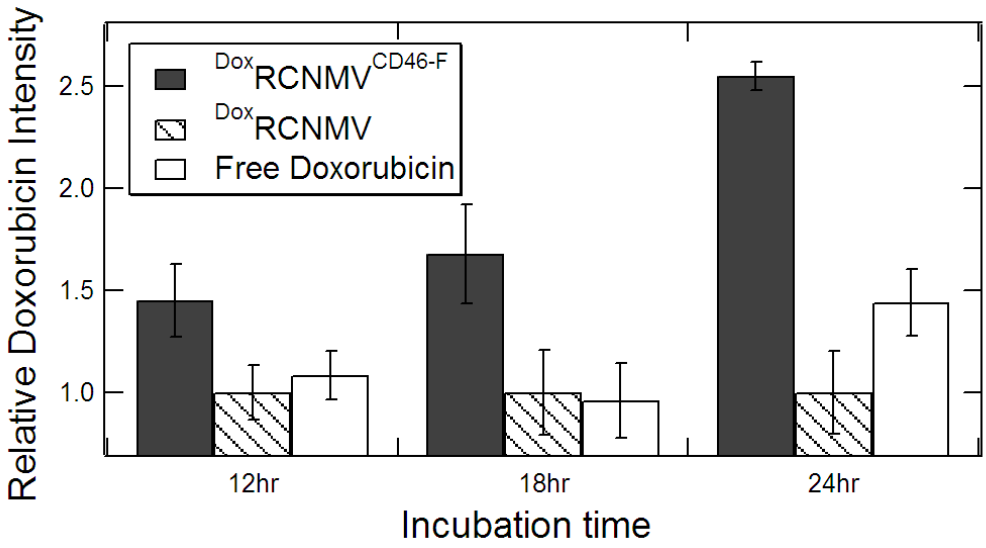

Figure 9.Delivery of ^{Dox}RCNMV$^{CD46\text{-}F}$, ^{Dox}RCNMV (not conjugated with CD46-F) at 100 pM, and free doxorubicin at equivalent concentration for various incubation times (12, 18 and 24 hours).

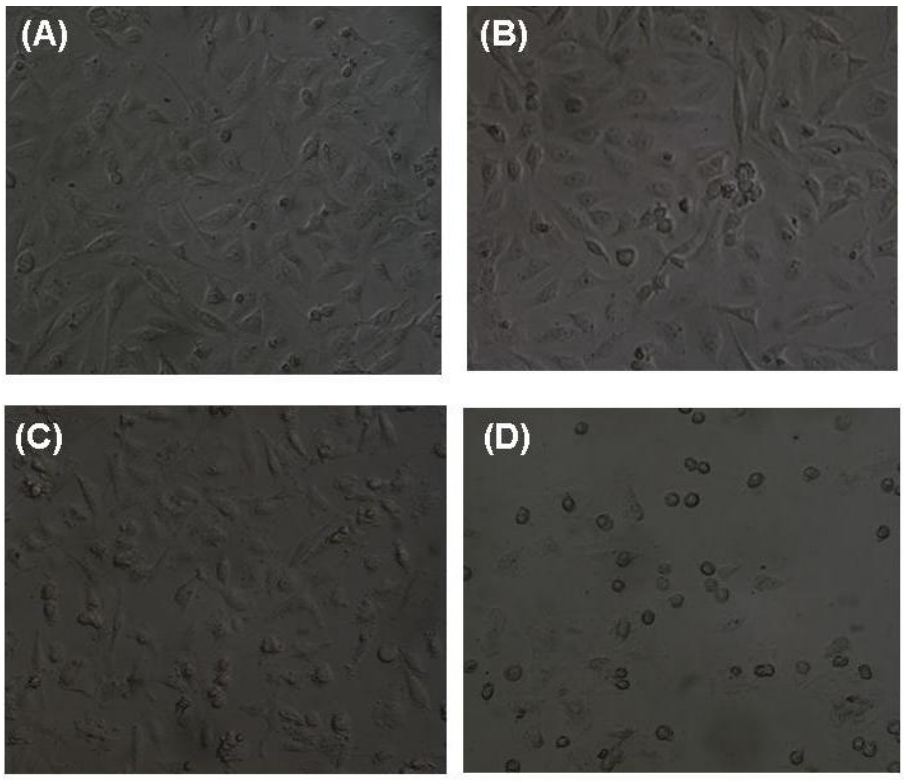

Figure 10.Morphological changes to HeLa cells (A) before and after treatment with (B)^{Dox}RCNMV, (C) free Doxorubicin and (D) ^{Dox}RCNMV$^{CD46\text{-}F}$ for 24 hours.

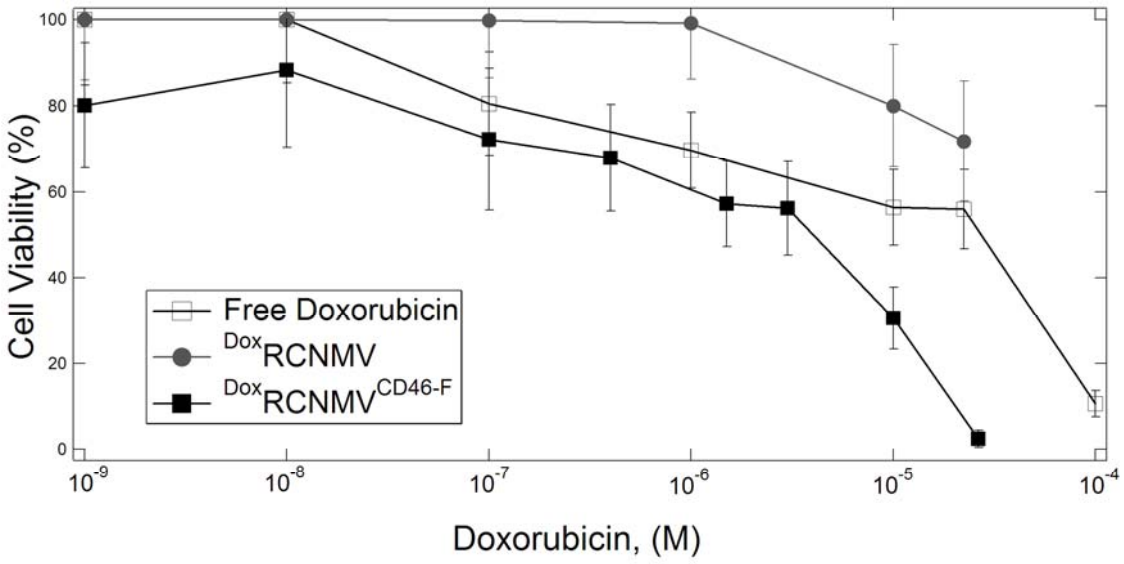

Figure 11.Cytotoxicity effect of infused and non-infused Doxorubicin on HeLa cells. ^{Dox}RCNMV$^{CD46\text{-}F}$, ^{Dox}RCNMV and free Doxorubicin were exposed to HeLa cells for 24

hours. At the end of the period, the medium was removed and the cells were washed with medium before assessed with ATP assay. Each point presented the mean of six replicates.

References

(1) Torchilin, V. P. *Advanced Drug Delivery Reviews* **2006**, *58*, 1532-1555.

(2) Kayser, O.; Lemke, A.; Hernandez-Trejo, N. *Current Pharmaceutical Biotechnology* **2005**, *6*, 3-5.

(3) Rawat, M.; Singh, D.; Saraf, S.; Saraf, S. *Biological & Pharmaceutical Bulletin* **2006**, *29*, 1790-1798.

(4) Frechet, J. M. J. *Science* **1994**, *263*, 1710-1715.

(5) Fernandez-Urrusuno, R.; Calvo, P.; Remunan-Lopez, C.; Vila-Jato, J. L.; Alonso, M. J. *Pharmaceutical Research* **1999**, *16*, 1576-1581.

(6) Kim, T. H.; Park, I. K.; Nah, J. W.; Choi, Y. J.; Cho, C. S. *Biomaterials* **2004**, *25*, 3783-3792.

(7) Aktas, Y.; Andrieux, K.; Alonso, M. J.; Calvo, P.; Gursoy, R. N.; Couvreur, P.; Capan, Y. *International Journal of Pharmaceutics* **2005**, *298*, 378-383.

(8) Luo, D.; Han, E.; Belcheva, N.; Saltzman, W. M. *Journal of Controlled Release* **2004**, *95*, 333-341.

(9) Soto, C. M.; Blum, A. S.; Vora, G. J.; Lebedev, N.; Meador, C. E.; Won, A. P.; Chatterji, A.; Johnson, J. E.; Ratna, B. R. *Journal of the American Chemical Society* **2006**, *128*, 5184-5189.

(10) Chatterji, A.; Ochoa, W. F.; Ueno, T.; Lin, T. W.; Johnson, J. E. *Nano Letters* **2005**, *5*, 597-602.

(11) BANCROFT, J. *Virology* **1967**, *31*, 354.

(12) Allen, M.; Bulte, J. W. M.; Liepold, L.; Basu, G.; Zywicke, H. A.; Frank, J. A.; Young, M.; Douglas, T. *Magnetic Resonance in Medicine* **2005**, *54*, 807-812.

(13) Wang, Q.; Kaltgrad, E.; Lin, T. W.; Johnson, J. E.; Finn, M. G. *Chemistry & Biology* **2002**, *9*, 805-811.

(14) Lewis, J. D.; Destito, G.; Zijlstra, A.; Gonzalez, M. J.; Quigley, J. P.; Manchester, M.; Stuhlmann, H. *Nature Medicine* **2006**, *12*, 354-360.

(15) Khor, I. W.; Lin, T. W.; Langedijk, J. P. M.; Johnson, J. E.; Manchester, M. *Journal of Virology* **2002**, *76*, 4412-4419.

(16) Chen, C.; Kwak, E. S.; Stein, B.; Kao, C. C.; Dragnea, B. *Journal of Nanoscience and Nanotechnology* **2005**, *5*, 2029-2033.

(17) Douglas, T.; Young, M. *Nature* **1998**, *393*, 152-155.

(18) Ren, Y.; Wong, S. M.; Lim, L. Y. *Bioconjugate Chemistry* **2007**, *18*, 836-843.

(19) Hooker, J. M.; Kovacs, E. W.; Francis, M. B. *Journal of the American Chemical Society* **2004**, *126*, 3718-3719.

(20) Uchida, M.; Flenniken, M. L.; Allen, M.; Willits, D. A.; Crowley, B. E.; Brumfield, S.; Willis, A. F.; Jackiw, L.; Jutila, M.; Young, M. J.; Douglas, T. *Journal of the American Chemical Society* **2006**, *128*, 16626-16633.

(21) Loo, R. H. G., Veronica R.Basnayake, Steven A.Lommel, Stefan Franzen *Journal of American chemical society* **2006**.

(22) Loo, L.; Guenther, R. H.; Lommel, S. A.; Franzen, S. *Chemical Communications (in press)* **2007**.

(23) Sherman, M. B.; Guenther, R. H.; Tama, F.; Sit, T. L.; Brooks, C. L.; Mikhailov, A. M.; Orlova, E. V.; Baker, T. S.; Lommel, S. A. *Journal of Virology* **2006**, *80*, 10395-10406.

(24) Tkachenko, A. G.; Xie, H.; Liu, Y. L.; Coleman, D.; Ryan, J.; Glomm, W. R.; Shipton, M. K.; Franzen, S.; Feldheim, D. L. *Bioconjugate Chemistry* **2004**, *15*, 482-490.

(25) Barabas, K.; Sizensky, J. A.; Faulk, W. P. *Journal of Biological Chemistry* **1992**, *267*, 9437-9442.

(26) Rodrigues, P. C. A.; Beyer, U.; Schumacher, P.; Roth, T.; Fiebig, H. H.; Unger, C.; Messori, L.; Orioli, P.; Paper, D. H.; Mulhaupt, R.; Kratz, F. *Bioorganic & Medicinal Chemistry* **1999**, *7*, 2517-2524.

(27) Fornari, F. A.; Randolph, J. K.; Yalowich, J. C.; Ritke, M. K.; Gewirtz, D. A. *Molecular Pharmacology* **1994**, *45*, 649-656.

(28) Fahmy, T. M.; Samstein, R. M.; Harness, C. C.; Saltzman, W. M. *Biomaterials* **2005**, *26*, 5727-5736.

(29) Hansen, C. B.; Kao, G. Y.; Moase, E. H.; Zalipsky, S.; Allen, T. M. *Biochimica Et Biophysica Acta-Biomembranes* **1995**, *1239*, 133-144.